



**Species-differences in the *in vitro* biotransformation of trifluoroethene
(HFO-1123)**

**Speziesunterschiede in der *in vitro* Biotransformation von Trifluorethen
(HFO-1123)**

Doctoral thesis for a doctoral degree
at the Graduate School of Life Sciences,
Julius-Maximilians-Universität Würzburg,
Section Biomedicine

submitted by

Raphael H. Dekant

from

Würzburg

Würzburg, 2022



Submitted on:

Office stamp

Members of the Thesis Committee

Chairperson: Prof. Dr. C. Wegener

Primary Supervisor: Prof. Dr. A. Mally

Supervisor (Second): Prof. Dr. L. Lehmann

Supervisor (Third): Dr. R. Bertermann

Parts of this thesis have already been published as following:

Publications

Dekant R., Bertermann R., Serban J., Sharma S., Shinohara M., Morisawa Y., Okamoto H., Brock W.J., Dekant W., Mally A.; Species-differences in the *in vitro* biotransformation of 1,1,2-trifluoroethene (HFO-1123); ***Manuscript in preparation.***

Presentation at international conferences

Dekant R., Serban J., Sharma S., Bertermann R., Shinohara M., Morisawa Y., Okamoto H., Brock W.J., Dekant W., Mally A. (2022); Investigation of possible species-differences in biotransformation of 1,1,2-trifluoroethene (HFO-1123) in subcellular liver and kidney fractions, Poster presentation at SOT 61st annual meeting, San Diego, USA, March 27-31, 2022.

In memoriam to my beloved grandparents,

Anna and Wilhelm Henzl.

Table of Contents

1 Abstract	1
2 Zusammenfassung	3
3 Introduction	6
3.1 A healthy world demands clean cooling – United Nation’s Sustainable Development Goals	6
3.2 Freon® - The beginning of modern refrigeration and its unforeseen climate hazards....	9
3.3 Hydrochlorofluorocarbons (HCFCs) and hydrofluorocarbons (HFCs) – an inadequate but necessary alternative for CFCs	14
3.4 Hydrofluoroolefins (HFOs) — Green refrigerants of the 21st century with increased potential for toxicity	18
3.5 The Mercapturic Acid Pathway – A common pathway in the bioactivation of haloalkenes	22
3.6 Trifluoroethene (HFO-1123) – Advanced climatic properties but marked health concerns	26
3.6.1 Inhalation exposure of experimental animals to HFO-1123.....	26
3.6.2 Potential role of HFO-1123 biotransformation in species-differences in toxicity.....	31
3.7 Objectives and aims	36
4 Materials & Methods	37
4.1 Chemicals & chemical syntheses	37
4.1.1 Chemicals	37
4.1.2 Chemical syntheses.....	37
4.2 <i>In vitro</i> incubations to study GST and β -lyase mediated biotransformation of HFO-1123.....	38
4.2.1 Sources of subcellular fractions.....	38
4.2.2 GST mediated biotransformation of HFO-1123 in S ₉ subcellular fractions.....	40
4.2.3 β -Lyase mediated biotransformation of 1123-CYS.....	43
4.3 Analytical methods.....	46
4.3.1 ¹⁹ F-NMR.....	46
4.3.2 Liquid chromatography coupled with mass spectrometry (LC-MS/MS).....	46
4.4 Cell culture experiments	48
4.4.1 Cell culture properties.....	48
4.4.2 Cell Viability	50
4.4.3 Quantitation of citrate.....	51
4.4.4 LC-MS/MS method to determine citrate levels	51
4.4.5 Statistical analysis	52
5 Results	53
5.1 GST dependent biotransformation of HFO-1123	53
5.1.1 Purity assessment of 1123-GSH by quantitative ¹⁹ F-NMR	53

5.1.2	Preliminary experiments to verify the experimental approach	54
5.1.3	Time-dependent formation of 1123-GSH in liver S ₉ incubated with HFO-1123.....	56
5.1.4	<i>In vitro</i> kinetics of GST mediated formation of 1123-GSH after incubating hepatic S ₉ fractions with HFO-1123	57
5.1.5	Species-differences in 1123-CYS formation in hepatic S ₉ fractions after incubation with HFO-1123	58
5.1.6	Impact of γ -GT and β -lyase inhibition on GSH dependent biotransformation of HFO-1123 in hepatic S ₉	59
5.1.7	Time-dependent formation of fluorine containing metabolites after incubation of hepatic S ₉ fractions with HFO-1123 by ¹⁹ F-NMR.....	61
5.1.8	Time-dependent formation of 1123-GSH and 1123-CYS in renal S ₉ fractions after incubation with HFO-1123	64
5.2	Determination of β -lyase mediated biotransformation of 1123-CYS in renal and hepatic cytosolic fractions.....	66
5.2.1	Confirmation of β -lyase mediated cleavage of 1123-CYS	68
5.2.2	Kinetics of β -lyase mediated cleavage of 1123-CYS in renal and hepatic cytosolic fractions	70
5.2.3	Fluorine containing metabolite formation from 1123-CYS in renal and hepatic cytosol monitored by ¹⁹ F-NMR.....	72
5.3	Effects of 1123-CYS and MFA on cell viability and cellular citrate levels in cell culture.....	81
5.3.1	Cytotoxicity of 1123-CYS and MFA	81
5.3.2	Effects of 1123-CYS on cellular citrate	82
5.3.3	LC-MS/MS analysis of 1123-CYS metabolites in human, rat and porcine proximal tubular cells	84
5.4	Summary of GST- and β -lyase dependent biotransformation of HFO-1123.....	86
6	Discussion	88
6.1	GST mediated formation of 1123-GSH in hepatic and renal S ₉	88
6.2	β -lyase mediated biotransformation of 1123-CYS in renal and hepatic cytosols.....	92
6.3	β -lyase mediated biotransformation of 1123-CYS and cytotoxicity in cell culture.....	94
6.4	Summary and Conclusion.....	97
7	Abbreviations.....	103
8	References	105
Appendix A	Additional Methods.....	117
Appendix B	Additional Figures & Tables.....	120
List of Figures	127
List of Tables	131

1 Abstract

1,1,2-trifluoroethene (HFO-1123, CAS# 359-11-5) is intended for use as a refrigerant. Inhalation studies on HFO-1123 in rats suggested a low potential for toxicity, with no-observed-adverse-effect levels $\geq 20,000$ ppm. However, single inhalation exposure of Goettingen[®] Minipigs (≥ 500 ppm, 6 hours) and New Zealand White Rabbits (NZW Rabbits) (≥ 1250 ppm, 6 hours) resulted in mortality. It was assumed that conjugation of HFO-1123 with glutathione, via glutathione S-transferase (GST), gives rise to S-(1,1,2-trifluoroethyl)-L-glutathione (1123-GSH), which is then transformed to the corresponding cysteine S-conjugate (S-(1,1,2-trifluoroethyl)-L-cysteine, 1123-CYS). Subsequent β -lyase mediated cleavage of 1123-CYS may result in monofluoroacetic acid (MFA), a potent inhibitor of aconitase. Species-differences in 1123-GSH formation and 1123-CYS cleavage to MFA may explain species-differences in HFO-1123 toxicity.

This study was designed to test the hypothesis, that GSH-dependent biotransformation and subsequent β -lyase mediated formation of monofluoroacetic acid (MFA), a potent inhibitor of aconitase in the citric acid cycle, may play a key role in HFO-1123 toxicity and to evaluate if species-differences in the extent of MFA formation may account for the species-differences in HFO-1123 toxicity. The overall objective was to determine species-differences in HFO-1123 biotransformation in susceptible vs. less susceptible species and humans as a basis for human risk assessment.

To this end, *in vitro* biotransformation of HFO-1123 and 1123-CYS was investigated in renal and hepatic subcellular fractions of mice, rats, humans, Goettingen[®] Minipigs and NZW Rabbits. Furthermore, cytotoxicity and metabolism of 1123-CYS was assessed in cultured renal epithelial cells. Enzyme kinetic parameters for β -lyase mediated cleavage of 1123-CYS in renal and hepatic cytosolic fractions were determined, and ¹⁹F-NMR was used to identify fluorine containing metabolites arising from 1123-CYS cleavage. Quantification of 1123-GSH formation in hepatic S₉ fractions after incubation with HFO-1123 was performed by LC-MS/MS and hepatic metabolism of HFO-1123 was monitored by ¹⁹F-NMR.

Rates of 1123-GSH formation were increased in rat, mouse and NZW Rabbit compared to human and Goettingen[®] hepatic S₉, indicating increased GSH dependent biotransformation in rats, mouse and NZW Rabbits. NZW Rabbit hepatic S₉ exhibited increased 1123-GSH formation in the presence compared to the absence of acivicin, a specific γ -GT inhibitor. This indicates increased γ -GT mediated cleavage of 1123-GSH in NZW Rabbit hepatic S₉ compared to the other species. ¹⁹F-NMR confirmed formation of 1123-GSH as the main metabolite of GSH mediated biotransformation of HFO-1123 in hepatic S₉ fractions next to F⁻. Increased F⁻ formation was detected in NZW Rabbit and Goettingen[®] Minipig hepatic S₉ in the

presence of an NADPH regenerating system, indicating a higher rate of CYP-450 mediated metabolism in these species. Based on these findings, it is possible that CYP-450 mediated metabolism may contribute to HFO-1123 toxicity.

In contrast to the increased formation of 1123-GSH in rat, mouse and NZW Rabbit hepatic S₉ (compared to human and Goettingen[®] Minipig), enzyme kinetic studies revealed a significantly higher β -lyase activity towards 1123-CYS in renal cytosol of Goettingen[®] Minipigs compared to cytosol from rats, mice, humans and NZW Rabbits. However, β -lyase cleavage in renal NZW Rabbit cytosol was slightly increased compared to rat, mouse and human renal cytosols. ¹⁹F-NMR analysis confirmed increased time-dependent formation of MFA in renal Goettingen[®] Minipig cytosol and NZW Rabbit (compared to human and rat cytosolic fractions). Three structurally not defined MFA-derivatives were detected exclusively in NZW Rabbit and Goettingen[®] Minipig cytosols. Also, porcine kidney cells were more sensitive to cytotoxicity of 1123-CYS compared to rat and human kidney cells.

Overall, increased β -lyase mediated cleavage of 1123-CYS to MFA in Goettingen[®] Minipig and NZW Rabbit kidney (compared to human and rat) may support the hypothesis that enzymatic cleavage by β -lyases may account for the species-differences in HFO-1123 toxicity. However, the extent of GST mediated biotransformation in the liver as the initial step in HFO-1123 metabolism does not fully agree with this hypothesis, since 1123-GSH formation occurs at higher rates in rat, mouse and NZW Rabbit S₉ as compared to the Goettingen[®] Minipig.

Based on the inconsistencies between the extent of GST and β -lyase mediated biotransformation of HFO-1123 obtained by this study, a decisive statement about an increased biotransformation of HFO-1123 in susceptible species with a direct linkage to the species-specific toxicity cannot be drawn. Resulting from this, a clear and reliable conclusion regarding the risk for human health originating from HFO-1123 cannot be made. However, considering the death of Goettingen[®] Minipigs and NZW Rabbits after inhalation exposure of HFO-1123 at concentrations ≥ 500 ppm and ≥ 1250 ppm, respectively, this indicates a health concern for humans under peak exposure conditions. For a successful registration of HFO-1123 and its use as a refrigerant, further *in vitro* and *in vivo* investigations addressing uncertainties in the species-specific toxicity of HFO-1123 are urgently needed.

2 Zusammenfassung

1,1,2-Trifluorethen (HFO-1123, CAS# 359-11-5) besitzt hervorragende klimatische und thermische Eigenschaften für den Einsatz als Kühlmittel. In Inhalationsstudien an Ratten, Kaninchen und Schweinen, die im Rahmen der regulatorischen Toxizitätsprüfung durchgeführt wurden, konnten ausgeprägte Speziesunterschiede in der Toxizität von HFO-1123 nachgewiesen werden. In Ratten zeigte HFO-1123 ein geringes Potential für akute und chronische Toxizität, mit NOAELs („No-Observed-Adverse-Effect Level“) ≥ 20.000 ppm. Im Gegensatz dazu führte die einmalige HFO-1123 Exposition von Goettingen[®] Minischweinen (≥ 500 ppm, 6 Stunden) und Weißen Neuseeländer Kaninchen (WN Kaninchen) (≥ 1250 ppm, 6 Stunden) zum Tod von Versuchstieren. Bereits die niedrigste verwendete Raumkonzentrationen von 65 ppm führten bei Goettingen[®] Minischweinen zu ausgeprägter Toxizität (Kardiotoxizität, Neurotoxizität). Auf Grundlage der inhalativen Toxizität, sowie detaillierter Kenntnis der Biotransformation strukturverwandten Substanzen wurde vermutet, dass Speziesunterschiede in der Toxizität auf einer speziesspezifischen Biotransformation von HFO-1123 beruhen. Der erste Schritt in der vermuteten Bioaktivierung von HFO-1123 könnte demnach eine Glutathion S-transferase abhängige Konjugation mit Glutathion beinhalten und zur Bildung von S-(1,1,2-trifluoroethyl)-L-Glutathion (1123-GSH) führen. Das gebildete Glutathion-Konjugat könnte γ -Glutamyltransferase (γ -GT), sowie Dipeptidase und Aminotransferase abhängig zu seinem korrespondierenden Cystein S-Konjugat, S-(1,1,2-trifluoroethyl)-L-Cysteine (1123-CYS) abgebaut werden. Wie andere Cystein S-Konjugate mit elektronegativen Substituenten am Schwefelatom, könnte dieses mittels Cysteininkonjugat- β -Lyasen (β -Lyasen) zu einem Thionoacylfluorid- Intermediat umgewandelt werden. Nach Hydrolyse entsteht voraussichtlich Monofluoressigsäure (MFA) als stabiler Metabolit. MFA greift in den Zitronensäurezyklus ein, indem das Enzym Aconitase irreversible gehemmt wird. Die Hemmung der Aconitase führt zu einem Abbruch des Zitronensäurezyklus und somit zu einem erheblichen Eingriff in die Energiegewinnung des Organismus. Speziesunterschiede in der Bildung von 1123-GSH sowie der Spaltung von 1123-CYS zu MFA könnten die speziesspezifische Toxizität von HFO-1123 erklären.

Ziel dieser Arbeit war es die im vorherigen Absatz aufgestellte Arbeitshypothese, einer Glutathion-abhängigen Biotransformation von HFO-1123, gefolgt von einer β -Lyase vermittelten Bildung von MFA zu überprüfen um deren Beitrag in der speziesspezifischen Toxizität von HFO-1123 einzuschätzen. Unterschiede im Ausmaß der Bildung von MFA könnten ursächlich für die Speziesunterschiede in der Toxizität von HFO-1123 sein. Ergebnisse dieser Untersuchungen sollen als Grundlage für die Risikobewertung von HFO-1123 im Menschen dienen.

Im Rahmen dieser Arbeit, wurde die *in vitro* Biotransformation von HFO-1123 und 1123-CYS in subzellulären Fraktionen von Leber und Niere der Spezies Ratte, Maus, Goettingen[®] Minischwein, WN Kaninchen und Mensch untersucht. Zusätzlich wurde die Zytotoxizität und der Metabolismus von 1123-CYS in Nierenepithelzellen überprüft. Die Bildung von 1123-GSH wurde mittel LC-MS/MS in hepatischen S₉ Fraktionen quantitativ bestimmt und die Entstehung weiterer Metabolite mittels ¹⁹F-NMR analysiert. Weiterhin wurde die Enzymkinetik der β -Lyase vermittelten Spaltung von 1123-CYS in cytosolischen Leberfraktionen bestimmt und fluorhaltige Metabolite dieser Spaltung mittels ¹⁹F-NMR aufgezeichnet.

In Leber S₉ Fraktionen von Ratten, Mäusen und WN Kaninchen wurde eine gesteigerte Bildung von 1123-GSH im Vergleich zu S₉ Fraktionen von Goettingen[®] Minischweinen und Menschen beobachtet. Dies deutet auf eine gesteigerte Glutathion-abhängige Biotransformation in Ratten, Mäusen und WN Kaninchen hin. Zusätzlich zeigten Leber S₉ Fraktionen von WN Kaninchen eine erhöhte Bildung von 1123-GSH in Anwesenheit von Acivicin, einem spezifischen γ -GT Inhibitor. Dies deutet auf eine gesteigerte γ -GT abhängige Spaltung von 1123-GSH in hepatischen S₉ Fraktionen von WN Kaninchen hin. Zusätzlich bestätigten ¹⁹F-NMR Untersuchungen - neben anorganischem Fluorid (F⁻) - 1123-GSH als Hauptmetaboliten der Glutathion-abhängigen Biotransformation von HFO-1123. Die erhöhte Bildung von F⁻ in Leber S₉ Fraktionen von Goettingen[®] Minischweinen und WN Kaninchen in Anwesenheit eines NADPH regenerierenden Systems, deutet weiterhin auf eine gesteigerte CYP-450 vermittelte Biotransformation in diesen Spezies hin. Jedoch ist der Beitrag der CYP-450 vermittelten Biotransformation von HFO-1123 zur speziesspezifischen Toxizität nicht geklärt.

Im Gegensatz zur gesteigerten Bildung von 1123-GSH in Leber S₉ Fraktionen von Ratten, Mäusen und WN Kaninchen (verglichen mit Leber S₉ Fraktionen von Goettingen[®] Minischweinen und Menschen), wurde in enzymkinetischen Untersuchungen eine erhöhte β -Lyase Aktivität gegenüber 1123-CYS in Nierenzytosol von Goettingen[®] Minischweinen im Vergleich zu zytosolischen Fraktionen von Ratten, Mäusen, Menschen und WN Kaninchen beobachtet. Trotz der niedrigeren β -Lyase Aktivität in WN Kaninchen (verglichen mit Goettingen[®] Minischwein), zeigte diese zytosolische Fraktion eine leicht erhöhte Aktivität im Vergleich zu Nierenzytosol von Ratten, Mäusen und Menschen. Im Einklang damit wurde eine erhöhte Bildung von MFA in Nierenzytosol von Goettingen[®] Minischweinen und WN Kaninchen (im Vergleich zu zytosolischen Fraktionen von Menschen und Ratten) mittels ¹⁹F-NMR beobachtet. Interessanterweise wurde ausschließlich im Zytosol von Goettingen[®] Minischweinen und WN Kaninchen die Bildung von drei strukturell nicht charakterisierten MFA-Derivaten nachgewiesen. Unterstützt wird die erhöhte β -Lyase Aktivität in Nierenzytosol von Goettingen[®] Minischweinen durch eine erhöhte Zytotoxizität von 1123-CYS in Nierenepithelzellen von Schweinen (Verglichen mit humanen und Ratten Nierenzellen).

Grundsätzlich bestätigt die erhöhte β -Lyase abhängige Spaltung von 1123-CYS zu MFA in Goettingen[®] Minischweinen und WN Kaninchen die Annahme, dass eine β -Lyase vermittelte Spaltung von 1123-CYS einen wichtigen Beitrag zur Toxizität von HFO-1123 leistet. Jedoch steht dem eine verminderte GST vermittelte Bildung von 1123-GSH in Goettingen[®] Minischwein Leber S₉ Fraktionen im Vergleich zu Ratten, Maus und WN Kaninchen entgegen.

Auf Basis der bisher erhobenen Daten ist der Beitrag der Glutathion-abhängigen und β -Lyase vermittelten Biotransformation zur Toxizität von HFO-1123 nicht abschließend geklärt und lässt eine eindeutige Aussage über eine vermehrte Biotransformation von HFO-1123 zu toxischen Metaboliten in empfindlichen Spezies im Zusammenhang mit der speziesspezifischen Toxizität nicht zu. Diese Unsicherheiten lassen keine Rückschlüsse über das Ausmaß der Biotransformation und Toxizität im Menschen zu. Für die Registrierung von HFO-1123 und seiner zukünftigen Verwendung als Kühlmittel sind weiter *in vitro* und *in vivo* Untersuchungen nötig, um die Sicherheit bei der Verwendung von HFO-1123 für die menschliche Gesundheit zu gewährleisten.

3 Introduction

3.1 A healthy world demands clean cooling – United Nation's Sustainable Development Goals

A cattle farmer in the Midwest of the United States transporting dairy and meat products to the market, a restaurant owner in Saudi Arabia storing perishable seafood, and a patient in central China undergoing hemodialysis due to renal malfunction - they all rely on efficient and functional refrigeration. Food and feed, medicine and vaccines depend on complex cool chains as they are vulnerable to variations in temperature. Without cooling of computer-servers, modern global communication and workflows would be impossible. Productivity and education in offices and schools in hot climatic regions would suffer without space cooling and air-conditioning.

The developed world consumes enormous amounts of energy for cooling and refrigeration. For example, in the United Arabian Emirates between 50 and 75% of the total electricity is used for space-cooling and refrigeration. In the United States more energy is needed for air-conditioning than the whole energy consumption of all African Nations combined (Peters, 2016). Today, developed countries use a tremendous amount of energy for cooling compared to emerging nations. However, this will change in the future. Most developing countries are in hot climate regions of Africa and Asia that are most affected by rising world temperatures. As their population and economic power are rapidly increasing, the need and use of refrigeration and air-conditioning will drastically increase and energy consumption as well as green-house gas emission will skyrocket. Prediction models from the United Nations imply that energy consumption for air-conditioning will increase 33-fold by 2100 (Arent *et al.*, 2015). In the overpopulated future world, with approximately 9 billion humans by 2050, up to three-quarters of manhood will be afflicted by heat and heat correlated health concerns (McGregor *et al.*, 2015). As the world's poorest are most affected by heat-derived health issues and food insecurity, the demand for governmental and personal action to deliver environmental-friendly and affordable cooling is more essential than ever.

Rising world temperatures and overpopulation set enormous challenges for a healthy world and a functional global society. In 2015, the *United Nations General Assembly* adopted the resolution 'Transforming our world: the 2030 agenda for sustainable development' (UN, 2016) which committed the global community to reach 17 Sustainable Development Goals (referred to as global goals), which endeavor to change the world for the better. Universal healthcare and well-being, ending poverty and hunger, increased worldwide education level, gender equality, and sustainable use of energy and resources are a selection of key goals that need to be achieved for a prosperous and healthy world. However, the challenge to reach these goals is tremendous and multifaceted. In the official debate about strategies to accomplish the

global goals, the importance of universal access to green refrigeration and air-conditioning is commonly underrated. According to the “*Clean Cold and Global Goals*” report of the Energy Department of the University of Birmingham (Peters, 2016), providing the world with effective, universal and clean cooling is an elementary step that needs to be taken to reach these 17 goals.

Figure 1 displays a selection of the global goals and how they relate to universal access to clean cooling. Ending world's poverty and hunger, the first and second goal, is a complex challenge that has no single answer. However, cooling plays a vital role in tackling these two issues. Poverty and hunger are directly correlated to food wastage and food insecurity. Worldwide, up to 30% of food is wasted after production within the food chain and a fair bit can be blamed on unavailable or insufficient cooling (Snel *et al.*, 2018). In developing countries, where poverty and hunger are most prevalent, malfunctions in the cold-chain can be accountable for up to 90% of food loss (Peters, 2016). As food insecurity will increase in the future due to drought and changing climate conditions the need for an efficient food supply management, with functional, universal, and affordable cold chains is inevitable for fighting world hunger. Nevertheless, cold chain related food wastage is not limited to the developing world. It is an ongoing problem in the developed world as well. Up to 55% of fruit and vegetable loss can be blamed on insufficient temperature management (Gustavsson *et al.*, 2011). As food wastage due to insufficient cooling or malfunction in temperature management is a worldwide problem, the need for improvements is universal and inalienable for a sustainable future.

**Universal and clean cooling technologies
contribute to the Sustainable Development Goals, because they:**



Figure 1 United Nations *Sustainable Development Goals* with regard to universal, cost-efficient clean refrigeration according to the *Clean Cold and the Global Goals* report of the Birmingham Energy Institute (2016). Logos of *Sustainable Developmental Goals* are courtesy of the United Nations and their informational use in non-commercial and non-profit publications does not require prior permission from the United Nations (UN, 2020).

Another emerging issue that is focused by the UN's global goals is taking action against man-made climate change. In the public opinion the human contribution to climate change is mainly caused by shipping, aviation, individual transportation (cars and buses) and energy-delivering industry. Refrigeration is often forgotten in debates about climate change, despite it being a main perpetrator in emission of greenhouse gases and energy consumption. Worldwide the cooling industry is accountable for over 10% of the global green-house gas exhaust, emitting more than shipping and aviation combined (Dong *et al.*, 2021). Leakage of refrigerants with a high global warming potential is accountable for around a quarter of this exhaust, the other three quarters are caused by the energy needed for cooling, that is generating CO₂ (Maidment, 2014). Refrigeration and effective cooling are emerging issues of today's world and a major challenge for a sustainable and healthy planet that urgently needs to be solved.

Knowledge about the history of refrigeration, with its major landmarks and arising climate issues, is inalienable to understand the challenges for the industry.

3.2 Freon® - The beginning of modern refrigeration and its unforeseen climate hazards

The history of modern refrigeration started with Thomas Midgley. In the 1920s, 1930s and 1940s, he was recognized as one of the most successful chemists of all time. He held more than 150 patents, received numerous awards, including the prestigious *Priestly Medal* of the American Chemical Society (ACS) and was assigned president of the ACS in 1944. However, two of his greatest inventions, tetraethyl lead (TEL) and dichlorodifluoromethane inverted his posthumous reputation:

“Thomas Midgley had more impact on the atmosphere than any other single organism in earth history” – J.R. McNeill (2000)

“The one-man environmental disaster” – New Scientist (2017)

“Thomas Midgley, the most harmful inventor of history” – BBVA-OpenMind (2021)

TEL revolutionized the automobile industry in the 1920th. It eliminated engine knocking, thus boosting engine power, automobile speed and fuel economy. Adding TEL to gasoline rapidly became a multimillion-dollar business. The great risk for public health originated from lead and lead derived substances was well known at the beginning of the 20th century, but greed for profits overruled health concerns. Profiting companies tried to keep medial interest and coverage of TEL related intoxications low. Thankfully, in 1986 the use of TEL as a gasoline additive was banned, due to emerging health hazards, more than half a century after its introduction. In 1992, it was estimated that human lead exposure was up to 625-times greater as compared to pre-industrial times (Flegal and Smith, 1992) and TEL was accountable for up to 90% of lead in the earth’s atmosphere (Kitman, 2000).

Spurred by the profitable invention of leaded gasoline, Midgley focused on solving the problem of refrigeration. By his time refrigeration posed tremendous safety hazards, due to the flammability and toxicity of substances, like ammonia, methyl chloride or sulfur dioxide used for refrigeration. Numerous incidents, as the death of more than 100 people in a single hospital in 1929 due to a refrigerant leak, lead to the public opinion of banning these hazardous chemicals from the refrigerant market (McGrayne, 2001). However, until the 1930s no ‘safe’ refrigerant alternative was available. In 1931 Midgley’s working group identified dichlorodifluoromethane as an inert, non-flammable, non-acute toxic gas with ideal physicochemical characteristics (e.g. specific heat, high insulating value and high vapor pressure) for refrigeration.

The ‘invention’ of dichlorodifluoromethane was the starting step of “modern refrigeration”. Dichlorodifluoromethane and other chlorofluorocarbons (CFCs, see Figure 2 for chemical structures) were trademarked as Freon™ by DuPont and rapidly used in global scale. Applications of CFCs were not limited to refrigeration, but widely distributed as aerosol spray propellants, solvents, and degreasing agents. During its peak (early 1970s) CFC production was a thriving industry, producing around 5 million tons per year with a revenue of 500 million dollars (ACSNCL, 2017).

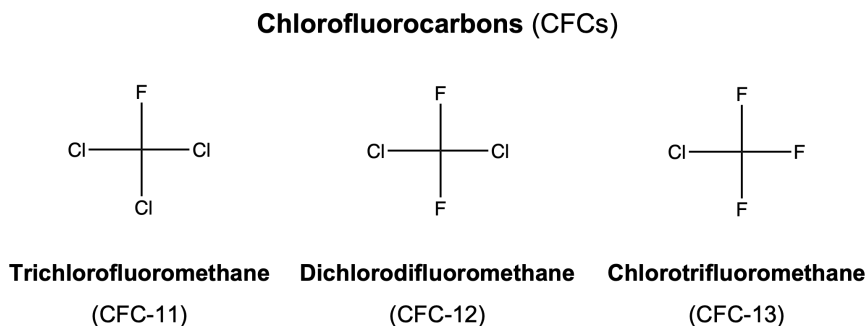


Figure 2 Chemical structures of exemplary CFCs

Considering the risk of CFCs for human health, most members of this group show acute but low long-term toxicity comparable with the general toxicity of solvents (see Casarett and Doll's toxicology (2013) for detailed summary). Pulmonary and to a lesser extent dermal uptake are the most common routes of CFCs exposure. Like other small and lipophilic molecules, they can induce central nervous system depression leading to narcosis and death after exposure to high concentrations. Additionally, cardiac sensitization to epinephrine after exposure to high CFC concentrations were noted (Reinhardt *et al.*, 1971). However, the mechanism of toxicity for narcosis is not completely elucidated, but it is postulated that alterations in lipid membrane fluidity lead to changes in neural messaging and subsequent central nervous toxicity (Wurzel, 2005). However, if acute exposure is survived, usually no chronic or long-term toxicity, as carcinogenicity or teratogenicity, is observed (Dekant, 1996; Wurzel, 2005). For example CFC-11 and CFC-12 are not cancerogenic or genotoxic *in vitro* and *in vivo*, but possess cardiotoxicity in mammals (NRC, 2000). The low long-term and chronic toxicity can be explained due to minimal biotransformation and quantitative exhalation of CFCs (Cox *et al.*, 1972; Mergner *et al.*, 1975).

CFCs revolutionized modern civilization as no other chemicals before them, and for over 40 years they were thought to be one of the greatest inventions in history. But this appraisal changed dramatically in the mid 1970th. Retrospective, the widespread use of CFCs was one of the greatest man-made hazards to world's climate. To get a deeper understanding about climate hazards originating from CFCs, detailed knowledge about earth's atmospheric properties is necessary.

Nitrogen (~78%), oxygen (~21%), argon (~0.9%) and carbon dioxide (~0.04%) are the most prevalent gases in the earth's atmosphere (Egger, 2003). However, nitrogen and oxygen form the majority of atmospheric gases and are inevitable for life itself. They do not have a great influence on earth's climate. Other gaseous components as carbon dioxide, ozone, methane, and sulfur dioxide are present only at minor concentrations but are far more accountable for the global climate. Especially, stratospheric ozone often referred to as the 'ozone-layer' is of remarkable importance. It inhibits harmful UV-light penetrating into the troposphere and the earth's surface, thus protecting humans, animals, and plants. It is of inevitable importance for the stability of the whole stratosphere and thus for the earth's climate (Rowland, 2006). UV-B light ($\lambda = 280\text{-}315\text{ nm}$), the main reason for sunburn and sun-exposure related basal-cell and squamous cell carcinomas (ACS, 2019), is to a great extent absorbed by stratospheric ozone. The percentage of UV-B light absorbed is dependent on the concentration of ozone being present (the more ozone in the stratosphere the more UV-B light is absorbed). However, stratospheric ozone is vulnerable. The ozone-layer represent approximately $4 \times 10^{-6}\%$ of the complete atmosphere but is accountable for absorbing most of the UV-B light emitted by the sun. To envision the low amount of ozone in more vivid words: If the ozone-layer would be completely compressed to one layer it would have a thickness of only 3 millimeters, compared to 8 kilometers of the whole atmosphere compressed (Newman, 2018). Dobson units are commonly used to describe the density of the stratospheric ozone-layer. One Dobson unit is defined as 'the number of molecules of ozone that would be required to create a layer of pure ozone 0.01 millimeters thick at a temperature of 0 degrees Celsius and a pressure of 1 atmosphere' (Newman, 2018). In general, the average ozone concentration in the stratosphere is approximately 300 Dobson Units. The infamous 'ozone-holes' do not describe areas that completely lack ozone, but where concentrations are only one third of the average value (roughly 100 Dobson units). Due to its low concentration, stratospheric ozone stands in a fragile balance of creation and destruction. Ozone is generally formed via UV-C light ($\lambda = 160\text{-}240\text{ nm}$) mediated dissociation of molecular oxygen (O_2) to two oxygen atoms that subsequently add to two separate molecular oxygen molecules. Degradation of atmospheric ozone is caused by radicals of natural and man-made origin. NO_x - and HO_x -radicals are of natural occurrence, while Cl_x -radicals are man-made (Braslavsky and Rubin, 2011). Cl_x radicals can be formed by a variety of chemicals, but CFCs are responsible for the majority of them.

Molina and Rowland (1974) were among the first to predict the ozone depleting potential of CFCs and the underlying chemical mechanism. Figure 3 illustrates the influence of CFCs on the ozone layer and associated consequences for humans and the earth's atmosphere. After CFCs are released into the troposphere (0-15 km altitude), they are relatively unreactive. Following their migration into stratospheric altitudes of 20-40 km their reactivity increases. UV-

radiation mediated cleavage of CFCs results in the formation of chlorine radicals. Chlorine radicals can break down ozone molecules resulting in the formation of molecular oxygen and chlorine monoxide radicals. Those chlorine monoxide radicals can be reactivated to chlorine radicals, by reaction with elementary oxygen and subsequently restart the ozone depletion cycle. As chlorine radicals are readily reactivated, one single CFC-molecule can destroy up to 200.000 ozone molecules (Biddle, 1998). Also, CFCs have a long atmospheric residence time, persisting in the atmosphere for of up to 625 years (Hodnebrog *et al.*, 2013). With increasing amounts of CFCs emitted and thus increased concentrations of chlorine radicals formed in the stratosphere, ozone is rapidly depleted and the ozone layer becomes less dense and more penetrable for UV-B light leading to an increased risk for human health, e.g., increasing incidence for skin cancer and cataract formation (Longstreth, 1988; Taylor *et al.*, 1988). Shortly after the detection of the *ozone depletion potential* (ODP) associated with CFCs, it was recognized that they additionally contribute directly to global warming. As they are potent absorbers of infrared (IR) light, they can trap and subsequently release heat in the atmosphere, leading to rising world temperatures (Ramanathan, 1975).

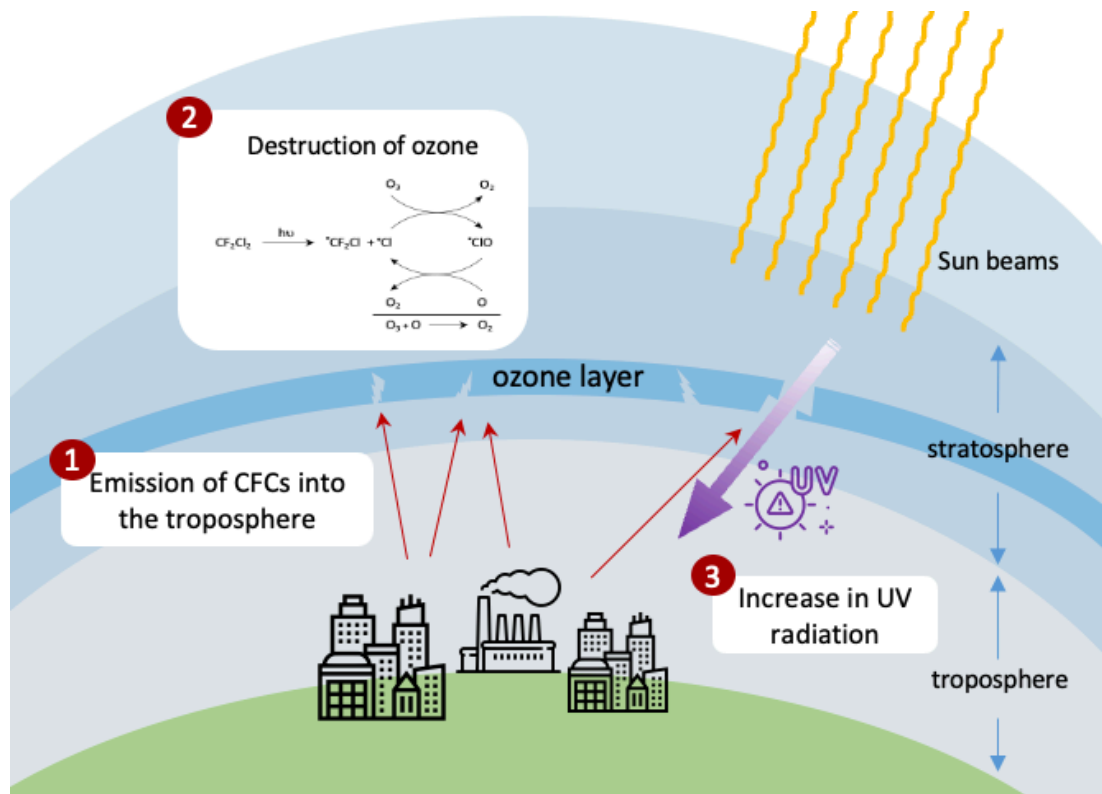


Figure 3 Negative influence of CFCs on stratospheric ozone and related health risks. After emission of CFCs (1) and migration into the stratosphere, they are photolytically cleaved by UV-B light leading to chlorine (Cl) radicals (2). Cl radicals degrade ozone molecules leading to decreased density of the stratospheric ozone layer. Due to the lower density of stratospheric ozone, increased amounts of UV-light can penetrate the troposphere and lead to human and animal health hazards (3).

Despite the enormous threats for health and the environment originating from the excessive use of CFCs, the public and governmental interest to ban CFCs usage was relatively low in the beginning. Governmental and medial interest arose in 1984, more than a decade after the first reports about CFC related hazards, as the first 'ozone hole' over Antarctica with a direct linkage to CFCs emission was discovered (Farman *et al.*, 1985). In an unprecedented effort of the United Nations the Montreal Protocol, an international treaty charted to protect stratospheric ozone by banning the use and production of CFCs, was ratified in 1989 (UNEP, 2009). In fact, this treaty was, first in history, accepted by all UN members, emphasizing the urgency and relevance to take action against CFC use and production.

Thanks to the Montreal Protocol, leading to the phase out of CFCs, unconceivable and unchangeable consequences for world's climate were prevented. In 2009, Newman and colleagues predicted the consequences for world's climate until the year 2065, if CFCs were not phased out (Newman *et al.*, 2009). According to their computational models (Figure 4), by 2065 approximately two-third of the stratospheric ozone would be depleted (compared to the 1970s) leading to an increase in UV-radiation penetrating the earth's surface of more than 500%. Such an increase in UV-radiation would dramatically increase the risk for skin cancer and other unpredictable harmful effects on plants, animals, and humans. In mid-latitude countries such as Portugal or Greece, the UV Index would have increased dramatically, leading to sunburn within minutes being exposed to sunlight. Increased UV-radiation would possibly contribute to food insecurity, as crop growth would be affected negatively, leading to a lower production of crop-based food. Especially in the equatorial regions of Africa and Asia, where cereal-based diets are most prevalent, reduced crop production would have aggravated poverty and hunger.

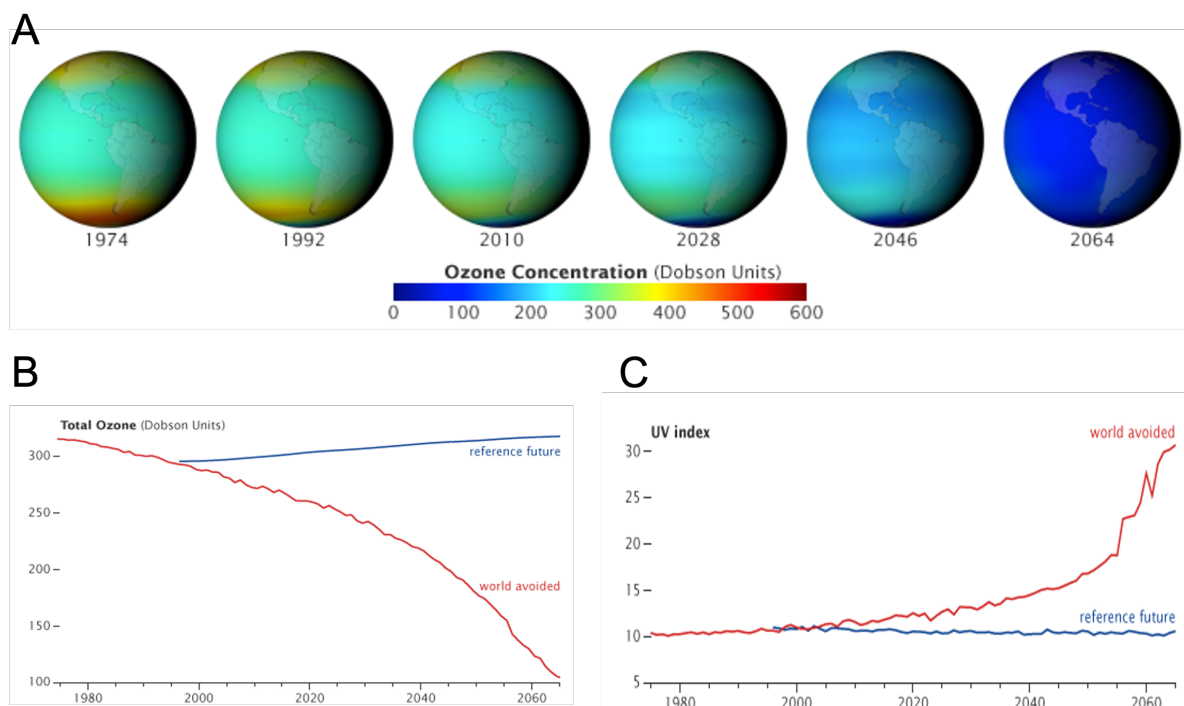


Figure 4 Computational model of global stratospheric ozone depletion from 1974 until 2064 (A and B) and changes in global in UV-index (C) if CFCs were not phased out. Figure modified from Carlowicz *et al.* (2009). Content of this figure is courtesy of NASA, but not subject to copyright in non-profit publications as stated in NASA's Media Usage Guidelines (NASA, 2022).

Thanks to the fundamental research of Rowland and Molina and other scientists as well as the rapid action of global policymakers and industry representatives, the world avoided a climatic collapse of inconceivable magnitude.

3.3 Hydrochlorofluorocarbons (HCFCs) and hydrofluorocarbons (HFCs) – an inadequate but necessary alternative for CFCs

The global phase out of CFCs set the need for safe and climate friendly alternatives. Hydrochlorofluorocarbons (HCFCs) and hydrofluorocarbons (HFCs) (Figure 5) were introduced as CFC replacement substances, as they exhibit similar beneficial thermodynamic and physiochemical properties (Fisher *et al.*, 1990). Additionally, they degrade rapidly in the troposphere and do not reach the stratosphere to the same extent as CFCs, thus having minimal (HCFCs) to zero (HFCs) ozone depleting potential. Their tropospheric lability relies on the carbon-hydrogen (C-H) bond(s), making them susceptible for thermal and chemical degradation. Despite the significantly lower ODP, they contribute excessively to global warming. HCFCs and HFCs have an up to 10.000 times increased GWP potential compared to carbon dioxide (Myhre *et al.*, 2013). The GWP of HCFCs and HFCs depends on the degree of fluorine substitution, increasing with the number of fluorine atoms present in the molecule (Hodnebrog *et al.*, 2013). Despite their contribution to global warming, they were accepted as

interim CFC substitutes and are still used in a broad range of industrial and domestic applications.

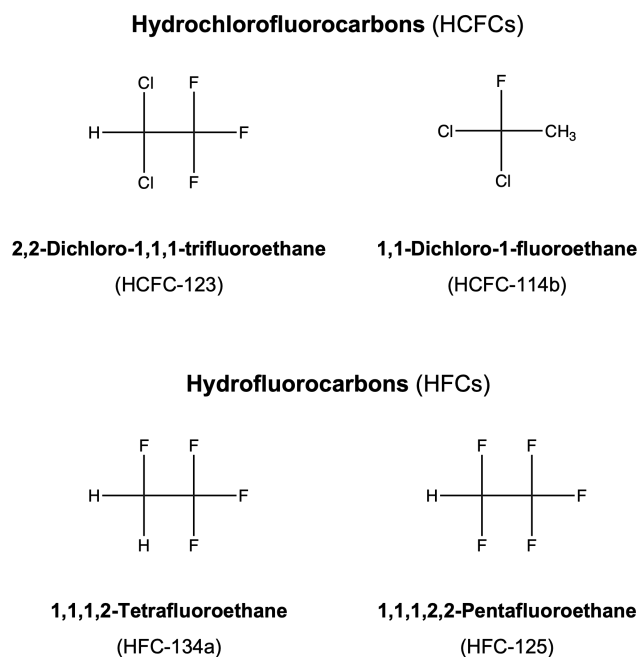


Figure 5 Chemical structures of exemplary HCFCs and HFCs

Their decreased chemical inertness is accompanied by increased biotransformation, leading to the formation of toxic metabolites. Several members of the HCFCs (e.g., 2,2-dichloro-1,1,1-trifluoroethane [HCFC-123], 1,1-dichloro-1-fluoroethane [HCFC-114b]) and HFCs (e.g., 1,1,1,2-tetrafluoroethane [HFC-134a], 1,1,1,2,2-pentafluoroethane [HFC-125]) are known to be hepatotoxic, cardiotoxic, toxic to the central nervous system, or carcinogenic in rodents and mammals at high room concentrations (Toxicity reviewed by Anders (1991), Dekant (1996) and Monographs of the European Centre of Ecotoxicology and Toxicology of Chemicals (ECETOC)). Despite the general low potential for toxicity, concerns for public health and safety remain as chronic and acute poisoning after HCFC and HFC exposure were reported in humans (Hoet *et al.*, 1997; Takebayashi *et al.*, 1998; Boucher *et al.*, 2003).

The toxicity of HFCs and HCFCs is generally based on oxidative metabolism mediated by Cytochrome P-450 enzymes (CYP-450), leading to reactive and stable metabolites which interfere with tissue-homeostasis and may lead to toxicity, such as hepatotoxicity. However, as their biological reactivity is increased compared to the CFCs, the biotransformation of HFCs and HCFCs is more complex. Oxidation and reduction by CYP-450 as well as a combination of CYP-450 reduction and glutathione (GSH) dependent biotransformation have been identified *in vitro* and *in vivo* with several HCFCs and HFCs. Figure 6 provides several metabolic pathways of HCFC-123 exemplary for other HCFCs, as it is one of the best studied representatives of this group.

HCFC-123 is oxidized by CYP-450 *in vitro* (Urban *et al.*, 1994) and *in vivo* (Urban and Dekant, 1994; Tanaka *et al.*, 1998) in rodents and humans. Multiple studies suggest CYP-450 2E1 to be the predominant isoform involved in the oxidative metabolism of HCFC-1123 in particular and in general for the majority of HCFCs and HFCs as well as other halogenated alkanes (e.g. halothane) (Godin *et al.*, 1993; Loizou *et al.*, 1994; Zanovello *et al.*, 2001). The CYP-450 mediated oxidation of HCFC-123 leads to the formation of an intermediate halohydrin. Hydrolysis of the intermediate forms the acyl halide trifluoroacetyl chloride (TFAC). On the one side, TFAC is an acetylating agent that can bind covalently via lysine residues to proteins, which is associated with immune-derived liver toxicity (Harris *et al.*, 1991; Lind *et al.*, 1995). On the other side, hydrolysis of TFAC leads to the formation of trifluoroacetic acid (TFA), which was identified as an urinary metabolite in rats and humans (Urban and Dekant, 1994; Tanaka *et al.*, 1998). A trifluoroacetylating intermediate is also the major metabolite of halothane and accountable for halothane induced idiosyncratic hepatitis (NIDDK, 2012) and may be associated with hepatotoxicity of HCFC-123 (Hoet *et al.*, 2001).

A second biotransformation pathways, that occurs both *in vitro* and *in vivo* involves the CYP-450 dependent dehydrohalogenation (reduction) of HCFC-1123, leading to the formation of the olefin 1,1-dichloro-2,2-difluoroethene (DCDFE). DCDFE is known to be nephro- and hepatotoxic (Commandeur *et al.*, 1987). Firstly, this olefin may undergo intramolecular chlorine migration, leading to the formation of chlorodifluoroacetic acid *in vitro*. Secondly, it is susceptible for glutathione (GSH) dependent biotransformation. As this metabolic pathway is relevant to a variety of pharmaceuticals and industrial xenobiotics, it is well characterised and also known as the 'mercapturic acid pathway' (see Hanna and Anders (2019) for detailed review and chapter 3.5). Biotransformation via this pathway leads to the bioactivation of several fluorinate and chlorinated olefins that are known as nephrotoxic agents. The addition of GSH leads to the formation of a GSH-conjugate. Cleavage of the GSH-conjugate of HCFC-123 leads to the formation of the corresponding cysteine S-conjugate S-(1,1-dichloro-2,2-difluoroethyl)-L-cysteine. Cysteine S-conjugates in general can be bioactivated by β -lyases or detoxified by *N*-acetyltransferases, leading to the excretion of a *N*-acetylcysteine derivative (known as mercapturic acid) into urine. Biotransformation of HCFC-123 via the mercapturic acid pathway is confirmed by the detection of *N*-acetyl-S-(1,1-dichloro-2,2-difluoroethyl)-L-cysteine, the mercapturic acid of HCFC-123 in urine of rats (Urban and Dekant, 1994). In the interest of completeness, a reductive metabolism of HCFC-123 is described *in vitro* under anaerobic conditions, leading to the formation of 1-chloro-2,2,2-trifluoroethane (CTFE) and 1-chloro-2,2-difluoroethene (Godin *et al.*, 1993). CTFE is a known testicular toxin, leading to Leydig cell adenomas in rats (Cook *et al.*, 1992). However, the relevance of the reductive metabolism and derived metabolites of HCFC-123 in humans and rodents is yet unknown.

In conclusion, HCFC-123 shows a multitude of biotransformation pathways, but the formation of TFA as the major metabolite of HCFC-123 is in general accountable for hepatotoxicity. Compared to their predecessors, the CFCs, HCFCs and HFCs show an increased biotransformation that is accountable for their elevated toxicity (compared to CFCs).

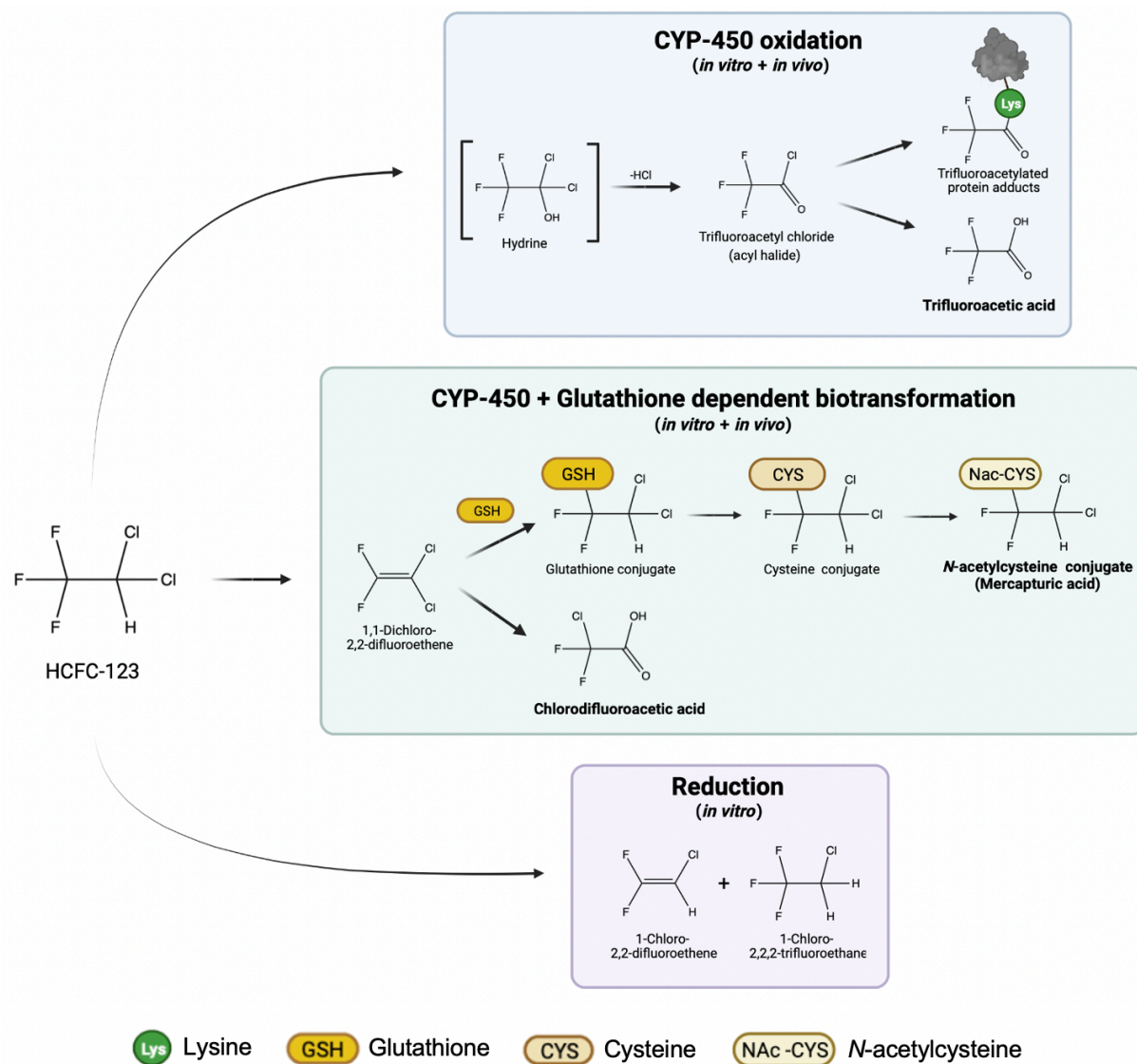


Figure 6 *In vitro* and *in vivo* biotransformation of HCFC-123. CYP-450 2E1 mediated oxidation of HCFC-123 leads to the formation of an intermediate hydrin, that is subsequently oxidized to trifluoroacetyl chloride (TFAC). TFAC may acetylate organ tissue via lysine residues or form trifluoroacetic acid, which is associated with hepatitis. Furthermore, CYP-450 dependent oxidation may form an olefin (1,1-dichloro-2,2-difluoroethene) which is susceptible for glutathione mediated biotransformation leading to the excretion of a mercapturic acid (*N*-acetylcysteine conjugate) into the urine. In addition, reductive metabolism under anaerobic conditions was also detected *in vitro*, but not *in vivo*. Figure created with BioRender.com.

Due to their increased global warming potential and their inarguable risks for public health, the production and application of HCFCs and HFCs will be phased out worldwide until 2047. This decision was ratified by the majority of the United Nations under the Kigali Amendment (ratified in 2016) to the Montreal Protocol (Heath, 2017). Due to the expiring use of HCFCs and HFCs,

the demand for novel refrigerants that are climate-friendly and safe is high and the search for such compounds is on-going.

3.4 Hydrofluoroolefins (HFOs) — Green refrigerants of the 21st century with increased potential for toxicity

One class of refrigerants, that are and will be used to replace HCFCs and HFCs, are hydrofluoroolefins (HFOs). Compared to their predecessors (CFCs, HCFCs and HFCs), HFOs exhibit zero *ozone depletion potential* (ODP), a significantly reduced global warming potential (see Table 1 for a comparison of climatic properties of CFCs, HCFC, HFCs and HFOs) and similar beneficial thermal properties, which enable their use in a variety of industrial applications (e.g. refrigeration, aerosols, drycleaners).

Table 1 Classes of refrigerants and their climatic properties

Class	Compound name	ODP relative to CFC-11	GWP for 100 years relative to CO ₂	Atmospheric lifetime	Literature
1. CFCs	Chlorotrifluoromethane (CFC-13)	1.0	13,893	640 years	(Dincer, 2018) (Hodnebrog <i>et al.</i> , 2013)
2. HCFCs	1-Chloro-1,1-difluoroethane (HCFC-142a)	0.01-0.07	1,982	17.2 years	(Dincer, 2018) (Hodnebrog <i>et al.</i> , 2013)
3. HFCs	Difluoromethane (HFC-32)	0	677	5.2 years	(Hodnebrog <i>et al.</i> , 2013) (Li <i>et al.</i> , 2014)
4. HFOs	1,1,2-trifluoroethene (HFO-1123)	0	0.3	1.6 days	(Hodnebrog <i>et al.</i> , 2013) (Mondal <i>et al.</i> , 2020)
	1,1,1,3-tetrafluoropropene (HFO-1234ze)	0	6	18 days	(Antiñolo <i>et al.</i> , 2017)

The missing ODP originates from the absence of chlorine atoms and the significantly reduced GWP relies on the carbon-carbon (C-C) double bond, which leads to a limited atmospheric lifetime of several days. However, these climate-beneficial properties are accompanied by an increased biological reactivity, exemplified by increased toxicity of several HFOs (compared to HCFCs, HFC and CFCs). C-C double bonds are accountable for an increased extent of biotransformation, which may increase the risk for toxicity through generation of reactive and stable metabolites. Haloalkenes (general term for halogenated alkenes including HFOs) can be susceptible for nucleophilic reactions with e.g. the sulfhydryl moiety of cysteine (CYS) or

glutathione (GSH), as well as for CYP-450 mediated oxidation. CYP-450 mediated oxidation as well as GSH conjugation (mercapturic acid pathway), alone or combined, are common starting steps of metabolic pathways in the biotransformation of halogenated xenobiotics and thus contribute to the metabolism of HCFCs, HFCs (see 2.3 for metabolism of HCFCs/HFCs) and HFOs. Whether CYP-450 or GSH mediated, biotransformation in general is an endogenous defense mechanism against potential toxic xenobiotics with the objective to eliminate the compound from the body. However, biotransformation can contribute to an increase in toxicity, due to the formation of metabolites that possess enhanced toxicity compared to their parent substance, representing bioactivation of the xenobiotic.

Several haloalkenes, such as vinyl chloride (CYP-450 oxidation dependent bioactivation), trichloroethene (TRI), tetrafluoroethene (TFE), hexafluoropropylene (HFP) (GSH dependent bioactivation) are metabolized extensively, leading to several metabolites responsible for *in vitro* and *in vivo* toxicity. TRI, TFE and HFP are renal and hepatic toxicants associated with liver and kidney carcinogenesis in rodents and are classified as potential carcinogen in humans (EPA, 2011; IARC, 2016; ECHA, 2022a,b). TRI was used in a variety of applications, e.g. as a medical anesthetic for surgery, a dry-cleaning agent, an additive in refrigerant systems and as a metal degreaser. A complex biotransformation resulting in a multitude of intermediates and stable metabolites is responsible for the mutagenic, carcinogenic, as well as renal and hepatotoxic potential of TRI (EPA, 2011). In general, biotransformation of TRI occurs through two pathways. TRI is metabolized by CYP-450 and by GSH dependent biotransformation, resulting in several toxic compounds (see Appendix B, Figure B.1 for detailed biotransformation of TRI). Toxic metabolites derived from CYP-450 mediated biotransformation include chloral hydrate, trichloroacetic acid and dichloroacetic acid, and these are associated with TRI mediated liver injury. GSH dependent metabolism of TRI via the mercapturic acid pathways leads to *S*-(1,2-dichlorovinyl)-*L*-glutathione (DCVG), *S*-(1,2-dichlorovinyl)-*L*-cysteine (DCVC) and DCVC sulfoxides as key metabolites linked to nephrotoxicity and renal carcinogenesis (Lash *et al.*, 2000). While CYP-450 dependent biotransformation of TRI is much more pronounced than GST mediated metabolism, GST derived metabolites (DCVC/DCVC sulfoxides) contributed for the most part to the overall toxicity of TRI (Dekant, 2003b).

Despite the severe toxicity of several haloalkenes, HFOs in currently in use possess a general low potential for toxicity. 2,3,3,3-tetrafluoropropene (HFO-1234yf) and trans-1,3,3,3-tetrafluoropropene (HFO-1234ze) are examples of HFOs that are currently used for mobile and space refrigeration. HFO-1234yf has an atmospheric lifetime of 11 days and atmospheric breakdown occurs via reaction of hydroxyl radicals with the double bond (Hodnebrog *et al.*, 2013). No acute toxicity was observed in rats (up to 405,800 ppm) and rabbits (up to 100,000 ppm) (Schmidt *et al.*, 2012; Tveit *et al.*, 2013). Also, no cardiac sensitization after exposure of

up to 120,000 ppm and a challenge dose of epinephrine was noted in beagle dogs. Furthermore, repeated exposure of rats revealed a NOEAL of 50,000 ppm (Tveit *et al.*, 2013). In contrast, NZW Rabbits showed mortality after repeated inhalation exposure of 5500 ppm. Based on necropsy findings, NOEALs were established as 1000 ppm for females and 500 ppm for males, respectively (Rusch, 2018). However, the NOAEL (symptomatic and histopathologic) in minipigs exposed up to 28 days to HFO-1234yf was 10,000 ppm (Rusch, 2018), indicating low toxicity. Based on these findings, the maximum permitted work place exposure level for HFO-1234yf is 500 ppm as an 8h time weighted average (TWA) (WEEL, 2009).

HFO-1234ze (trans-1,3,3,3-tetrafluoropropene) exhibits an atmospheric lifetime of 10 days (Hodnebrog *et al.*, 2013). Practically, no acute toxicity was observed in rats (NOAEL of 207,000 ppm) (Rusch *et al.*, 2013). Repeated dose inhalation exposure in NZW Rabbits revealed histological changes in the heart (cardiac muscle vacuolation and mononuclear cell infiltrations) and the liver (inflammation and vacuolation) at 20,000 ppm and above, indicating the heart and liver as target organs of intoxication (Rusch *et al.*, 2013). Based on these findings, a workplace exposure level for HFO-1234ze of 800 ppm was established as an 8h TWA (WEEL, 2012).

In general biotransformation of HFO-1234yf and HFO-1234ze follow the two major pathways (CYP-450 mediated oxidation and GSH dependent conjugation) already described for HCFCs, HFCs and haloalkenes. Figure 7 summarizes the *in vitro* and *in vivo* biotransformation of HFO-1234ze. CYP-450 dependent biotransformation leads to the formation of an intermediate epoxide which can be either conjugated with GSH and eliminated into urine or oxidized to 3,3,3-trichlorolactic acid. Direct GSH addition to HFO-1234ze, mediated by glutathione S-transferases, leads to the formation of the corresponding GSH S-conjugate, which is subsequently cleaved to its cysteine S-conjugate (1234ze-CYS). 1234ze-CYS can be cleaved by cysteine S-conjugate transaminases, *N*-acetyltransferases or cysteine S-conjugate β -lyases, leading to the urinary metabolites 1234ze-mercaptolactic acid, 1234ze-CYS-NAc and 3,3,3-trifluoropropionic acid, respectively.

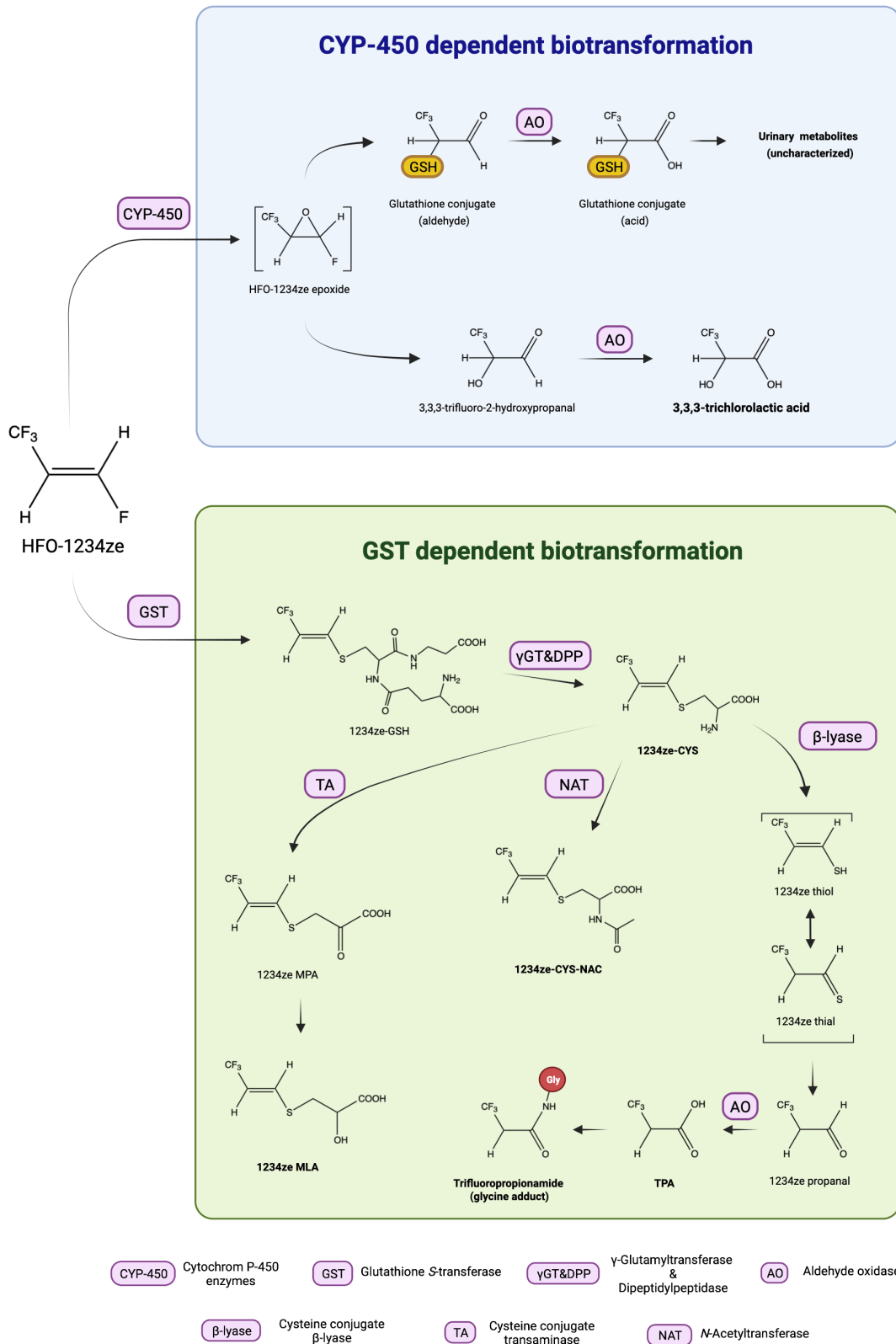


Figure 7 CYP-450 and GST dependent biotransformation of HFO-1234ze in rodents. 1234ze-GSH – *trans*-S-(3,3,3-trifluoropropenyl)-L-glutathione; 1234ze-CYS – *trans*-S-(3,3,3-trifluoropropenyl)-L-cysteine; 1234ze MPA – *trans*-S-(3,3,3-trifluoropropenyl)-L-mercaptopyruvic acid; 1234ze MLA – *trans*-S-(3,3,3-trifluoropropenyl)-L-mercaptolactic acid; 1234ze-CYS-NAc – *trans*-N-acetyl-S-(3,3,3-trifluoropropenyl)-L-cysteine; TPA – 3,3,3-trifluoropropionic acid. Urinary metabolites are marked in bold. Figure adapted from Schuster *et al.* (2009). Figure created with BioRender.com.

Despite the anticipated low potential for toxicity of HFO-1234yf and HFO-1234ze, species-differences in toxicity are prevalent and hamper the evaluation of health risks associated with new HFOs. As the mercapturic acid pathway play an important role in bioactivation of haloalkanes and haloalkenes, a more detailed discussion of reactions and enzymes involved is outlined in the following.

3.5 The Mercapturic Acid Pathway – A common pathway in the bioactivation of haloalkenes

The mercapturic acid pathway (MAP) plays a vital role in the detoxification and bioactivation of xenobiotics. Especially, in the biotransformation of halogenated alkanes (HCFCs) and alkenes (TRI, TFE, HFP, HFOs) the MAP is of great importance. Figure 8 gives a comprehensive overview of possible metabolic fates of substrates processed via this pathway.

This pathway is initiated by the direct coupling of a MAP substrate (e.g. haloalkene) with GSH. The coupling of xeno- and endobiotics with GSH is usually catalyzed by glutathione S-transferases (GSTs; EC 2.5.1.18), which can be divided in three superfamilies based on their cellular location (cytosolic GSTs, microsomal membrane-associated proteins in eicosanoid and glutathione metabolism and mitochondrial Kappa-class GSTs) (Hanna and Anders, 2019). GST are prevalent in most mammalian tissues, with an increased content being present in the liver (greater than 3-10% of entire soluble protein present). Both cytosolic and microsomal fractions possess GST activity towards haloalkenes. However, the activity of the respective fractions towards GSH conjugations depends on structural properties of the haloalkene (Cooper and Hanigan, 2010). In general, three mechanisms of GST-catalyzed conjugation of GSH and haloalkenes are known. Addition of GSH to the double bond occurs with tetrafluoroethylene and an addition-elimination reaction is observed with trichloroethylene (See Appendix B, Figure B.1). Also, the reaction of GSH with a reactive epoxide moiety (generated by CYP-450 mediated oxidation) was observed with several haloalkenes (e.g. HFO-1234ze, Figure 7).

Breakdown of GSH conjugates via the MAP is initiated by the enzymatic cleavage of the γ -glutamyl bond, mediated by γ -glutamyltransferases (γ -GT, EC 2.3.2.2) leading to a cysteinylglycine S-conjugate. γ -GT is predominantly expressed on the surface of the proximal tubule of the kidney, but their appearance is not limited to renal tissue. Glands and ducts of several organs (e.g. testes, liver, prostate, sweat glands) also possess γ -GT activity. The γ -GT mediated breakdown of GSH conjugates can be inhibited by several glutamine analogues as acivicin or L-azaserine (Taniguchi and Ikeda, 1998). The product resulting from γ -GT mediated breakdown – the corresponding cysteinylglycine S-conjugate – is a potential target of aminopeptidase N (APN, EC 3.4.11.2)) or cysteinylglycine dipeptidase (DPP, EC 3.4.13.19)

cleavage. Like γ -GT, APN and DPP are to a great extent located in renal proximal tubular epithelial cells (Taniguchi, 2012), but also appear in the liver and other organs. The cleavage of the cysteinylglycine S-conjugate may occur intra- or extracellular with APN and DPP activity being present in microsomal as well as in cytosolic fractions, and in the brush border membrane, respectively (Hanna and Anders, 2019). However, activity of APN and DPP in tissue and subcellular fractions differs significantly between mammalian species. This may lead to a difference in the extent of cleavage of the cysteinylglycine S-conjugate between species. Usually, APN and DPP attack the N-terminal amino acid of the cysteinylglycine conjugate, leading to the formation of a cysteine S-conjugate.

Cysteine S-conjugates play a decisive role in the detoxification and bioactivation of glutathione adducts via the mercapturic acid pathway. They can either be processed by N-acetyltransferases (NAT, EC 2.3.1.80) to N-acetyl derivatives (mercapturic acids) which are usually excreted into the urine, or, depending on structure, bioactivated by cysteine S-conjugate β -lyases (β -lyase, EC 4.4.1.13) to reactive metabolites.

N-acetylation of cysteine S-conjugates derived from haloalkenes via NAT is usually a detoxification mechanism. One reason is that N-acetyl-S-cysteine (NAc-CYS) conjugates are more polar than their precursors and are substrate to organic acid transporters, leading to elimination into urine. A second reason is that NAc-CYS conjugates are not accessible for β -lyase cleavage, which does not lead to the formation of reactive and potential toxic breakdown products (in contrast to cysteine S-conjugates). However, NAT derived metabolism of cysteine S-conjugates does not solely lead to a detoxification. Several mercapturic acids derived from haloalkenes can be metabolized to sulfoxides, which are associated with renal and hepatic toxicity (Werner *et al.*, 1996; Lash *et al.*, 2000). NAT activity is present in the kidney and liver, with increased activity in renal tissue (Ozaki *et al.*, 1998). Within the kidney NAT are located in the proximal tubules on the cytosolic surface of the endoplasmic reticulum (Okajima *et al.*, 1984). Activity of NAT was observed with several cysteine S-conjugates derived from haloalkenes, indicating an NAT mediated metabolism of HFO-1123.

In addition to detoxification via NAT, bioactivation of cysteine S-conjugates by β -lyases may occur. β -Lyases are pyridoxal 5-phosphate dependent enzymes, that are involved in endogenous in amino acid metabolism. To perform at maximal activity, β -lyases need the presence of α -aminoketo acids (e.g., α -Keto- γ -methiolbutyrate) (Cooper, 1998). β -lyase activity is present in several tissues (e.g., liver, kidney) from various species (rat, human, etc.), with particularly high activity in the kidney (Cooper *et al.*, 2011). Despite endogenous compounds (e.g., leukotrienes, catecholamines, estrogens), multiple pharmaceuticals (e.g., cisplatin, methazolamide) are metabolized and may also be bioactivated by β -lyase (Kishida *et al.*, 1990; Monks and Lau, 1994; Montine *et al.*, 2000; Townsend *et al.*, 2003; Murphy and

Gijón, 2007). Several groups tried to introduce functional groups to existing pharmaceuticals that are β -lyase cleavable to obtain specific drug release (Elfarra and Hwang, 1993). For example, effort was put in the development of β -lyase specific prodrugs of 6-mercaptopurin (6-MP). As an anticancer agent, 6-MP causes a variety of severe adverse effects due to unspecific organ release. These adverse effects could be minimized if the drug would only act in the target organ. As β -lyase activity is most prevalent in kidney tissue, it was anticipated that a β -lyase cleavable prodrug of 6-MP would increase organ selectivity in the kidney and lower adverse side effects, while boosting anticancer activity. Despite promising results, currently no β -lyase active prodrugs of 6-MP are approved by FDA or EMA.

In addition to pharmaceuticals, β -lyases are involved in the metabolism of several haloalkenes. Various cysteine *S*-conjugates derived from haloalkenes including *S*-(1,2-dichlorovinyl)-*L*-cysteine [DCVC], *S*-(1,1,2,2-tetrafluoroethyl)-*L*-cysteine [TFEC], *S*-(1,2,2-trichlorovinyl)-*L*-cysteine [TCVC] are known to be toxic to rats (liver, brain and especially to kidney) and to kidney derived cell systems of rats, pigs (LLC-PK1 cells) and humans (Reviewed by Cooper and Pinto (2006), Cristofori *et al.* (2015) and Cooper and Hanigan (2018)). Especially the renal proximal tubules are target of cysteine *S*-conjugates derived from haloalkenes. The important role of β -lyases in the bioactivation of (nephro-)toxic cysteine *S*-conjugates was demonstrated in several renal proximal tubular cell lines in the presence of the β -lyase inhibitor, aminoxyacetic acid (AOAA). Renal proximal tubular cells of different mammalian species (e.g. rat, human and pig) could be protected completely or in part from the cytotoxicity of cysteine *S*-conjugates derived from haloalkenes in the presence of AOAA. Interestingly, rat renal tissue seems to be more susceptible towards the toxicity of cysteine *S*-conjugates as compared to human renal tissue, indicating species differences in the specific activity of β -lyases (Lash *et al.*, 1990; Iyer and Anders, 1996).

Despite an increase in renal β -lyase activity was observed after incubation with nephrotoxic cysteine *S*-conjugates derived from haloalkenes, the total β -lyase activity is reduced (MacFarlane *et al.*, 1993). Reduced overall β -lyase activity may be associated with a syncatalytic inactivation of β -lyases induced by the cleavage of the cysteine *S*-conjugate. This can be interpreted as an endogenous protective mechanism against the formation of toxic β -lyase derived metabolites (Cooper and Hanigan, 2018). In subcellular fractions of rats and by purified β -lyases, as well as with β -lyase activity present in bacteria, the cleavage of fluorine and chlorine containing cysteine *S*-conjugates derived from halogenated alkenes results in the formation of pyruvate, ammonia, and a reactive thionoacyl species (Green and Odum, 1985; Dekant *et al.*, 1986; Dekant *et al.*, 1988). These reactive thionoacyl compounds and metabolites derived thereof were identified to be a main cause of toxicity observed with cysteine *S*-conjugates derived from haloalkenes. In addition to cysteine *S*-conjugate derived

metabolites that are responsible for toxicity, tissue damage by covalent binding of cysteine *S*-conjugate (e.g., *S*-(1,1,2,2-tetrafluoroethyl)-*L*-cysteine)) is associated with carcinogenesis (Nelson and Pearson, 1990).

In the interest of completeness, detoxification of reactive intermediates originated from β -lyase cleavage of the cysteine *S*-conjugate via glucuronidation was detected *in vivo* in rodents leading to the urinary elimination of the glucuronic acid conjugates (Elfarra and Hwang, 1990).

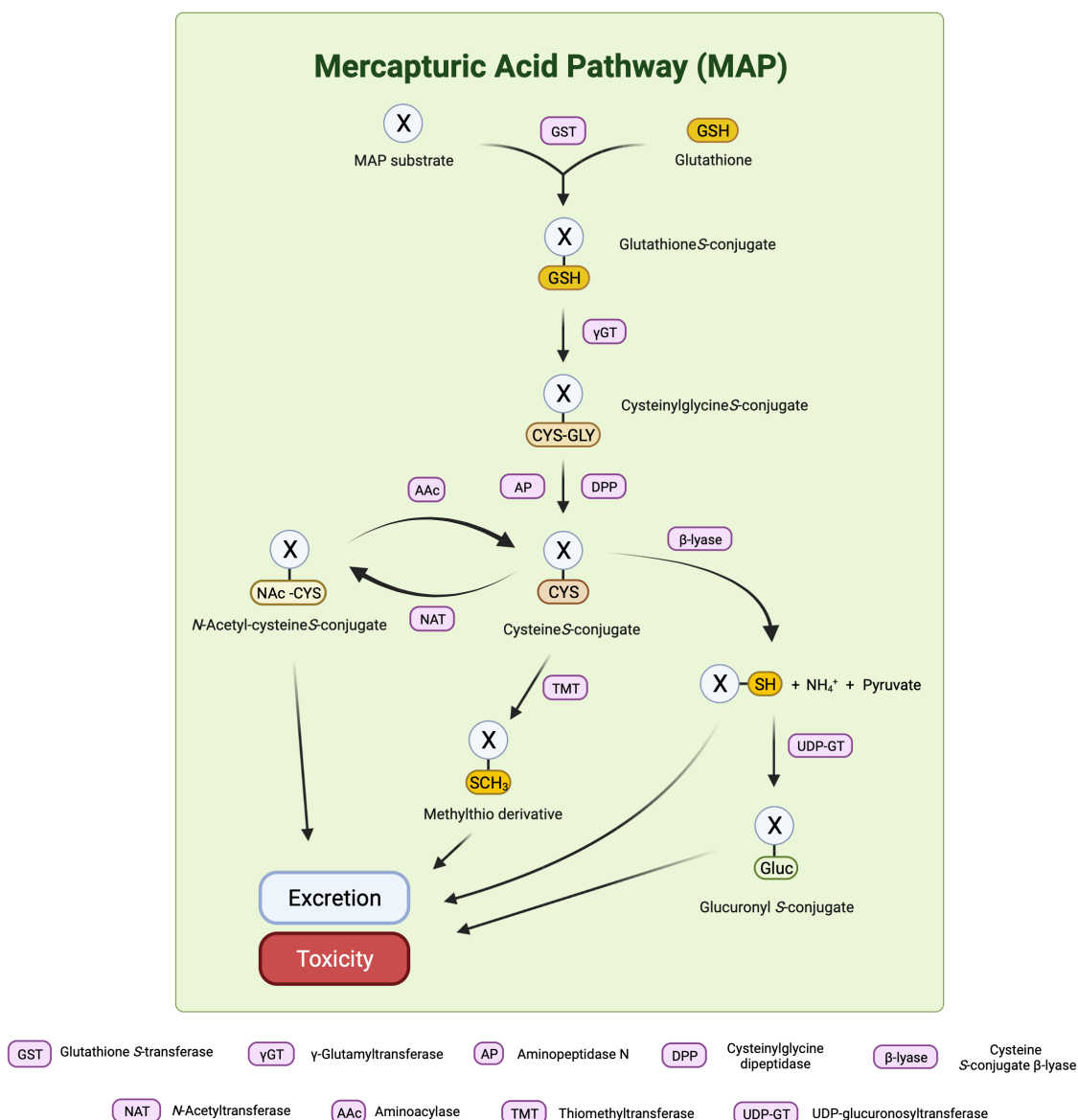


Figure 8 The mercapturic acid pathway in bioactivation and detoxification of xeno- and endobiotics. Figure modified from Cooper and Hanigan (2010) and created with BioRender.com.

In summary, biotransformation of chemicals via the MAP is an endogenous mechanism, designed to detoxify potentially hazardous electrophiles. However, in case of several haloalkenes MAP mediated biotransformation leads to the formation of reactive metabolites being responsible for toxicity, thus representing a bioactivation. Based on the chemical structure of an individual haloalkene it is challenging to predict whether it will be bioactivated

or detoxified via the MAP. A detailed knowledge of *in vivo* metabolite monitoring and *in vitro* kinetics of involved enzymes is necessary to explain observed toxicity.

3.6 Trifluoroethene (HFO-1123) – Advanced climatic properties but marked health concerns

3.6.1 Inhalation exposure of experimental animals to HFO-1123

Due to the phasing out of high-GWP refrigerants like HCFCs and HFCs and the continuing demand for refrigeration which is expected to increase even further due to climate change, the need for safe and low-GWP refrigerants is greater than ever. One chemical currently considered as a promising new refrigerant is 1,2,2-trifluoroethene (HFO-1123, CAS# 359-11-5). As a member of the hydrofluoroolefins, it exhibits zero ODP due to the absence of chlorine. Compared to other HFOs that are currently used as refrigerants, its GWP of 0.6 (compared to CO₂) and atmospheric lifetime of 1.6 days is low (HFO-1234ze: GWP, 6 (compared to CO₂); atmospheric lifetime, 18 days) (Hodnebrog *et al.*, 2013; Antiñolo *et al.*, 2017; Mondal *et al.*, 2020). HFO-1123 is not anticipated for sole use within air-conditioning units (due to its increased flammability), but as a mixture with other refrigerants. In combination with other refrigerants, flammability is reduced and refrigeration performance is increased (Hashimoto *et al.*, 2019).

Due to the increased potential for toxicity and observed species-differences in toxicity of haloalkenes (Tetrafluoroethene, Trichloroethene, HFO-1234yf), the safety and risk for human health of new HFOs must be assessed prior to official approval and introduction to the market. Several animal studies were performed with HFO-123 following the testing guidelines for fluorocarbon refrigerants issued by the *Program of the Development of Alternative Fluorocarbon Toxicity Testing* as a scientific basis for toxicology evaluation (Rusch, 2018). Table 2, Table 3 and Table 4 summarize design and results of the inhalation toxicity studies conducted with HFO-1123 in mammals.

In rats, a single-dose inhalation study with HFO-1123 revealed no mortality or signs of intoxication at exposure concentrations up to 200,000 ppm (Wako, 2014c). Repeated dose inhalation studies with HFO-1123 for 14 days (6 hours/day, 5 days/week) and concentrations up to 20,000 ppm, including a developmental toxicity study, suggested a low toxic potential of HFO-1123, with no-observable-adverse-effect-levels (NOAELs) \geq 20,000 ppm (Wako, 2014a).

As cardiac toxicity occurs with several fluorinated carbons, cardiac sensitization needs to be evaluated as a critical endpoint in all novel halogenated refrigerants (ECETOC, 2009). No evidence for cardiac sensitization or other symptoms of intoxication were observed in beagle dogs, exposed to HFO-1123 at up to 75,000 ppm, indicating a low potential for cardiac toxicity





(Coffee, 2015). Results of inhalation studies conducted with rats and beagle dogs thus indicate a low acute, chronic, reproductive, and cardiac toxicity of HFO-1123.

However, short term inhalation exposures of Goettingen[®] Minipigs to HFO-1123 resulted in mortality at exposure levels ≥ 500 ppm (Wako, 2017). Clinical symptoms of intoxication, including emesis, convulsions, hunched posture and decreased locomotor activity were observed at concentrations as low as 65 ppm (Wako, 2018b) indicating the central nervous system as the target organ of HFO-1123 toxicity. In addition to visual signs of intoxication, necropsy revealed hemorrhage of the epicardium and interstitium, basophilic granulation of the myocardium and cell inflammation of the epicardium in several moribund and surviving animals (Wako, 2018b). Also, increased troponin levels and aspartate aminotransferase activity were observed in plasma of most Goettingen[®] Minipigs exposed to HFO-1123. Both, necropsy findings and altered blood parameters indicate the heart as a target for toxicity of HFO-1123.

Similarly, a developmental toxicity study in New Zealand White (NZW) Rabbits exposed to HFO-1123 via inhalation recorded mortality at levels ≥ 1250 ppm after first exposure (Wako, 2016). Necropsy findings revealed edema and reddish patches in the lung, hemorrhage in the trachea, focal white changes in the heart, as well as ascites and hydrothorax. These changes could not unequivocally be linked to HFO-1123 exposure as they were also consistent with post-mortem changes. However, mortality and moribundity of NZW Rabbits revealed an increased sensitivity to HFO-1123 toxicity compared to rats.



Interestingly, a great variability in the response to HFO-1123 between individual Goettingen[®] Minipigs and NZW Rabbits was observed. Death or absence of symptoms of intoxication occurred in both species and within all dose groups. Comparable effects have been noted with HCFC-123 (Lind *et al.*, 1995; Hoet *et al.*, 2001). In the case of HCFC-123, differences in the extent of GSH liver content and variations in CYP-450 activity (differences in the extent of CYP-450 or GSH mediated biotransformation) were discussed to be linked to the interindividual susceptibility. If this effects also play a key role with HFO-1123 is yet unknown.

Table 2 Study design and results of acute toxicity and *in vivo* biotransformation studies conducted with HFO-1123 in experimental animals

	 Rat	 Goettingen® Minipig	 Chimeric mice (HU-liver TK-NOG mice)	 Beagle dogs
Acute toxicity studies & biotransformation studies				
Study design	a) 4h, female/male, 3 animals/sex/dose b) 4h, male	4h, female	4h, male	10 min, 6 males/dose, epinephrine dose after 5 min exposure (cardiac sensitization)
HFO-1123 concentrations [ppm]	a) 2500, 20,000, 200,000 b) 20,000	85, 200	20,000 ppm	25,000, 50,000, 75,000
Symptoms of intoxication	n.d.	n.d.	n.d.	n.d.
Necropsy findings	n.e.	n.e.	no abnormalities	n. e.
Clinical parameters	a) n. e. b) normal plasma citrate levels	Increased plasma citrate level, MFA detected in urine	MFA detected in urine, no increase in plasma citrate levels	no cardiac sensitization
Literature	a) (Wako, 2013), (Wako, 2014c) b) (Wako, 2019b)	(Wako, 2019a)	(Wako, 2018a)	(Coffee, 2015)



n.e. – not evaluated; n.d. - none detected

Table 3 Study design and results of repeated dose toxicity studies conducted with HFO-1123 in experimental animals

	 Rat	 Goettingen® Minipig
Repeated dose toxicity studies		
Study design	a) 2-week exposure, 5 d/week, 6h/d, female/male, 6/sex/dose b) 13-week exposure, 5d/week, 6h/d,	a) 2-week exposure, 7d/week, 6h/d, female, 3 animals/dose b) 2-week exposure, 7d/week, 6h/d, female, 3 animals/dose
HFO-1123 concentrations [ppm]	0, 1000, 5000, 10,000, 20,000	a) 0, 1000, 5000, 10,000 b) 0, 65, 130, 500
Effect levels [ppm]	a) NOEL: 20,000 b) LOAEL: 1030	n.e.
Symptoms of intoxication	n.d.	a) Mortality after first inhalation in all groups, emesis, convulsions b) Mortality after first inhalation (500 ppm), emesis
Necropsy findings	a) No abnormalities b) Vacuolation of VNO (≥ 5000 ppm)	(a, b) Hemorrhage of epicardium and interstitium of the heart, focal inflammatory cell infiltration in the epicardium and basophilic granulation of myocardium, Thickening of intramural artery media
Clinical parameters	no abnormalities	(a, b) increased troponin levels, lower neutrophil counts, increased aspartate aminotransferase activity
Literature	(Wako, 2014a), (Wako, 2014b)	(Wako, 2018b), (Wako, 2017)

n.e. – not evaluated; n.d. - none detected

Table 4 Study design and results of developmental and reproductive toxicity studies conducted with HFO-1123 in experimental animals

	 Rat	 NZW Rabbit
Developmental and reproductive toxicity studies		
Study design	a) 12/sex/group, male: 28 days prior to mating females for 14 days prior to mating and through gestation day 19 b) female (20/group), exposed from GD 6 to GD 19	female, 5 animals/group, 6h/day, from GD 6 to GD 27
HFO-1123 concentrations [ppm]	a) 0, 1000, 5000, 10,000, 20,000 b) 0, 5000, 10,000, 20,000	0, 1250, 2500, 5000, 10,000, 20,000
Symptoms of intoxication	none detected	Mortality observed in all dose groups
Necropsy findings	a) Vacuolation of VNO of parental animals b) no abnormalities in parental animals and offspring	Ascites and/or hydrothorax, focal white change in the heart, edema and dark reddish patch in the lungs, hemorrhage in the trachea
Clinical parameters	n.e.	n.e.
Literature	(Wako, 2015b), (Wako, 2015a)	(Wako, 2016)

3.6.2 Potential role of HFO-1123 biotransformation in species-differences in toxicity

The observed marked differences in toxicity in exposed animals may be due to species-specific biotransformation resulting in the formation of toxic metabolites in susceptible species. It is thus hypothesized that the higher sensitivity of Goettingen[®] Minipigs and NZW Rabbits as compared to rats may be explained by species-differences in the routes or extent of HFO-1123 biotransformation. For several structural related HFOs, HCFCs and HFCs, differences in the extent of biotransformation, toxicity and carcinogenicity between species have been observed and described in the literature (Koob and Dekant, 1991; Elfarra *et al.*, 1998; Dekant, 2003a; Anders, 2008; Tveit *et al.*, 2013; Cristofori *et al.*, 2015; Rusch, 2018).

In principle, oxidative biotransformation mediated by CYP-450 enzymes and biotransformation via the Mercapturic Acid Pathways may contribute to the biotransformation of HFO-1123. In previous chapters both biotransformation pathways were described in detail, as they play an important role in both bioactivation and detoxification of HCFC-123, TRI and HFO-1234ze (Figure 6, Figure C.11 and Figure 7). In the following, CYP-450 and MAP derived biotransformation will be discussed regarding their contribution to HFO-1123 metabolism. Figure 9 gives a brief overview of uptake, hepatic transport and proposed pathways involved in the biotransformation of HFO-1123 with regard to the observed toxicity in Goettingen[®] Minipigs and NZW Rabbits.

CYP-450 mediated oxidation of HFO-1123 may generate an intermediate epoxide, which may further react with glutathione (GSH) in an enzymatic reaction mediated by glutathione transferases (GST) to form a glutathione conjugate. Subsequent processing of the GSH conjugate to its corresponding cysteine S-conjugate may lead to renal excretion in the form of the corresponding mercapturic acid or hydrolysis to inorganic fluoride (F⁻). Since selectively toxic intermediates are not anticipated to be formed via this pathway, CYP-450 mediated biotransformation is not considered to play a primary role in HFO-1123 toxicity.

Bioactivation of HFO-1123 may involve biotransformation via the mercapturic acid pathway (MAP) (see chapter 3.5 for a detailed summary of involved enzymes and reactions). Regarding HFO-1123, the first potential metabolite formed via the MAP is the corresponding glutathione conjugate, S-(1,1,2-trifluoroethyl)-L-glutathione (1123-GSH). It is expected that 1123-GSH is sequentially cleaved by γ -GT and APN/DPP resulting in the corresponding cysteine S-conjugate, S-(1,1,2-trifluoroethyl)-L-cysteine (1123-CYS). Cysteine S-conjugates play a decisive role in the detoxification and bioactivation of glutathione adducts via the mercapturic acid pathway. They can either be processed by *N*-acetyltransferases to *N*-acetyl derivatives (mercapturic acids) which are usually excreted into the urine, or, depending on structure, bioactivated by cysteine S-conjugate β -lyases to reactive metabolites. Various cysteine S-conjugates derived from haloalkenes are known to be toxic to rats and to kidney derived cell

systems of rats and humans (Cooper and Pinto, 2006; Cristofori *et al.*, 2015). In subcellular fractions of rats and by purified β -lyases, as well as with β -lyase present in bacteria, the cleavage of fluorine and chlorine containing cysteine S-conjugates results in the formation of pyruvate, ammonia, and a reactive thionoacyl species (Green and Odum, 1985; Dekant *et al.*, 1986; Dekant *et al.*, 1988). These reactive thionoacyl compounds and metabolites derived thereof were identified to be a main cause of toxicity observed with cysteine S-conjugates.

One possible metabolite derived from thionoacyl species formed from fluoride containing haloalkenes is monofluoroacetic acid (MFA). MFA is a stable end-product of biotransformation of several halogenated alkanes (Keller *et al.*, 1996) and based on the structure of 1123-CYS, formation of MFA can be expected to occur during β -lyase mediated biotransformation of 1123-CYS.

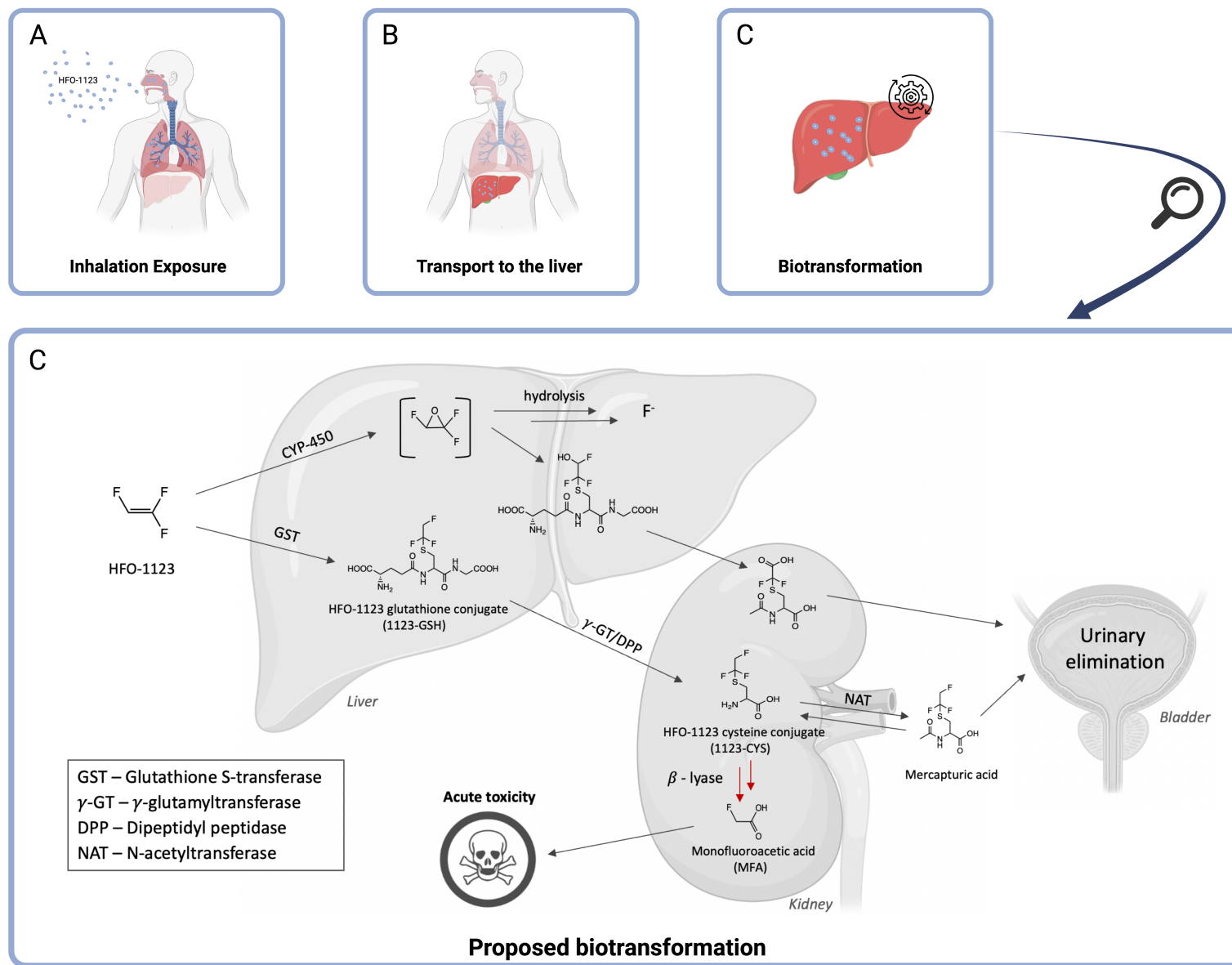


Figure 9 Pulmonary uptake (A), hepatic transport (B) and proposed biotransformation (C) of HFO-1123 with account for its toxicity in sensitive species. Cytochrome P450 (CYP-450) mediated biotransformation may result in hydrolysis of the epoxide into F⁻ or subsequent conjugation with GSH and urinary excretion of a mercapturic acid. The mercapturic acid pathway (lower pathway) is expected to be responsible for HFO-1123 toxicity. HFO-1123 may be conjugated to glutathione, likely mediated by glutathione S-transferases (GST), to form S-(1,1,2-trifluoroethyl)-L-glutathione (1123-GSH). This conjugate may be cleaved by γ-glutamyltransferases (γ-GT) to form the corresponding cysteine S-conjugate (1123-CYS). 1123-CYS can either be eliminated by N-acetyltransferases or bioactivated by β-lyases. The latter reaction may give rise to monofluoroacetic acid (MFA) as the ultimate toxic agent expected to be responsible for HFO-1123 toxicity. Figure created with BioRender.com.

MFA is a potent inhibitor of aconitase (citrate hydro-lyase, EC 4.2.1.3) in the tricarboxylic acid (TCA) cycle and therefore highly toxic (Goncharov *et al.*, 2006). Inhibition of the TCA cycle by MFA leads to a multitude of cellular effects (Figure 10), e.g. lactate acidosis, glutamine depletion, ketosis and adenosine triphosphate (ATP) depletion (Proudfoot *et al.*, 2006) resulting in cardiac arrest, ventricular fibrillation or central nervous system depression accompanied with cardiovascular or respiratory disorders. Reduced ATP production is causal for a decreased activity of cellular processes that demand a great amount of energy, like gluconeogenesis. Also, inhibition of aconitase is associated with the accumulation of citrate, as citrate is no longer converted into isocitrate (Buffa and Peters, 1949; Egyed and Brisk, 1965; Buffa *et al.*, 1973). Increased citrate levels can lead to hypocalcemia, resulting in cardiac arrest, convulsion, and central nervous system depression (Buffa and Peters, 1949; Pattison, 1959; Bosakowski and Levin, 1986; Goh *et al.*, 2005).

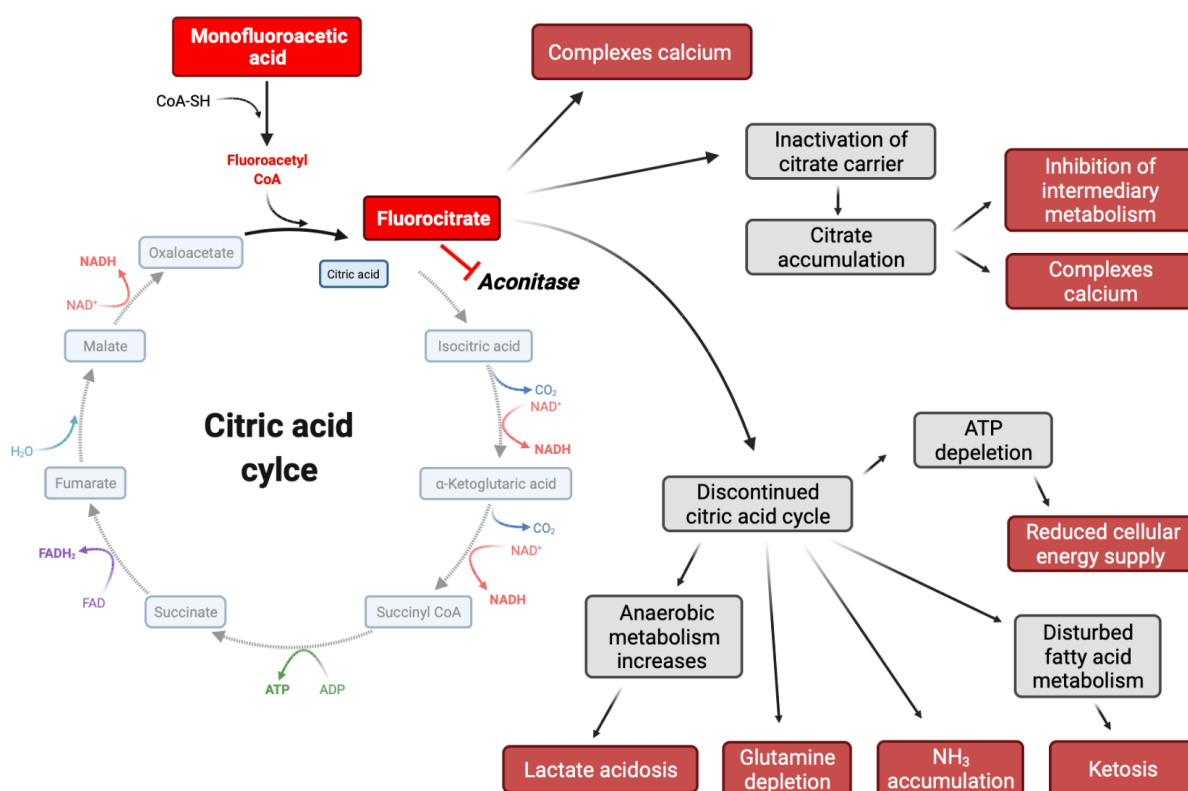


Figure 10 Cellular effects of monofluoroacetic acid (MFA) that may contribute to its toxicity according to Proudfoot *et al.* (2006). MFA is incorporated as fluoroacetyl-CoA in the citric acid cycle. Subsequent formation of fluorocitrate leads to suicide inhibition of aconitase, resulting in discontinuation of the citric acid cycle, causing lactate acidosis, glutamine and ATP depletion, NH₃ accumulation and ketosis. Fluorocitrate can further lead to direct calcium chelation and citrate accumulation, leading to the inhibition of enzymes involved in intermediary metabolism e.g., phosphofructokinase. Figure modified from Proudfoot *et al.* (2006) and created with BioRender.com.

Increased citrate levels after HFO-1123 exposure may thus be an indicator of MFA formation as a result of 1123-CYS mediated cleavage (Keller *et al.*, 1996). Rats exposed to HFO-1123 (> 20.000 ppm) did not show significant changes in plasma citrate levels and also no toxicity (Wako, 2019b). However, in Goettingen[®] Minipigs exposed to HFO-1123 (85-200 ppm) a

concentration dependent increase in plasma citrate levels was recorded (Wako, 2019a). Using ^{19}F -NMR, traces of MFA were also detected in urine of Goettingen[®] Minipigs administered 200 ppm of HFO-1123 for 4 hours (Wako, 2019a). These biochemical changes were associated with clinical signs of intoxication consistent with symptoms of MFA poisoning and support a linkage between β -lyase mediated cleavage of 1123-CYS, increased citrate levels and HFO-1123 toxicity in experimental animals.

To get initial insight into biotransformation derived toxicity of HFO-1123 in humans, biotransformation of HFO-1123 was evaluated in a chimeric mouse model with a humanized liver. Chimeric mice with a humanized liver (Hu-liver mice) are used in drug development as a model to predict human drug metabolism and to identify potential toxic metabolites (Nishimura *et al.*, 2013). Wako *et al.* (2018a) exposed Hu-liver TK-NOG mice for four hours with HFO-1123 at concentrations of 20,000 ppm. No signs of toxicity or abnormalities in histopathological examination or clinical parameters were observed compared to unexposed controls. However, MFA was observed as a urinary metabolite after HFO-1123 exposure indicating MAP associated biotransformation.

Urine analysis of rats, Goettingen[®] Minipigs and chimeric mice exposed to HFO-1123 suggested species-differences in the formation of MFA. The detection of MFA as a urinary metabolite in chimeric mice and Goettingen[®] Minipigs following HFO-1123 exposure, confirms the involvement of the mercapturic acid pathway in HFO-1123 biotransformation. As MFA formation was absent in the rat but present in the Goettingen[®] Minipig, its formation may further play a key role in the toxicity of HFO-1123 in susceptible species (Goettingen[®] Minipig, NZW Rabbit). Further investigation on biotransformation, with special focus on the enzymatic formation and cleavage of HFO-1123 derived metabolites in susceptible and less susceptible species as well as human are of major importance to evaluate human safety.

3.7 Objectives and aims

The general aim of this work was to experimentally support the hypothesis that species-differences in the extent of GSH dependent biotransformation and subsequent β -lyase mediated formation of MFA may account for the species-differences in HFO-1123 toxicity by investigating HFO-1123 biotransformation in subcellular fractions of susceptible (Goettingen[®] Minipig, NZW Rabbit) versus less susceptible species (SD rats, CD1 mice) and humans as a basis for human risk assessment.

The first specific aim of this work was to determine the extent of GSH dependent biotransformation of HFO-1123 in hepatic S₉ fractions of SD rats, CD-1 mice, Goettingen[®] Minipigs, NZW Rabbits and humans through quantitation of 1123-GSH by LC-MS/MS and identification of potential fluorine containing metabolites by ¹⁹F-NMR.

The second specific aim was to understand if species-differences in HFO-1123 toxicity may be due to differences in cysteine S-conjugate β -lyase mediated biotransformation. Enzyme kinetics of β -lyase mediated cleavage of 1123-CYS in renal and hepatic cytosolic fractions of susceptible vs. less susceptible species were assessed using a modified UV/VIS spectrometric assay based on the method described by *Lash et al.* (Lash, 2007). ¹⁹F-NMR was used to analyze the formation of fluorine containing metabolites derived from β -lyase mediated cleavage of 1123-CYS.

An ancillary aim of the work was to assess cytotoxicity and biotransformation of 1123-CYS in human (HK-2), rat (NRK-52E) and pig (LLC-PK1) renal proximal tubular epithelial cell lines in the presence and absence of a β -lyase inhibitor to further support the role of β -lyase mediated cleavage of 1123-CYS.

Results of this work were expected to provide detailed information about enzyme kinetics of GST and β -lyase mediated biotransformation of HFO-1123 derived metabolites and species-differences in HFO-1123 metabolism, that can be used to evaluate the safety of HFO-1123 in humans.

4 Materials & Methods

4.1 Chemicals & chemical syntheses

4.1.1 Chemicals

S-(1,2,2-trichlorovinyl)-L-cysteine (TCVC) and monofluoroacetic acid (MFA) were purchased from Toronto Research Chemicals (North York, Canada). HFO-1123 and crude 1123-CYS were supplied by AGC Inc. (Tokyo, Japan). 1123-CYS was purified by HPLC at the Institute of Pharmacology and Toxicology of the University Wuerzburg, yielding a purity of approximately 98% (Appendix A, Chapter A.1). Purity of 1123-CYS was characterized by LC-MS/MS and ^{19}F -NMR. 1123-GSH was synthesized, purified, and characterized at the Institute of Pharmacology and Toxicology of the University of Wuerzburg according to procedures described below. *N*-acetyl-S-(1,1,2-trifluoroethyl)-L-cysteine (1123-CYS-NAc) was synthesized at the Institute of Pharmacology and Toxicology of the University of Wuerzburg according to procedure described below. Unless otherwise indicated, all other chemicals were purchased from Merck (Darmstadt, Germany), Sigma Aldrich (Taufkirchen, Germany) or Roth (Karlsruhe, Germany) in the highest purity available. For cell culture media and related supplements see chapter 4.4.

4.1.2 Chemical syntheses

Synthesis of S-(1,1,2-trifluoroethyl)-L-glutathione (1123-GSH)

1123-GSH was synthesized according to the method described by McKinney *et al.* (1957) with minor modifications. Reactions were carried out at -80°C (cooled by a mixture of methanol/ CO_2). Sodium (3 mmol) was dissolved in liquefied ammonia (50 mL). To this solution, L-glutathione (3 mmol) was added and dissolved. Finally, an excess of HFO-1123 was added and the obtained solution was stirred for 5 hours. The reaction was stopped by removing the reaction flask from the cooling source. It was then stored at 25°C overnight in a fume hood to evaporate any remaining HFO-1123 and NH_3 . The obtained crystal residue was dissolved in water and acidified to pH 3 with 2 N hydrochloric acid. The obtained crude synthesis product was purified by HPLC (Appendix A, Chapter A.3), characterized by LC-MS/MS and one- and two-dimensional $^1\text{H}/^{19}\text{F}/^{13}\text{C}$ -NMR (Appendix B, Figures B.2 to B.6).

Synthesis of N-acetyl-S-(1,1,2-trifluoroethyl)-L-cysteine (1123-CYS-NAc)

N-acetyl-S-(1,1,2-trifluoroethyl)-L-cysteine (1123-CYS-NAc) was synthesized by *N*-acetylation of 1123-CYS to serve as an analytical standard to enable LC-MS/MS analysis of 1123-CYS-NAc formation in cell cultures treated with 1123-CYS. The synthesis was carried out at $2\text{--}5^{\circ}\text{C}$ in an ice-bath. 1123-CYS (0.02 mmol) was dissolved in 1 mL of water. To this solution, 0.024 mmol acetic anhydride was gradually added. The pH of the solution was monitored after every addition of acetic anhydride and was adjusted to pH 7 by addition of 0.25 M sodium hydroxide.

After addition of the total volume of acetic anhydride, the reaction was stirred for further 30 minutes and was finally neutralized to pH 7 by addition of 0.1 M formic acid. Successful synthesis of 1123-CYS-NAc was confirmed by characteristic fragmentation obtained by *Enhanced Product Ion* (EPI; see chapter 4.3 for analytical method) scans in positive and negative ionization (Appendix B, Figure B. 7).

4.2 *In vitro* incubations to study GST and β -lyase mediated biotransformation of HFO-1123

4.2.1 Sources of subcellular fractions

Origin of animals used for preparation of subcellular fractions

Tissue from a Goettingen[®] Minipig (sex: male; bodyweight: 42.4 kg; Date of birth: 24.07.2015; Date of sacrifice: 13.05.2020; Identification Nr. 23428) was obtained from the Department of Animal Sciences of the University of Goettingen (Goettingen, Germany). The liver of a male New Zealand White Rabbit was kindly provided by the *Department for Functional Materials in Medicine and Dentistry* of the University of Wuerzburg. Immediately after sacrifice, kidneys and liver were harvested. Kidneys were rinsed with 0.9% sodium chloride solution through the renal artery to clean the kidneys from circulating blood. The liver was rinsed with 0.9% sodium chloride solution through the portal vein. Kidneys and liver were sectioned, flash frozen and stored at -80°C. Cytosolic and S₉ fractions were prepared as described below.

S₉ subcellular fractions

Liver and kidney S₉ fractions from SD rats (liver: male, pool of 97 donors; kidney: male, pool of 150 donors) and humans (liver: mixed gender, pool of 50 donors; kidney: mixed gender, pool of 8 donors,) and hepatic S₉ from CD1 mice (male, pool of 1745 donors) were obtained from XenoTech (Kansas City, USA). Renal and hepatic S₉ fractions from Goettingen[®] Minipigs (male, 1 donor) and hepatic S₉ fractions of NZW Rabbits (male, 1 donor) were prepared in-house at the Institute of Pharmacology and Toxicology following standard operating procedure (SOP A51) as described below.

All working steps were performed at 4°C and equipment was pre-cooled to 4°C. Kidney or liver tissues were weighted, subsequently dissected into small pieces, and homogenized with a glass homogeniser after adding 0.154 M potassium chloride solution (pH 7.4, three times the organ weight in mL). Homogenates were centrifuged at 9,000 x g and 4°C for 20 min. After centrifugation, floating fat and precipitates were discarded. Obtained supernatants (S₉ fractions) were aliquoted into 1 mL vials, immediately flash frozen in liquid nitrogen and stored at -80°C. For method validation hepatic S₉ fractions of Goettingen[®] Minipigs (male, 1 donor) were obtained from Primacyt[®] (Schwerin, Germany).

Cytosolic fractions

Hepatic and renal cytosolic fractions from humans (kidney: pool of 4 donors, mixed gender; liver: pool of 10 donors, male), SD rats (kidney: 150 donors, male; liver: 454 donors, male) and CD1 mice (kidney: pool of 250 donors; liver: pool of 1200 donors, male) were obtained from XenoTech® (Lenexa, USA). Hepatic and renal cytosolic fractions from Goettingen® Minipigs (male; 1 donor) and NZW Rabbits (male, 1 donor) were prepared in-house at the Institute of Pharmacology and Toxicology following standard operating procedure (SOP 21-A/2) as described below.

All working steps were performed at 4°C and equipment was pre-cooled to 4°C. Kidney or liver tissues were weighted, subsequently dissected into small pieces, and homogenized with a glass homogeniser after adding 0.154 M potassium chloride solution (pH 7.4, three times organ weight in [mL]). Homogenates were centrifuged at 12,000 $\times g$ and 4°C for 10 min. The supernatants were transferred into ultracentrifuge vials and centrifuged at 154,000 $\times g$ and 4°C for 60 minutes. The precipitates were discarded. After ultracentrifugation of the supernatant, floating fat was discarded. The obtained supernatants (cytosolic fraction) were aliquoted into 1 mL vials, immediately flash frozen in liquid nitrogen and stored at -80°C.

Determination of protein concentration in subcellular fractions prepared in-house

Cytosolic and S₉ protein concentrations were determined using the DC™ Protein assay kit (Bio-Rad® Laboratories, Hercules, USA) and bovine serum albumin (BSA) as a standard (SOP 1-S/3). The initial step in this assay is the interaction of Cu²⁺ ions with peptide bonds, resulting in a violet-blue complex, known as the biuret reaction. In a subsequent reaction, Cu²⁺ ions are reduced to Cu¹⁺ by peptide bond oxidation. Folin-Ciocalteu reagent (mixture of phosphotungstate and phosphomolybdate) added to the sample is reduced by the peptide-bound Cu⁺ ions. Reduced Folin-Ciocalteu reagent leads to the formation of tungsten pentoxide, that can be quantified at 750 nm (Lowry *et al.*, 1951). Before protein quantitation, cytosolic fractions were diluted 1:20 with ice-cold 10 mM phosphate buffer, pH 7.4. Calibration standards (0 to 1 mg/mL) were prepared by diluting BSA in 10 mM phosphate buffer, pH 7.4. 20 μ L of samples or standards were added to 100 μ L of reagent A and vortexed for 10 seconds. Immediately after addition of reagent B (800 μ L), samples and standards were vortexed for 30 seconds and incubated for 15 minutes at 25°C. Absorbance was determined at 750 nm using a U-2000 UV/VIS spectrometer (Hitachi Ltd., Tokyo, Japan). Protein concentrations were determined by linear equation obtained from calibration standards.

4.2.2 GST mediated biotransformation of HFO-1123 in S₉ subcellular fractions

To investigate GST mediated biotransformation of HFO-1123 *in vitro*, hepatic and renal S₉ fractions were incubated with HFO-1123 according to the method described by Schmidt *et al.* (Schmidt *et al.*, 2013) with the following modifications. Briefly, HFO-1123 was added to subcellular fractions in gas-tight vials. Following incubations for up to 12h, aliquots of the incubations were processed for sample workup for ¹⁹F-NMR and LC-MS/MS analysis (Figure 11). The amounts of HFO-1123 added to the incubations were calculated based on the assumption that HFO-1123 acts as an ideal gas (1 mol HFO-1123 corresponds to a gas-volume of 22.4 L).

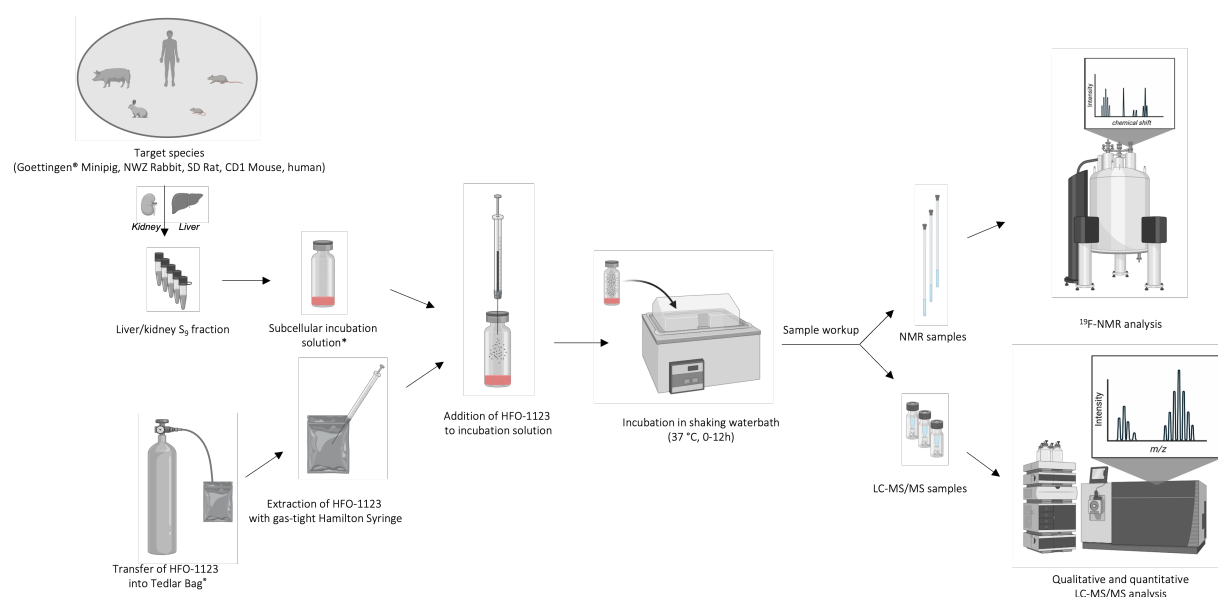


Figure 11 Overview of the experimental approach for determining GST mediated formation of 1123-GSH after incubation of HFO-1123 with subcellular S₉ fractions of Goettingen® Minipigs, NZW Rabbits, SD rats, CD1 mice and humans. Figure created with BioRender.com.

Method validation – Incubations of TRI with hepatic S₉

To demonstrate the suitability of the experimental set-up to assess GST mediated biotransformation of HFO-1123, formation of S-(1,2-dichlorovinyl)-L-glutathione (DCVG) was monitored in hepatic S₉ fractions after incubation with trichloroethylene (TRI)

TRI (1 mM) was incubated with hepatic S₉ subcellular fractions (3 mg protein/mL) of Goettingen® Minipigs, rats, mice and humans in sealed 20 mL GC vials (Supelco® Inc., Bellefonte, USA). Incubations (total volume of 1.1 mL) were performed in the presence of GSH (10 mM) in potassium phosphate buffer (100 mM, pH 7.4, containing 1 mM EDTA). The incubations were carried out in a shaking water bath at 37°C for up to 12 h. 200 µL aliquots were extracted before the start (prior to the addition of TRI), at the beginning (0 h) and 1, 6 and 12 h after the start of the incubation. Each aliquot was added to 0.3 mL ice-cold acetonitrile and centrifuged at 4°C and 20,000 x g for 15 minutes. The obtained pellet was resolubilized in

0.3 mL acetonitrile and again centrifuged (4°C, 20,000 x g, 15 minutes). The supernatants were combined and the acetonitrile/water phase was evaporated under reduced pressure. The dried residue was resolved in 200 µL H₂O + 0.1% formic acid (FA), transferred to LC vials and stored at -20°C until analysis.

Incubations of HFO-1123 with hepatic S₉ – time-dependent formation of 1123-GSH

HFO-1123 (0.4 mmol) was incubated with hepatic S₉ subcellular fractions (3 mg protein/mL) of Goettingen[®] Minipigs, NZW Rabbits, rats, mice and humans and renal S₉ subcellular fractions of Goettingen[®] Minipigs, rats and humans (3 mg protein/mL) in sealed 20 mL GC vials (Supelco[®] Inc, Bellefonte, USA). Incubations (total volume of 1.1 mL) were carried out in the presence of GSH (10 mM) and a NADPH regenerating system (10 mM NADP, 10 mM glucose-6-phosphate and 0.5 units/mL glucose-6-phosphate dehydrogenase) or 10 mM glutathione (GSH) in potassium phosphate buffer (100 mM, pH 7.4, containing 1 mM EDTA). To evaluate potential γ -GT mediated cleavage of 1123-GSH formed, additional incubations containing GSH (10 mM) and hepatic S₉ (3 mg protein/mL) were performed in the presence of the specific γ -GT inhibitor acivicin (0.5 mM). Additional incubations containing GSH (10 mM) and hepatic S₉ (3 mg protein/mL) were performed in the presence of AOAA (5 mM), a specific β -lyase inhibitor to evaluate potential β -lyase mediated cleavage of 1123-CYS which may be formed from 1123-GSH.

All incubations were carried out in a shaking water bath at 37°C for up to 12 hours. Aliquots (200 µL) were extracted before the start (prior to the addition of HFO-1123), and at 0, 1, 6 and 12h after addition of HFO-1123. Incubations were stopped by addition of 0.3 mL ice-cold acetonitrile to each aliquot and centrifugation at 4°C and 20,000 x g for 15 minutes. The obtained pellet was resolubilized in 0.3 mL acetonitrile and centrifuged (4°C, 20,000 x g, 15 minutes). The supernatants of both centrifugation steps were combined and the acetonitrile/water phase was evaporated under reduced pressure. The dried residue was resolved in 100 µL H₂O + 0.1% formic acid (FA), transferred to LC vials and stored at -20°C until analysis. All incubations were performed in triplicates.

Incubations of HFO-1123 with hepatic S₉ – enzyme kinetics

To determine *in vitro* kinetics of the GST mediated formation of 1123-GSH, hepatic S₉ subcellular fraction (3 mg protein/mL) of Goettingen[®] Minipigs, NZW Rabbits, rats, mice and humans were incubated with 0.18 mmol (4 mL), 0.27 mmol (6 mL), 0.36 mmol (8 mL), 0.45 mmol (10 mL), 0.53 mmol (12 mL) and 0.89 mmol (20 mL) HFO-1123 injected via a gas-tight syringe into the gas phase of sealed 20 ml GC vials (Supelco[®] Inc, Bellefonte, USA). Incubations (total volume of 1.1 mL) were carried out in the presence of GSH (10 mM) in potassium phosphate buffer (100 mM, pH 7.4, containing 1 mM EDTA). Incubations were carried out in a shaking water bath at 37°C for up to 12 hours. Aliquots were extracted before

the start (prior to the addition of HFO-1123), and at 0, 1, 6 and 12 h after addition of HFO-1123, whereby the 6 h time-point was selected to determine *in vitro* kinetics. Sample workup was performed as described above. All incubations were performed in triplicates.

Incubations of HFO-1123 with hepatic S₉ – sample work-up for ¹⁹F-NMR

To monitor the formation of fluorine containing metabolites in the biotransformation of HFO-1123, hepatic S₉ subcellular fractions (3 mg protein/mL) of Goettingen[®] Minipigs, NZW Rabbits, rats, mice and humans were incubated with 0.89 mmol (20 ml) HFO-1123 in the presence or absence of either a NADPH regenerating system (10 mM NADP, 10 mM glucose-6-Phosphate and 0.5 units/mL glucose-6-phosphate dehydrogenase) or glutathione (10 mM). Incubations were carried out in a shaking water bath at 37°C for 6 h. Aliquots (500 µL) were extracted at beginning (0 h) and at the end (6 h) of the incubation. Reactions were stopped by addition of 0.6 mL acetonitrile and centrifugation at 4°C and 20,000 x g for 15 minutes. The obtained pellet was resolubilized in 0.6 mL acetonitrile and centrifuged (4°C, 20,000 x g, 15 minutes). The supernatants obtained from both centrifugation steps were combined and the acetonitrile/water phase was evaporated under reduced pressure. The dried residue was dissolved in 550 µL D₂O and stored at -20° C until analysis. Immediately before analysis, the solution was transferred to NMR tubes.

4.2.3 β -Lyase mediated biotransformation of 1123-CYS

β -Lyase mediated cleavage of 1123-CYS was determined in renal and hepatic cytosolic fractions of Goettingen[®] Minipigs, NZW Rabbits, rats, mice, and humans. *In vitro* kinetics were determined by a spectrometric 96 well-plate assay and formation of fluorine containing metabolites were monitored by ¹⁹F-NMR.

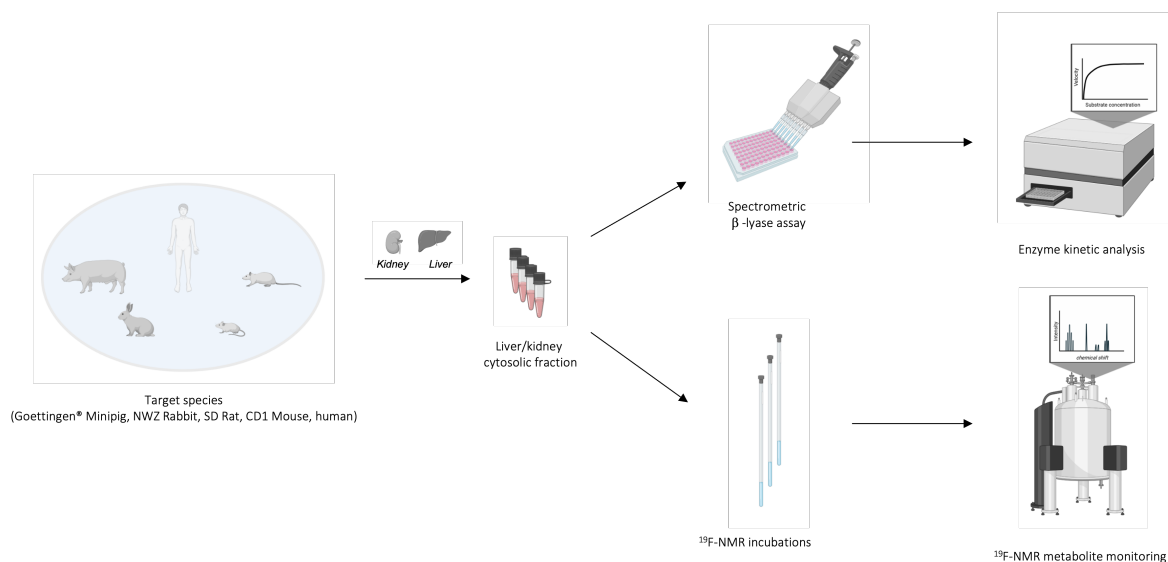


Figure 12 Overview of the experimental approach to determine β -lyase mediated cleavage of 1123-GSH after incubation of HFO-1123 with renal and hepatic cytosolic fractions of Goettingen[®] Minipigs, NZW Rabbits, SD rats, CD1 mice and humans. Figure created with BioRender.com.

Spectrometric β -lyase assay

Cysteine S-conjugates are substrates of β -lyases mediated cleavage, leading to the formation of pyruvate, ammonia and a reactive thionoacyl species, which is frequently responsible for the toxicity of the corresponding cysteine S-conjugate (Cooper and Hanigan, 2018). Pyruvate is produced in the same stoichiometric amount as the thionoacyl species. The amount of pyruvate formed can be quantified indirectly by addition of *D*-lactate dehydrogenase (*D*-LDH), which mediates the conversion of pyruvate to lactate. As reduced nicotinamide adenine dinucleotide (NADH/H⁺) is consumed for this conversion, the concentration of pyruvate formed, respectively cleaved cysteine S-conjugate, can be quantified by monitoring the reduction of a known concentration of NADH/H⁺ (Figure 13). To obtain optimal β -lyase activity, α -keto- γ -(methylthio)-butyrate (KMB) was incorporated into the assay. KMB and other short chain α -ketoacids are known to optimize β -lyase activity of cleavage of several cysteine S-conjugates derived from haloalkenes (Elfarra *et al.*, 1987; Cooper, 1998). An UV/VIS spectrometric assay based on this principle is described in the literature (Lash, 2007). The assay was modified to fit a 96-well plate format and experimental procedures are outlined below.

Table 5 Pipetting scheme for sample and blank incubations used to determine β -lyase mediated cleavage of cysteine *S*-conjugates in cytosolic fractions. Concentrations marked in brackets refer to final concentration per well. Solutions used were prepared in K_2HPO_4/KH_2PO_4 buffer (100 mM, pH 7.4).

Blank	<p>A. 0.05 ml of cytosolic fractions (hepatic, renal; rat, mouse, Goettingen[®] Minipig, NZW Rabbit, human) containing 1 [final concentration 0.5 mg protein/mL], 2 [final concentration 1 mg protein/mL] or 4 mg protein/mL [final concentration 2 mg protein/mL]</p> <p>B. 0.025 mL of 0.4 mM KMB solution [final concentration 0.1 mM]</p> <p>C. 0.025 mL of a 0.4 mM NADH/H⁺ solution [final concentration 0.1 mM] 1 μL of a 10 units/mL D-LDH solution [final concentration 0.1 units/mL]</p>
Sample	<p>A. 0.05 ml of cytosolic fraction (hepatic, renal; rat, mouse, Goettingen[®] Minipig, NZW Rabbit, human) containing 1 [final concentration 0.5 protein mg/mL], 2 [final concentration 1 protein mg/mL] or 4 mg protein/mL [final concentration 2 protein mg/mL]</p> <p>B. 0.025 mL of either 2, 4, 8, 12, 16 or 20 mM cysteine <i>S</i>-conjugate [final concentrations 0.5 mM, 1, 2, 3, 4, 5 mM] in 0.4 mM KMB [final concentration 0.1 mM]</p> <p>C. 0.025 mL of a 0.4 mM NADH/H⁺ solution [final concentration 0.1 mM]</p> <p>D. 1 μL of a 10 units/mL D-LDH solution [final concentration 0.1 units/mL]</p>

After homogenization, the decrease in absorbance ($A_{340\text{ nm}}$) at a wavelength of 340 nm was measured for 20 minutes. Decrease in $A_{340\text{ nm}}$ of the blank incubations were subtracted from decrease in $A_{340\text{ nm}}$ of the samples. The amount of pyruvate formed was calculated using a calibration curve prepared as described below. To confirm β -lyase dependent cleavage of 1123-CYS, some incubations were performed in the presence of the β -lyase inhibitor AOAA (0.625 mM).

Calibration curves were established as following: Pyruvate standard solutions (0, 0.005, 0.01, 0.025, 0.05 mM) were mixed with a NADH (0.1 mM) solution (final volume of 0.1 mL). The solution was homogenized and the absorbance ($A_{340\text{ nm}}^{\text{start}}$) was measured. After addition of 1 μ L of D-LDH (0.1 units/mL), the solution was homogenized and the absorbance ($A_{340\text{ nm}}^{\text{end}}$) was recorded (after being stable for one minute). Subtracted of $A_{340\text{ nm}}^{\text{end}}$ from $A_{340\text{ nm}}^{\text{start}}$ results in absorbance values which correspond to the amount of oxidized NADH and thus converted pyruvate. Unknown pyruvate concentrations were determined by linear equation (R^2 -values of calibration curves need to be ≥ 0.99).

¹⁹F-NMR based analysis of fluorine containing metabolites

To study fluorine metabolite formation, 1123-CYS (5 mM) containing KMB (0.1 mM) was incubated with human, SD rat, NZW Rabbit and Goettingen[®] Minipig renal and hepatic cytosol (5 mg protein/mL) in a final volume of 1 mL. Incubations were performed for 60 min at 37°C in a shaking water bath. To monitor β -lyase dependent cleavage of 1123-CYS, some incubations were performed in the presence of AOAA (5 mM). 0.5 mL aliquots were extracted at 0 and 60

min after the start of the reaction. For sample workup, aliquots were placed on ice and immediately centrifuged at 164,000 $\times g$ and 4°C for 30 minutes. D₂O was added to the supernatants, yielding a total volume of 0.8 mL. Until analysis, samples were stored at -80°C. During method development several modified sample workup procedures were performed with the extracted aliquots and analysed by ¹⁹F-NMR. The aim of these modified sample workup procedures was to effectively stop the enzymatic reaction at the end of the incubation period without producing artefacts in the NMR-spectra to allow identification of fluorine containing metabolites formed via the β -lyase reaction. A summary of all sample workup procedures is outlined in Appendix A, Table A.1.

4.3 Analytical methods

4.3.1 ¹⁹F-NMR

¹⁹F – NMR spectra for *in vitro* biotransformation studies were recorded in D₂O at 25 °C on a Bruker 500 MHz NMR spectrometer (Bruker Corporation, Billerica, USA) equipped with a 5 mm BB/H&F Prodigy Cryoprobe operating at 470.59 MHz. ¹⁹F chemical shifts were referenced to external CFCl₃. The acquisition time was set to 0.799 sec and 5120 scans were recorded. Spectral processing was performed with 0.05 Hz line broadening. ¹⁹F-NMR spectra were acquired without proton decoupling and a spectral width of 212.5 ppm (-33.4 to -245.9 ppm).

Characterization of 1123-GSH synthesis product was performed with ¹H-, ¹⁹F-, ¹⁹F{¹H}-; ¹⁹F-, ¹⁹F COSY-; ¹⁹F,¹H HMQC-, ¹³C{¹H}-, ¹³C DEPT135-, ¹³C DEPT90-, ¹³C{¹⁹F}-, ¹³C-,¹⁹F HMQC-, ¹H,¹H COSY-, ¹³C,¹H HSQC-, ¹³C,¹H HMBC-, ¹H- with water suppression and ¹H DOSY-NMR on a Bruker 400 MHz or 500 MHz NMR spectrometer (Bruker, Corporation, Billerica, USA).

Before analysis, accurate baseline correction and spectra phasing was performed. NMR spectra were analyzed with TopSpin 4.1.1 software (Bruker Corporation, Billerica, USA) for MAC OS 11.5.2. To describe NMR spectra the following abbreviations were used: s = singlet, d = doublet, t = triplet, dd = doublet of doublets, m = multiplet.

4.3.2 Liquid chromatography coupled with mass spectrometry (LC-MS/MS)

LC–MS/MS analyses were performed on an Agilent 1100 series LC coupled to an API2000/Q-Trap mass spectrometer (Applied Biosystems/MDS Sciex, Darmstadt, Germany). Samples were injected into the LC–MS/MS system through an Agilent 1100 series autosampler. Separations were carried out on a ReproSil-Pur C18 AQ column (2 mm \times 150 mm, 5 μ m; Dr. Maisch; Ammerbuch, Germany). Gradient elution was carried out with water + 0.1% formic acid (FA) (solvent A) and acetonitrile + 0.1% FA (solvent B). Initially, solvent A was held isocratic for 5 min at 100%, followed by a linear gradient to 95% B in 5 min. These conditions were held for further 5 min. Within 1 min, the gradient decreased linearly to 0% B and remained



at initial conditions until the end of analysis (30 min). A flow rate of 0.2 mL/min was used. For each run, 10 μ L of the respective sample were injected by the autosampler. The API 2000/Q-Trap mass spectrometer was operated with a Turbo Ion Spray source in negative or positive ion mode with a voltage of -4000 V. Spectral data were recorded with N₂ as the heater gas at 450°C and as the collision gas (CAD = -2) in multiple reaction monitoring mode (MRM). HFO-1123 derived metabolites and other monitored ions as well as their *m/z* transitions are summarized in Table 6.

Enhanced product ion spectra for *m/z* 390.1 (1123-GSH), *m/z* 246.2 (1123-CYS-NAc) and *m/z* 203.8 (1123-CYS) were recorded over the range of *m/z* 100–500 amu on an API 2000/Q-Trap mass spectrometer operating in negative or positive ion mode. The collision gas was N₂ at CAD = 2, and the collision energy was 30 V.

Method validation parameters such as limit of detection (LOD) and quantification (LOQ) were determined according to European Commission Regulation 657/2002/EC (E.U, 2002). The LOD and LOQ of 1123-GSH, MFA and the LOD of 1123-CYS were determined by serial dilution of S₉ subcellular fractions spiked with 1123-GSH, 1123-CYS or MFA. LODs and LOQs were obtained using a signal-to-noise (S/N) ratio of 3:1 and 7:1, respectively. **1123-GSH** – LOD: 0.013 μ M (5 ng/mL), LOQ: 0.025 μ M (10ng/mL); **1123-CYS** – LOD: 0.005 μ M (1 ng/mL); **MFA** – LOD: 0.5 μ M (40 ng/mL); LOQ: 1 μ M (80 ng/mL). Calibration for 1123-GSH was linear in the range from 10 ng/mL to 800 ng/mL.

Table 6 Mass spectrometer settings Q1 (m/z), Q3 (m/z) and Collision Energy (V) used for LC-MS/MS analyses

Analyte	Q1 (m/z)	Q3 (m/z)	Collision Energy (V)
Positive ionization			
<i>S</i> -(1,1,2-trifluorethyl)- <i>L</i> -glutathione (1123-GSH)	390.1	221.0	23
	390.1	175.0	30
	390.1	118.2	47
<i>trans</i> -(1,2-difluorethenyl)- <i>L</i> -glutathione (1123-GSH derivate)	370.1	241.1	30
	370.1	138.1	30
	370.1	118.1	30
<i>S</i> -(1,1,2-trifluorethyl)- <i>L</i> -cysteine (1123-CYS)	203.8	118.1	21
	203.8	164.0	13
<i>S</i> -(1,2-dichlorovinyl)- <i>L</i> -glutathione (DCVG) ¹	402.0	272.8	19
	402.0	255.8	23
	402.0	169.9	29
<i>N</i> -acetyl- <i>S</i> -(1,1,2-trifluorethyl)- <i>L</i> -cysteine (1123-CYS-NAc)	246.2	163.9	13
	246.2	118.0	21
Negative ionization			
Monofluoroacetic acid (MFA)	77.1	77.1	-15
	77.1	57.0	-15

¹used for method validation

4.4 Cell culture experiments

Cell culture experiments were carried out in collaboration with Johanna Serban, who was responsible for tissue culture maintenance, cell treatment and cytotoxicity testing. Raphael Dekant provided purified 1123-CYS and established the LC-MS/MS method for analysis of cellular citrate. Data acquisition and data analysis were performed by Raphael Dekant.

4.4.1 Cell culture properties

Cell viability and cellular citrate levels were determined in proximal tubular cell cultures of pigs (LLC-PK1 cell line), rats (NRK-52E cell line) and humans (HK-2 cell line) exposed to 1123-CYS. HK-2, NRK-52E and LLC-PK1 cells were obtained from the European Collection of Cell Cultures (Porton Down, England) and the American Type Culture Collection (Manassas, USA). Cells were cultured in Corning® T75 cell culture flasks (Sarstedt AG, Nürmbrecht, Germany) under standard cell culture conditions (37°C, 5% CO₂). Cell culture media and supplements are listed in Table 7. Composition of cell-specific media are listed in Table 8.

Table 7 List of cell culture media and supplements

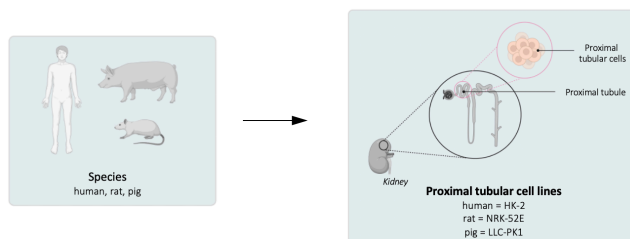
Cell culture media and supplements	Supplier
Dulbecco's Modified Eagle's Medium (DMEM)/Nutrient Mixture F-12 Ham F12	Sigma-Aldrich, Taufkirchen, Germany
Fetal bovine serum superior (FBS)	Merck Millipore, Darmstadt, Germany
GlutaMAX™-I	ThermoFisher Scientific, GmbH, Dreieich, Germany
Penicillin / Streptomycin	Sigma-Aldrich, Taufkirchen, Germany
HEPES	Sigma-Aldrich, Taufkirchen, Germany
Gibco™ MEM Non-Essential Amino Acids Solution (NEAA)	ThermoFisher Scientific, GmbH, Dreieich, Germany

Table 8 Origin of proximal tubular kidney cells and composition of cell-specific culture media

Cell Line	HK-2	NRK-52E	LLC-PK1
Origin	Human kidney immortalized by transduction with human papilloma virus 16 (HPV-16) E6/E7 genes	Rat (rattus norvegicus)	Pig (sus scrofa)
Cell-specific Medium	<ul style="list-style-type: none"> • DMEM/Nutrient Mixture F-12 Ham F12 (1:1) with 3.15 g/L glucose • 10% FBS • 1% Penicillin / Streptomycin • 2 mM GlutaMAX™-I 	<ul style="list-style-type: none"> • DMEM with 4.5 g/L glucose • 10% FBS • 1% Penicillin / Streptomycin • 1% GlutaMAX™-I • 1% NEAA 	<ul style="list-style-type: none"> • DMEM with 1.0 g/L glucose • 10% FBS • 1% Penicillin / Streptomycin • 1% GlutaMAX™-I • 25 mM HEPES

Figure 14 exhibits a summary of cell cultures used as well as an experimental overview of performed investigations. Experimental details are outlined below.

A. Proximal tubular cell lines



B. Cell culture investigations

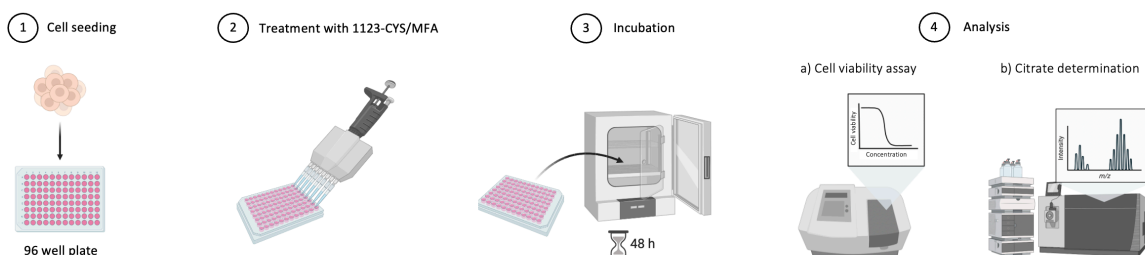


Figure 14 Cell systems (A) and cell culture investigations (B) used to evaluate cytotoxicity and cellular citrate which may arise from β -lyase mediated cleavage of 1123-CYS to MFA and subsequent inhibition of aconitase. Cell viability (4a) and cellular citrate levels (4b) after 1123-CYS exposure were determined in porcine, human and rat proximal tubular cells.

4.4.2 Cell Viability

Cells were seeded into 96-well plates at a density of 0.01×10^6 cells and allowed to grow to 90-100% confluency for 48h. To determine cytotoxicity of 1123-CYS, cells were then treated with 1123-CYS at 0, 39.1, 78.1, 156.3, 312.5, 625, 1,250, 2,500, 5,000 and 10,000 μM in the presence (0.125 mM for HK-2 and NRK-52E and 0.25 mM for LLC-PK1 cells) and absence of AOAA for 48h under standard cell culture conditions (37°C , 5% CO_2). Cytotoxicity of MFA was studied after incubation of cells with MFA at 0, 0.5, 1.4, 4.1, 12.3, 37.0, 111.1, 333.3, 1,000, 3,000 and 9,000 μM for 48h. Treatment solutions were prepared by serial dilution of stock solutions of 1123-CYS (10,000 μM) and MFA (9,000 μM) in cell-specific culture media. After treatment, cell viability was determined using the CellTiter-Glo[®] Luminescent Cell Viability Assay (Promega, Fitchburg, USA) according to the manufacturer's instructions. Each assay was performed in three independent experiments carried out in triplicates.

4.4.3 Quantitation of citrate

To determine effects of 1123-CYS and MFA on concentrations of cellular citrate, cells were seeded in 48-well plates at a density of 0.03×10^6 and allowed to grow to 90-100% confluency for 48h. Cells were then treated with MFA at 0, 0.01, 1 and 3 mM or 1123-CYS at 0, 0.1, 0.3, 1 and 3 mM for 48h under standard cell culture conditions (37°C, 5% CO₂). After treatment, cell supernatants were transferred into 1.5 mL reaction vials and were centrifuged (10 min, 4°C, 972 x g). The supernatants were discarded and the pellet was kept at 0°C until further processing. To the adherent cells remaining in the 48 well-plate, 0.2 mL of Pierce™ IP Lyse Buffer (Thermo Fisher Scientific Inc., Waltham, USA) was added and cells were lysed for 15 minutes. The cell lysates were then transferred into the 1.5 mL reaction vials containing the pellet. After centrifugation at 13.000 x g for 10 min and 4°C, the supernatants were removed and the protein concentration was determined using the Pierce™ BCA Protein Assay Kit (Thermo Fisher Scientific Inc., Waltham, USA) following manufacturer's instructions. The protein concentration of the samples was adjusted to 0.5 mg protein/mL by diluting with H₂O. To 0.1 mL of the diluted cell lysates 0.15 ml acetonitrile was then added and the samples were centrifuged twice at 20.000 x g and 4°C for 10 minutes to precipitate protein. The supernatants were removed and dried at reduced pressure. The remaining dry material was dissolved in 0.1 mL H₂O + 0.1% formic acid, transferred into LC vials and immediately analyzed by LC-MS/MS.

4.4.4 LC-MS/MS method to determine citrate levels

LC-MS/MS analyses were performed on an Agilent 1100 series LC coupled to an API2000/Q-Trap mass spectrometer (Applied Biosystems/MDS Sciex, Darmstadt, Germany). Samples were injected into the LC-MS/MS system through an Agilent 1100 series autosampler. Separations were carried out on a ReproSil-Pur C18 AQ column (2 mm x 150 mm, 5 µm; Dr. Maisch; Ammerbuch, Germany). Gradient elution was carried out with water + 0.1% formic acid (FA) (solvent A) and acetonitrile + 0.1% FA (solvent B). Initially, solvent A was held isocratic for 5 min at 100%, followed by a linear gradient to 95% B in 5 min. These conditions were held for further 5 min. Within 1 min, the gradient decreased linearly to 0% B and remained at initial conditions until the end of analysis (30 min). A flow rate of 0.2 mL/min was used. For each run, 10 µL of the respective sample were injected by the autosampler. The API 2000/Q-Trap mass spectrometer was operated with a Turbo Ion Spray source in negative ion mode with a voltage of -4000 V. Spectral data were recorded with N₂ as the heater gas at 450°C and as the collision gas (CAD = -2) in multiple reaction monitoring mode (MRM). Characteristic fragments of citrate (qualifier: 191/111 Da, quantifier: 191/87 Da) were analyzed with a collision energy of -30 V. The LOD (0.05 µM; 10 ng/mL) and LOQ (0.4 µM, 70 ng/mL) of citrate were determined by serial dilution of whole cell lysate spiked with citrate. A signal-to-noise (S/N)

ratio of 3:1 and 7:1 was used to determine LOD and LOQ, respectively. Calibration for citrate was linear from 100 ng/mL to 1000 ng/mL.

4.4.5 Statistical analysis

The one-way ANOVA followed by Dunnett's post hoc test was used to determine statistically significant changes in citrate levels of MFA/1123-CYS treated cells compared to untreated controls (Confidence interval: 95%; P-values: $p < 0.05$ (*), $p < 0.01$ (**), $p < 0.001$ (***)). GraphPad Prism version 9.1.2 (GraphPad Software, San Diego, USA) for Mac OS 11.5.2 was used for calculations.

5 Results

5.1 GST dependent biotransformation of HFO-1123

5.1.1 Purity assessment of 1123-GSH by quantitative ^{19}F -NMR

Following chemical synthesis, 1123-GSH was purified by HPLC-DAD and purity was assessed by one- and two-dimensional ^1H -, ^{13}C - and ^{19}F -NMR. While ^1H -, ^{13}C - and ^{19}F -NMR confirmed successful synthesis of 1123-GSH (Figure 15; Appendix B, Figures B.3 — B.6), another fluorine containing GSH conjugate was detected. Chemical shifts and coupling constants suggest that signals correspond to *S-trans*-(1,2-difluoroethenyl)-*L*-glutathione. Figure 15 shows the quantitative ^{19}F -NMR of the purified product of 1123-GSH synthesis. Quantitative spectral analysis revealed a ratio of 1:0.875 for 1123-GSH: *S-trans*-(1,2-difluoroethenyl)-*L*-glutathione. Due to the similar chemical structure of 1123-GSH and *S-trans*-(1,2-difluoroethenyl)-*L*-glutathione, separation of both compounds by preparative HPLC was not possible.

However, the ratio of 1123-GSH to *S-trans*-(1,2-difluoroethenyl)-*L*-glutathione enabled determination of the amount of 1123-GSH in the mixture obtained by HPLC. The dried mixture obtained by HPLC was resolved in water to give a 1123-GSH stock solution with a concentration of 1 mg/mL based on the ratio of 1123-GSH to *S-trans*-(1,2-difluoroethenyl)-*L*-glutathione obtained by quantitative ^{19}F -NMR. Calibration solutions for LC-MS/MS quantitation of 1123-GSH were prepared by serial dilution from this 1123-GSH stock solution.

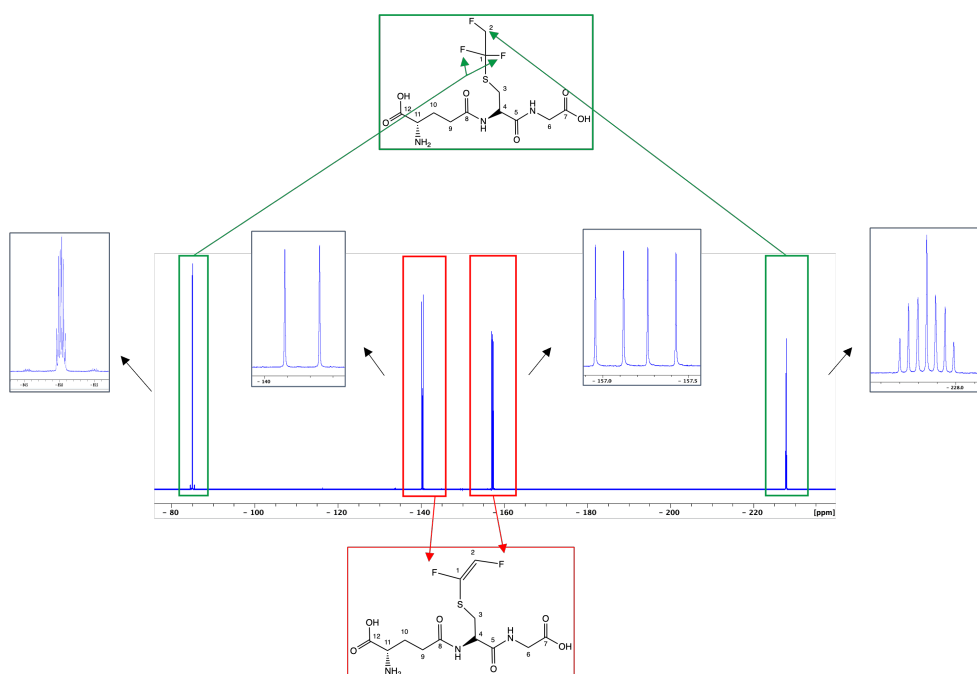


Figure 15 ^{19}F -NMR analysis of the purified 1123-GSH synthesis product. Besides 1123-GSH ($\delta = -85.0$ ppm, m; $\delta = -227.8$ ppm, m), a second GSH conjugate was found to be present. Chemical shifts and coupling constants suggest that this corresponds to *S-trans*-(1,2-difluoroethenyl)-*L*-glutathione ($\delta = -140.0$ ppm, d; $\delta = -157.2$ ppm, dd). Quantitative analysis revealed a ratio of 1:0.875 for 1123-GSH:trans-(1,2-difluoroethenyl)-*L*-glutathione.

5.1.2 Preliminary experiments to verify the experimental approach

To evaluate the suitability of the *in vitro* incubation system to determine the formation of 1123-GSH in incubations of hepatic S₉ fractions and HFO-1123, initial *in vitro* incubations were performed with trichloroethylene (TRI). TRI is a substrate for GST mediated biotransformation leading to S-(1,2-dichlorovinyl)-L-glutathione (DCVG) as main metabolite (Capinha *et al.*, 2021).

Figure 16 shows the LC-MS/MS chromatograms of the time-dependent formation of DCVG in mouse, rat, human and Goettingen[®] Minipig hepatic S₉ incubated with TRI (1 mM). Increased formation of DCVG (R_t: 13.58-14.21 min) was observed in incubations of mouse and rat hepatic S₉ compared to human and Goettingen[®] Minipig fractions. This is in line with published data suggesting increased formation of DCVG in rat compared to human subcellular fractions (Green *et al.*, 1997; Capinha *et al.*, 2021). Data for Goettingen[®] Minipig and mouse subcellular fractions are not available in the literature. Furthermore, two signals detected in incubations with rat and mouse S₉ fractions indicate formation of DCVG positional isomers, consistent with literature (Dekant *et al.*, 1990; Capinha *et al.*, 2021). Only one of the two positional isomers was found in human and Goettingen[®] Minipig S₉ fractions, possibly due to low signal intensity and coelution of the positional isomers.

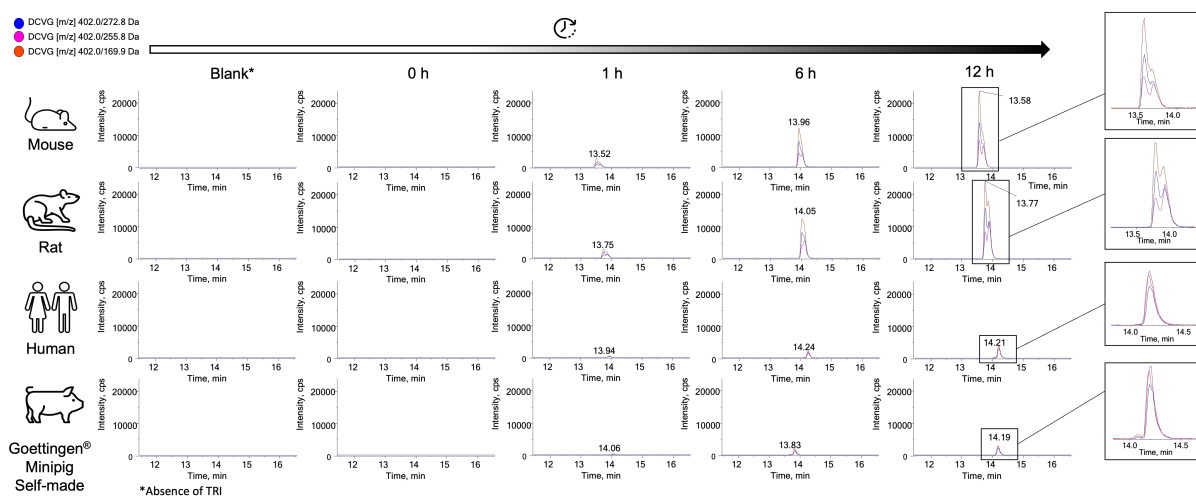


Figure 16 LC-MS/MS chromatograms showing time-dependent formation of DCVG in mouse, rat, human and Goettingen[®] Minipig hepatic S₉ after incubation with TRI (1 mM).

To verify the suitability of S₉ fractions prepared in-house, commercially available Goettingen[®] Minipig hepatic S₉ fractions were also incubated with HFO-1123 and formation of 1123-GSH was quantified. Quantification of 1123-GSH formation in *in-house prepared vs. purchased* Goettingen[®] Minipig S₉ fraction showed no significant differences between both S₉ fractions and thus confirmed the suitability of the S₉ fractions prepared in-house (Figure 17).

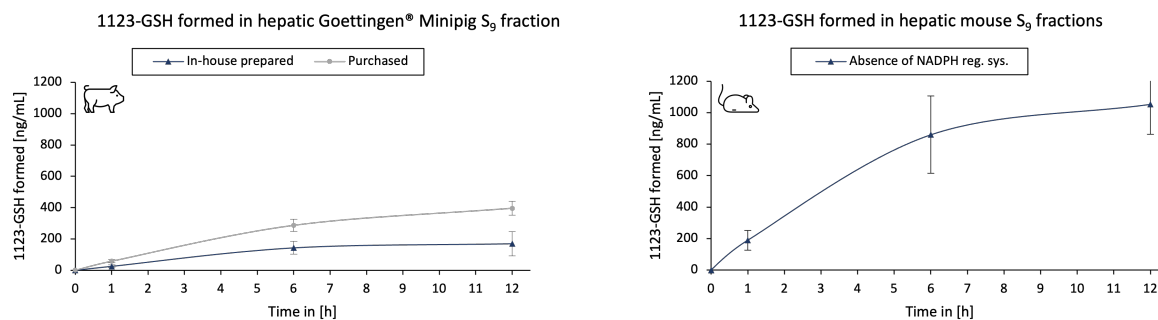


Figure 17 Comparison of 1123-GSH formation in purchased vs. in-house prepared Goettingen® Minipig S₉ (left graph) and mouse hepatic S₉ (right graph), showing no significant differences in the activity of 1123-GSH formation between both Goettingen® Minipig S₉, thus confirming the suitability of S₉ prepared in-house for further investigations.

These preliminary experiments demonstrate the suitability of the experimental set-up to investigate GST mediated biotransformation of HFO-1123 in S₉ fractions.

5.1.3 Time-dependent formation of 1123-GSH in liver S₉ incubated with HFO-1123

Formation of 1123-GSH in Goettingen[®] Minipig, NZW Rabbit, human, rat and mouse hepatic S₉ fractions incubated with 0.4 mmol HFO-1123 in the presence of GSH and a NADPH regenerating system or in the absence of the NADPH regenerating system was monitored for 1, 6 and 12h. Generally, significantly lower amounts of 1123-GSH were detected in the presence as compared to the absence of the NADPH regenerating system, indicating increased CYP-450 mediated biotransformation in the presence of the NADPH regenerating system (Figure 18, Table 9). In the absence of the NADPH regenerating system, 1123-GSH formation was significantly increased in mouse, rat and NZW Rabbit hepatic S₉ fractions as compared to human and Goettingen[®] Minipig fractions. These results suggest increased GST mediated formation of 1123-GSH in rat, mouse and NZW Rabbit compared to human and Goettingen[®] Minipig hepatic S₉ fraction.

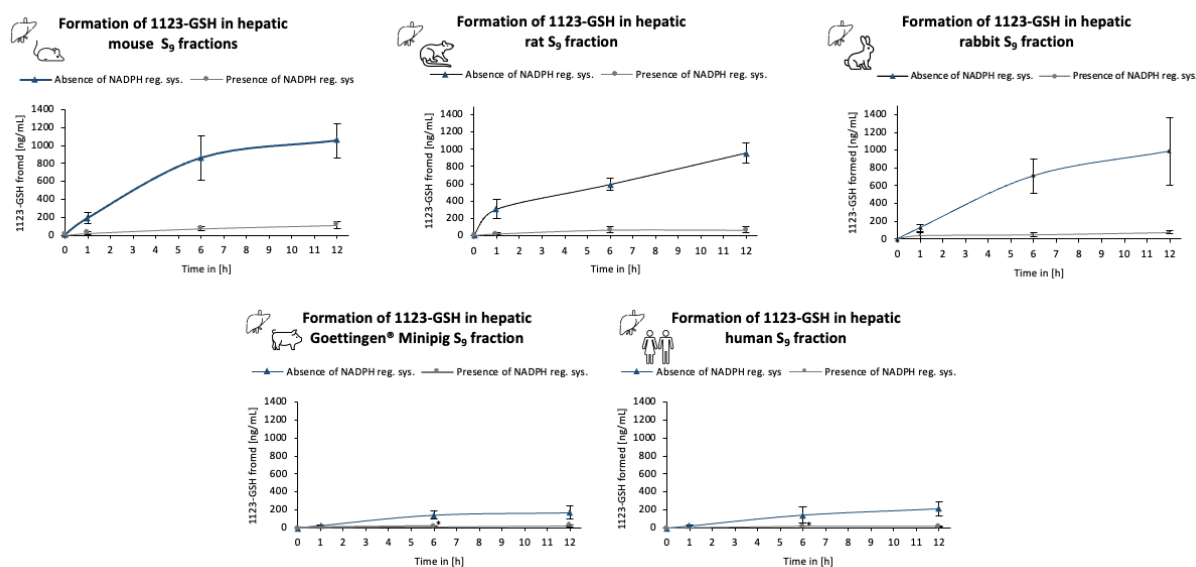


Figure 18 Time-dependent formation of 1123-GSH (ng/mL) in hepatic S₉ fractions of mice, rats, NZW Rabbits, Goettingen[®] Minipigs and humans in the presence (marked in grey) or absence (marked in blue) of the NADPH regenerating system. Results are presented as mean \pm standard deviation of three independent experiments.

Table 9 Concentration of 1123-GSH (ng/mL) formed after incubation of mouse, rat NZW Rabbit, Goettingen[®] Minipig and human hepatic S₉ fractions with 0.4 mmol HFO-1123. Results are presented as mean ± standard deviation (n = 3).

	Mouse	Rat	NZW Rabbit	G. Minipig	Human
Absence of NADPH reg. sys.					
1h	188.9 ± 63.2	305.4 ± 112.1	124.9 ± 38.5	25.4 ± 9.0	21.6 ± 6.3
6h	859.7 ± 245.3	593.4 ± 65.8	710.6 ± 192.9	143.5 ± 41.2	143.2 ± 85.6
12h	1053.3 ± 189.8	960.2 ± 118.0	986.9 ± 379.7	169.9 ± 77.4	214.0 ± 78.6
Presence of NADPH reg. sys.					
1h	22.3 ± 14.0	19.5 ± 11.4	38.2 ± 30.4	10 (LOQ)*	10 (LOQ)*
6h	74.3 ± 18.0	66.4 ± 31.7	48.8 ± 18.2	11.3 ± 2.2**	11.6 ± 1.8**
12h	112.1 ± 37.6	65.5 ± 35.0	76.7 ± 22.1	19.8 ± 8.3	14.8 ± 4.9

*To calculate 1123-GSH concentrations below the LOQ, the upper bound approach was used. Results below the LOQ were replaced by the numeric value of the LOQ (10 ng/mL).

**1123-GSH concentration of one replicate was above the LOQ, in the other replicates below the LOQ (10 ng/mL). Calculation was performed based on upper bound approach.

5.1.4 *In vitro* kinetics of GST mediated formation of 1123-GSH after incubating hepatic S₉ fractions with HFO-1123

In vitro kinetics of GST mediated 1123-GSH formation in hepatic S₉ fractions incubated with different amounts of HFO-1123, ranging from 4 mL up to 20 mL for 6 h, were assessed to characterize enzyme parameters (K_M and V_{MAX}) of GST mediated formation of 1123-GSH. As can be seen from the velocity of 1123-GSH formed [ng (1123-GSH)/mL/h] plotted against the amount of HFO-1123 in the gas phase (Figure 19), significantly higher rates of 1123-GSH formation were detected in NZW Rabbit followed by rat and mouse hepatic S₉ fractions. The lowest velocity of 1123-GSH formation was detected in human and Goettingen[®] Minipig hepatic S₉ fractions, indicating increased GST mediated biotransformation of HFO-1123 in NZW Rabbit, rat and mouse compared to Goettingen[®] Minipig and human hepatic S₉.

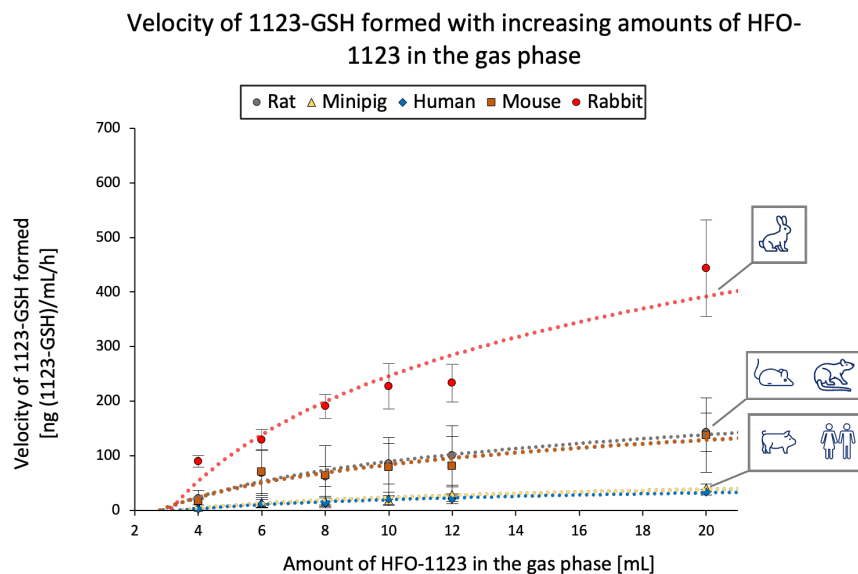


Figure 19 Velocity of 1123-GSH formed (ng 1123-GSH/mL/h) in hepatic S₉ fractions of mice, rats, NZW Rabbits, Goettingen[®] Minipigs and humans after incubation with HFO-1123 (4, 6, 8, 10, 12, 20 mL) in the gas phase. Results are presented as mean ± standard deviation (n = 3).

Due to the relatively low amounts of 1123-GSH formed at low HFO-1123 concentrations in the gas phase, plots to derive K_M and V_{MAX} did however not show the required linearity to reliably determine K_M and V_{MAX} .

5.1.5 Species-differences in 1123-CYS formation in hepatic S₉ fractions after incubation with HFO-1123

Incubations with hepatic S₉ fractions (Goettingen[®] Minipig, NZW Rabbit, human, rat, mouse) and 20 mL HFO-1123 performed during analysis of *in vitro* kinetics of GST mediated formation of 1123-GSH were also analyzed for formation of 1123-CYS to determine the extent of 1123-GSH cleavage to 1123-CYS by hepatic S₉.

Consistent with previous experiments, 1123-GSH was formed at significantly higher rates (6 to 10-fold) in NZW Rabbit, rat and mouse hepatic S₉ as compared to Goettingen[®] Minipig and human hepatic S₉ (Figure 20). 1123-CYS was not detected in incubations with rat and mouse S₉. In contrast, signals corresponding to 1123-CYS were detected in human and Goettingen[®] Minipig hepatic S₉, despite the lower rate of 1123-GSH formation. NZW Rabbit hepatic S₉ showed increased formation of both 1123-GSH and 1123-CYS compared to other species (Figure 20). This may indicate an increased cleavage of 1123-GSH to 1123-CYS in NZW Rabbit, human and Goettingen[®] Minipig compared to rat and mouse hepatic S₉.

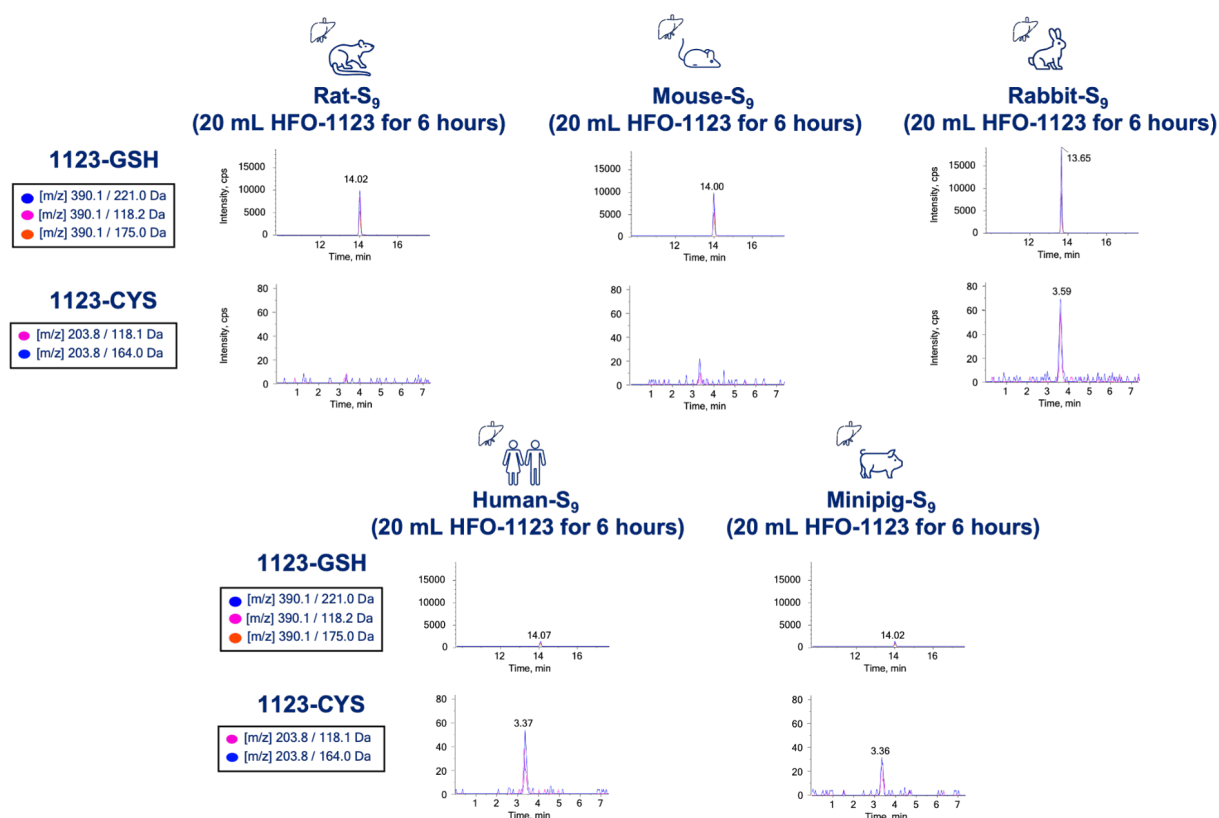


Figure 20 LC/MS-MS analysis of 1123-GSH and 1123-CYS formed in 6h-incubations of 20 mL HFO-1123 with hepatic S₉ fractions (rat, mouse, NZW Rabbit, human, and Goettingen[®] Minipig). Representative LC-MS/MS chromatograms are shown. The complete dataset is available in Appendix B, Figure B.8.

5.1.6 Impact of γ -GT and β -lyase inhibition on GSH dependent biotransformation of HFO-1123 in hepatic S₉

Since γ -GT has a key role in processing of GSH conjugates, it was further evaluated if species-differences in γ -GT activity towards 1123-GSH formed in hepatic S₉ fractions, resulting in 1123-CYS formation, may contribute to the species-differences in HFO-1123 toxicity. Acivicin, an inhibitor of mammalian γ -GT (Gardell and Tate, 1980), was used to evaluate the extent of γ -GT mediated cleavage of 1123-GSH formed in NZW Rabbit, rat, mouse, human and Goettingen[®] Minipig hepatic S₉ fractions incubated with HFO-1123. Figure 21 displays the amounts of 1123-GSH formed in hepatic S₉ of the target species in the presence and the absence of acivicin.

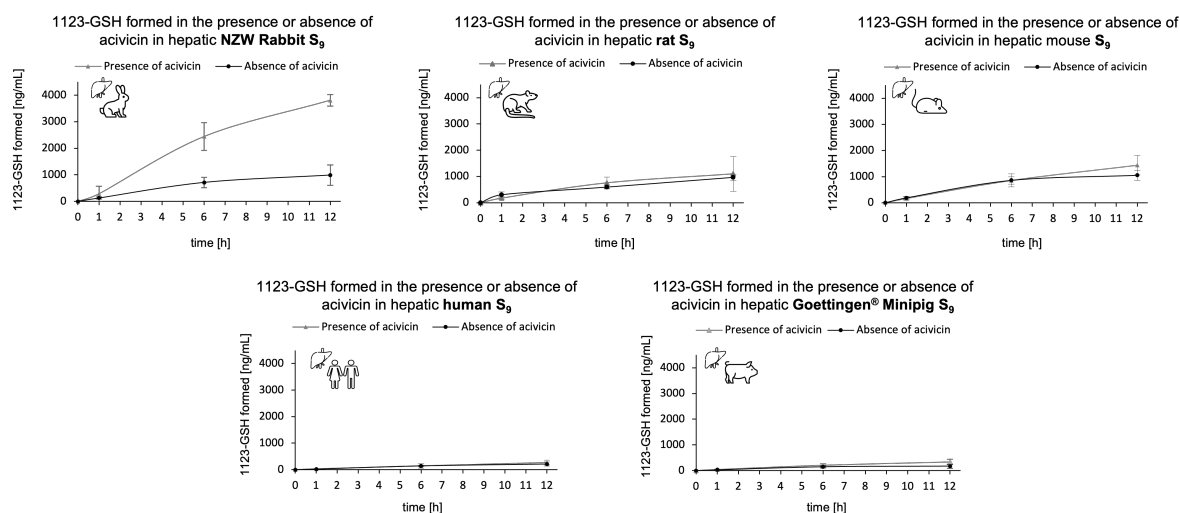


Figure 21 Time-dependent formation of 1123-GSH (ng/mL) in hepatic S₉ fractions of mice, rats, NZW Rabbits, Goettingen[®] Minipigs and humans in the presence or absence acivicin. Results are presented as mean ± standard deviation (n = 3).

While acivicin had no significant effect on the concentration of 1123-GSH in rat, mouse, human and Goettingen[®] Minipig hepatic S₉ incubated with HFO-1123, an increase in 1123-GSH formation was detected in the presence of acivicin in NZW Rabbit hepatic S₉ (Figure 21). This indicates increased γ -GT mediated cleavage of 1123-GSH in NZW Rabbit hepatic S₉ compared to the other species. However, as judged by relative signal intensities, γ -GT mediated cleavage of 1123-GSH was not paralleled by an increase in the concentration of 1123-CYS. This suggests either that the extent of the second enzymatic step in the processing of 1123-GSH to its corresponding cysteine S-conjugate, i.e. dipeptidase/aminopeptidase mediated cleavage of the cysteinylglycine conjugate, is low, or alternatively that any 1123-CYS formed is rapidly cleaved by β -lyases.

To assess if 1123-CYS formed from 1123-GSH is readily cleaved via β -lyase activity of S₉, Goettingen[®] Minipig, NZW Rabbit, mouse, rat, and human hepatic S₉ fractions were incubated with HFO-1123 (0.04 mmol/8.8 mL) in the presence and absence of aminoxy acetic acid (AOAA), an inhibitor of β -lyases.

Intensities of LC-MS/MS signals corresponding to 1123-CYS ([m/z]: 203.18/118.1 Da, 203.18/164.0 Da) obtained from incubations in the presence of AOAA were compared to those obtained in the absence of AOAA.

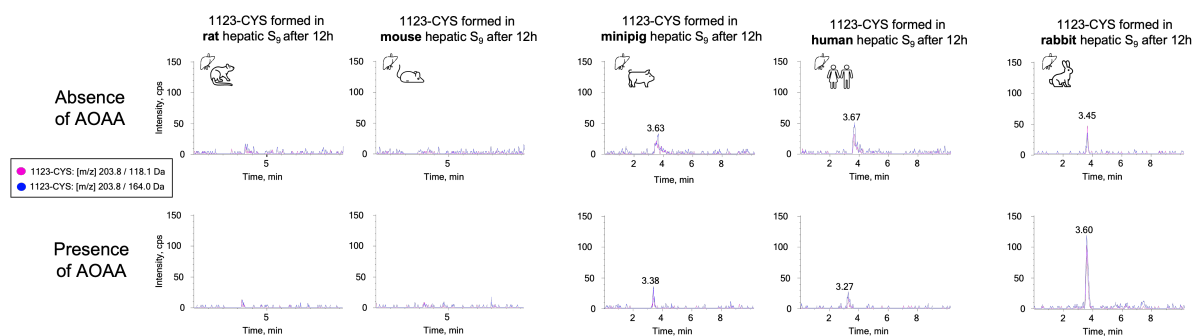


Figure 22 LC-MS/MS analysis of 1123-CYS ([m/z]: 203.18/118.1 Da, 203.18/164.0 Da) in 12h-incubations of hepatic S₉ of rats, mice, Goettingen[®] Minipigs, humans and NZW Rabbits with HFO-1123. Representative LC-MS/MS chromatograms are shown. The complete dataset is available in Appendix B, Figure B.9.

In incubations of rat and mouse hepatic S₉ fractions, no signals corresponding to 1123-CYS above the LOD (1 ng/mL) were detected either in the presence or absence of AOAA (Figure 22). Incubations of Goettingen[®] Minipig and human hepatic S₉ revealed signal intensities of 1123-CYS close to the LOD (1 ng/mL) independent of the presence or absence of AOAA (Figure 22). In contrast, a significant increase in 1123-CYS signal intensity was found in incubations with NZW Rabbit S₉ in the presence of AOAA (S/N-ratio: 12/1) as compared to its absence (S/N-ratio: 3/1), indicating AOAA mediated inhibition of β -lyase cleavage of 1123-CYS. These findings suggest a slightly increased β -lyase activity towards 1123-CYS in NZW Rabbit hepatic S₉ fractions compared to hepatic S₉ of the other species investigated.

5.1.7 Time-dependent formation of fluorine containing metabolites after incubation of hepatic S₉ fractions with HFO-1123 by ¹⁹F-NMR

While 1123-GSH, which was analyzed by LC-MS/MS, is expected to be the major metabolite formed by GST mediated metabolism of HFO-1123, it is also possible that other potentially toxic metabolites may be formed during GST mediated metabolism. Thus, incubations of hepatic S₉ and HFO-1123 were screened by ¹⁹F-NMR to identify any fluorine containing metabolites formed. To this end, Goettingen[®] Minipig, NZW Rabbit, mouse, rat and human hepatic S₉ fractions were incubated in the presence or absence of GSH or a NADPH regenerating system with HFO-1123 for up to 6 hours and screened for fluorine containing metabolites by ¹⁹F-NMR.

Consistent with LC-MS/MS analysis showing increased 1123-GSH formation in rat and NZW Rabbit hepatic S₉ compared to S₉ of other species, ¹⁹F-NMR-signals corresponding to 1123-GSH ($\delta = -85.1$ ppm, m) were detectable only in hepatic rat and NZW Rabbit S₉ fractions in the presence of GSH (Figure 23). In contrast to synthesized 1123-GSH, which is characterized by two signals ($\delta = -85.0$ ppm, m; $\delta = -227.9$ ppm, m) corresponding to the C₁ fluorine atoms and the C₂ fluorine atom, respectively (Figure 15), only the signal corresponding to the C₁ bound fluorine atoms was detected in the S₉ incubations, with signal intensities close to the limit of

detection. The absence of the signal corresponding to the C₂ bound fluorine atom may thus be explained by the lower sensitivity of ¹⁹F-NMR as compared to LC-MS/MS.

In addition to 1123-GSH, time-dependent formation of F⁻ ($\delta = -121.9$ ppm – -122.2 ppm; s), judged by an increase in signal intensity, was detected in all examined hepatic S₉ fractions, with highest F⁻ levels in Goettingen[®] Minipig and NZW Rabbit S₉ compared to rat, mouse and human S₉. F⁻ formation was further increased in the presence of the NADPH-regenerating system compared to the absence, with highest F⁻ levels being formed in Goettingen[®] Minipig and NZW Rabbit S₉. Collectively, these data suggest a higher rate of CYP-450 dependent metabolism of HFO-1123 in these species.

Concluding from this, ¹⁹F-NMR analysis revealed that the time-dependent formation of fluorine containing compounds other than F⁻ and 1123-GSH was not observed in hepatic S₉ fractions incubated with HFO-1123. 1123-GSH can be expected as the main GSH conjugate formed by GST mediated biotransformation of HFO-1123. Furthermore, increased F⁻ formation detected in Goettingen[®] Minipig and NZW Rabbit hepatic S₉ in the presence of the NADPH regenerating system indicates increased CYP-450 mediated metabolism of HFO-1123 in this species. Whether increased CYP-450 mediated biotransformation is involved in the susceptibility of these two species is currently unknown.

Species-differences in the *in vitro* biotransformation of trifluoroethene (HFO-1123)

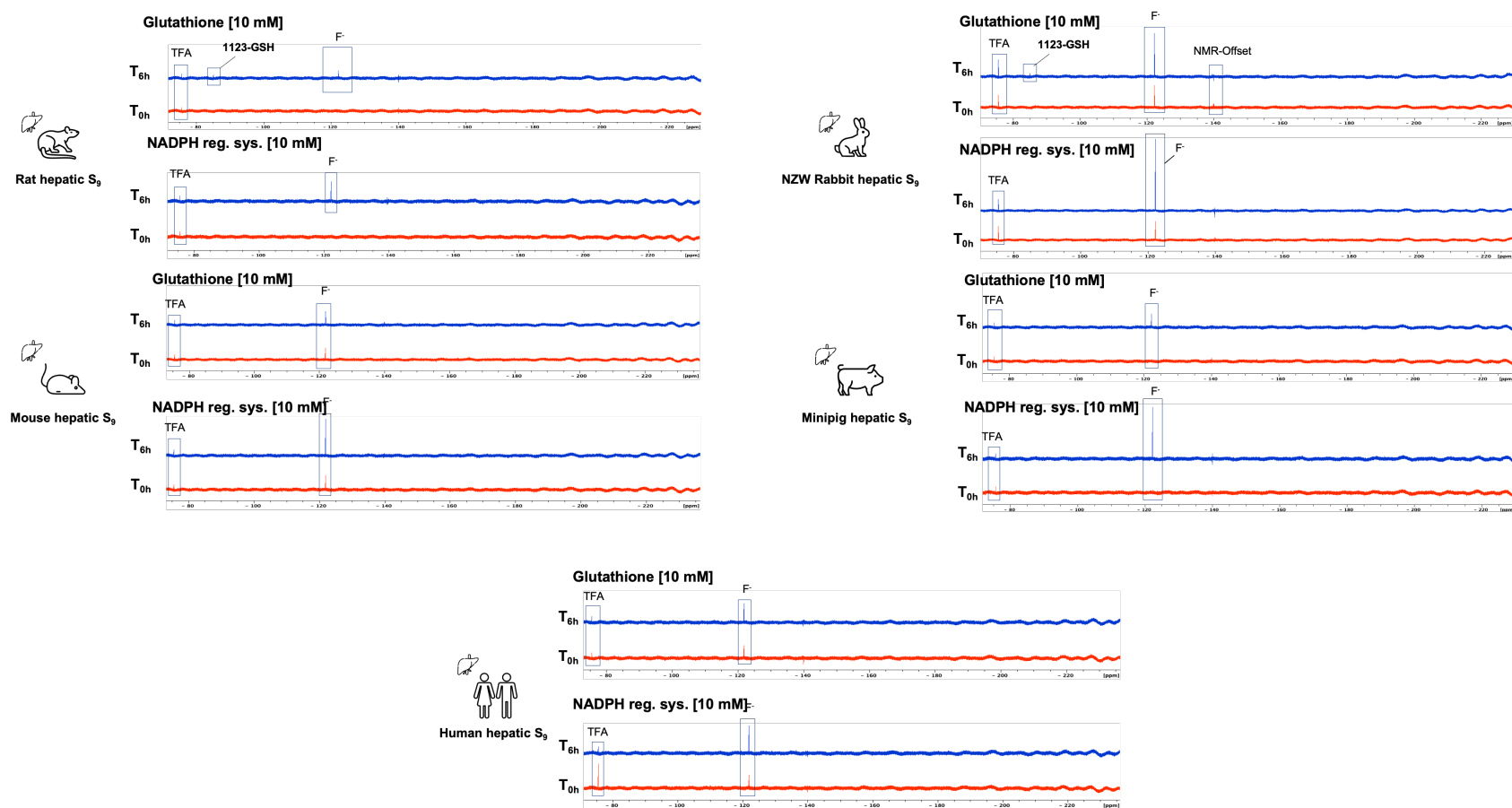


Figure 23 ^{19}F -NMR spectra of rat, mouse, human, Goettingen[®] Minipig and NZW Rabbit hepatic S_9 subcellular fractions incubated with HFO-1123 (0.89 mmol / 20 ml) in the presence and absence of either GSH (10 mM) or the NADPH regenerating system (10 mM). The red spectra show fluorine containing metabolites present at the beginning of the incubation (T_{0h}) and the blue spectra reveal fluorine containing metabolites after 6 hours of incubation (T_{6h}). ^{19}F -NMR-signals corresponding to 1123-GSH ($\delta = -85.1$ ppm, m) were detected in hepatic rat and NZW Rabbit S_9 fractions in the presence of GSH, but not in S_9 of other species. Compared to human, mouse, and rat S_9 , increased F^- formation was detected in Goettingen[®] Minipig and NZW Rabbit hepatic S_9 in the presence of the NADPH regenerating system, indicating increased CYP-450 mediated metabolism of HFO-1123 in these species. Of note, a signal ($\delta = -75.6$ ppm, s) presumably corresponding to trifluoroacetic acid (TFA) based on chemical shift and signal multiplicity, was evident in all incubations with similar signal intensities. It is assumed that TFA may have been introduced as a contaminant. Similarly, signals corresponding to F^- were detected in some incubations at the beginning (T_{0h}) of the incubations. This may be explained by F^- contamination of water used for the preparation of incubation buffers or S_9 fraction.

5.1.8 Time-dependent formation of 1123-GSH and 1123-CYS in renal S₉ fractions after incubation with HFO-1123

Since renal tissue also exhibits GST and γ -GT activity (reviewed by Hanna and Anders (2019)), it was speculated that GSH dependent biotransformation of HFO-1123 to 1123-GSH and 1123-CYS in the kidney may contribute to the species-differences in HFO-1123 toxicity. Renal S₉ fractions of human, rat and Goettingen[®] Minipig were thus incubated with HFO-1123 and analyzed by LC-MS/MS for time-dependent formation of 1123-GSH and 1123-CYS. Renal S₉ from mouse and NZW Rabbits were not commercially available and were therefore omitted.

Time-dependent formation of 1123-GSH and 1123-CYS was observed in incubation of HFO-1123 with human, Goettingen[®] Minipig and rat kidney S₉, although minor differences between triplicates of each species were observed (Figure 24). Compared to incubations of HFO-1123 with hepatic S₉, the amount of 1123-GSH formed in renal S₉ was significantly lower (20 to 50-fold) as judged by the signal intensities, whereas 1123-CYS appeared to be formed at comparable levels in renal and hepatic fractions. This is consistent with lower GST activity but higher γ -GT activity in kidney as compared to liver (Hanna and Anders, 2019). Based on these data, the kidney is unlikely to play a significant role in the initial steps of GSH dependent biotransformation of HFO-1123.

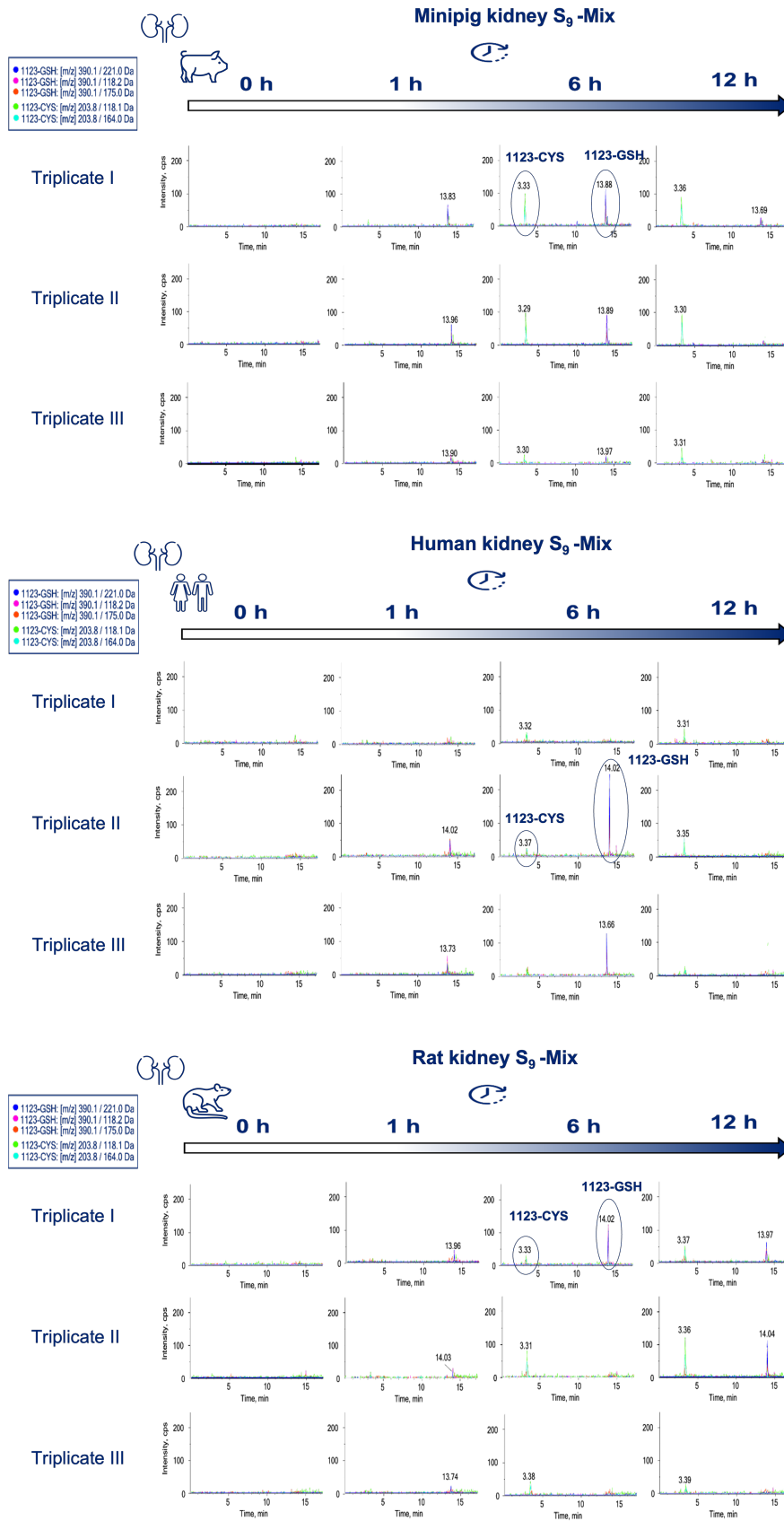


Figure 24 Time-dependent formation of 1123-GSH ([m/z]: 390.1/221.0 Da, 390.1/118.2 Da, 390.1/175.0 Da) and 1123-CYS ([m/z]: 203.8/118.1 Da, 203.8/164.0 Da) in Goettingen® Minipig, human and rat renal S₉ fractions. Results are shown from three independently performed incubations (Triplicate I, Triplicate I, Triplicate III).

5.2 Determination of β -lyase mediated biotransformation of 1123-CYS in renal and hepatic cytosolic fractions

Cysteine S-conjugate β -lyases (β -lyases) play a key role in the biotransformation of haloalkenes via the mercapturic acid pathway. Bioactivation of cysteine S-conjugates derived from haloalkenes is predominantly mediated by β -lyases. To test if 1123-CYS (the cysteine S-conjugate of HFO-1123) is cleaved by β -lyases leading to the formation of MFA *in vitro*, Goettingen[®] Minipig, NZW Rabbit, rat, mice, and human cytosolic fractions (renal and hepatic) were incubated with 1123-CYS. Enzyme kinetics of β -lyases mediated cleavage of 1123-CYS were determined by a spectrometric 96-well plate assay, while 1123-CYS derived fluorine metabolites were evaluated by ¹⁹F-NMR.

As an analytical standard, 1123-CYS was synthesized by AGC. Inc. and purified at the Institute of Pharmacology and Toxicology of the University of Wuerzburg. Purification of crude 1123-CYS was performed as described in Appendix A, chapter A.1 . Comparative LC-MS/MS (Figure 25) analysis of the crude and purified 1123-CYS batch demonstrates successful purification by HPLC. Before HPLC purification, impurities of 1123-CYS-ester (t_r = 14.56 min) and cystine (t_r = 1.96 min) were detected. HPLC purification proved to be successful, as no signal of 1123-CYS-ester and a significantly reduction of cystine was detected. Cystine traces were anticipated to have minimal effect on further investigations regarding 1123-CYS biotransformation. Based on the relative response of LC-MS/MS (Figure 25) and peak area integration by HPLC, the purity of the 1123-CYS batch was assessed as approximately 98%. Furthermore, the purity of 1123-CYS from fluorine containing compounds was assessed with ¹⁹F-NMR (Figure 26).

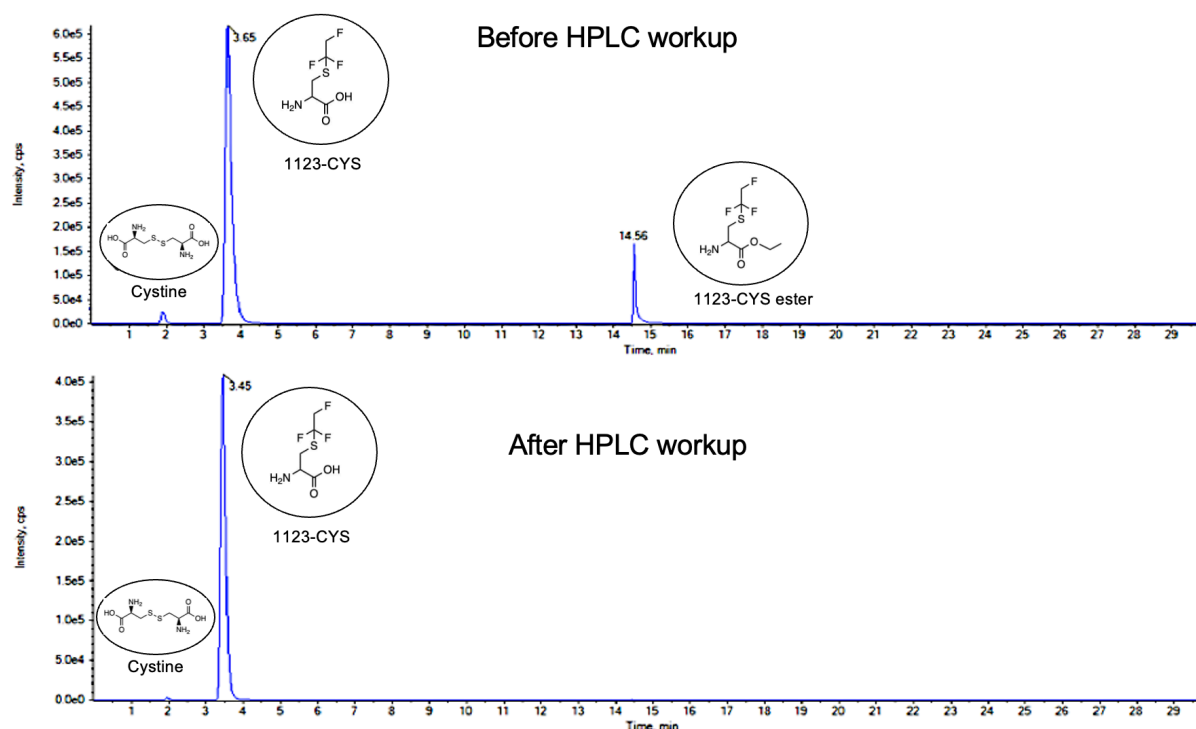


Figure 25 LC-MS/MS chromatograms of 1123-CYS batch before and after purification via HPLC. Before HPLC purification distinct signals of 1123-CYS ester ($t_r = 14.56$ min) and cystine ($t_r = 1.96$ min) were detected next to 1123-CYS ($t_r = 3.65$ min), revealing a contamination with both substances. After HPLC purification, the 1123-CYS batch was free of 1123-CYS-Ester impurity. Cystine impurity seem to be present in trace levels.

Absence of 1123-CYS ester was furthermore supported by ^{19}F -NMR. The two multiplets (m) (**Figure 26**, box a and d) were caused by the F_2 -moiety ($\delta = -84.6$ ppm; m) and the F_1 -moiety ($\delta = -228.3$ ppm; m) of 1123-CYS, respectively. The absence of similar signals with smaller intensities in the surrounding area of these multiplets implies the absence of the 1123-CYS-Ester. However, signals with low intensity assigned to MFA (Figure 26, box c; $\delta = -216.9$ ppm; t, $J_{\text{HF}} = 48.4$ Hz) and F^- (Figure 26, box b; $\delta = -120.3$ ppm; s) were detected. Based on the mechanism of β -lyase mediated cleavage of cysteine S-conjugates and the significantly lower signal intensities compared to signals assigned to 1123-CYS, these impurities were considered to have no or minimal impact on the spectrometric enzyme kinetic studies.

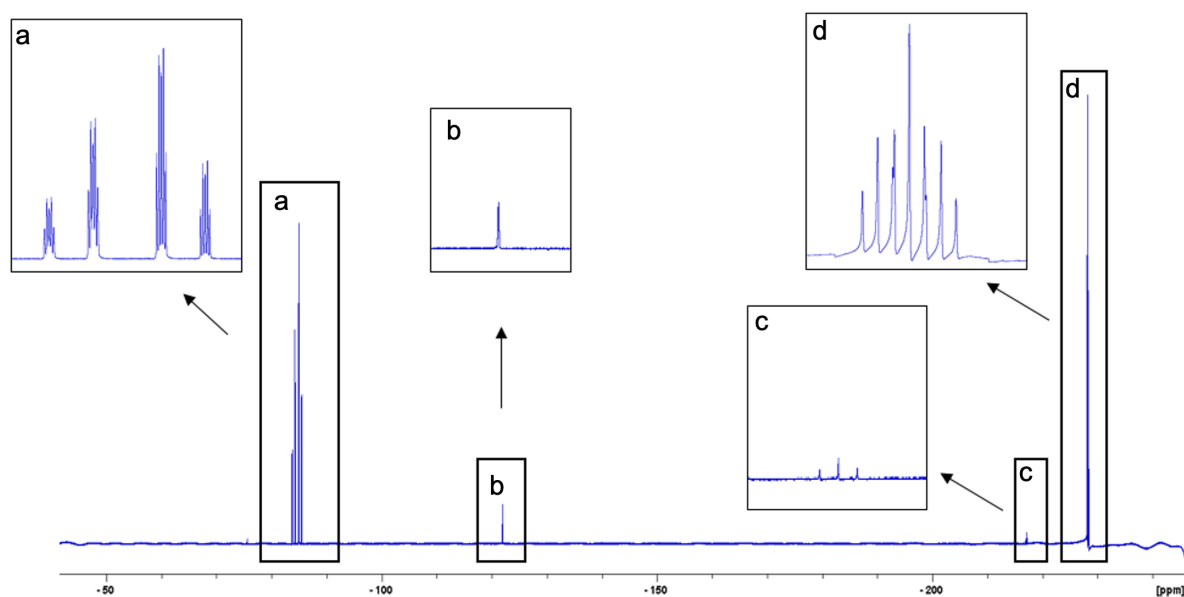


Figure 26 ^{19}F -NMR Spectra of purified 1123-CYS (20 mM). Resonances were assigned to 1123-CYS (F_2 -moiety (box a, $\delta = -84.6$ ppm; m), F_1 -moiety (box d, $\delta = -228.3$ ppm; m)); F^- (box b, $\delta = -120.3$ ppm; s); MFA (box c, $\delta = -216.9$ ppm; t, $J_{\text{HF}} = 48.4$ Hz). MFA and F^- signal intensity is significantly lower than signals assigned to 1123-CYS.

5.2.1 Confirmation of β -lyase mediated cleavage of 1123-CYS

Protein-concentration dependency of reaction rates

To evaluate protein concentration dependency of β -lyase mediated cleavage of 1123-CYS (1.25 mM), incubations were conducted with cytosolic fractions containing 0.5 mg protein/mL, 1 mg protein/mL and 2 mg protein/mL. As a positive control for β -lyases mediated cleavage, incubations with TCVC (1.25 mM) were performed and compared with results from 1123-CYS. TCVC is the corresponding cysteine *S*-conjugate of tetrachloroethene formed via the mercapturic acid pathway and a target of β -lyase cleavage (Dekant *et al.*, 1988; Lash and Parker, 2001). Hepatic Goettingen[®] Minipig and human renal cytosol were used exemplary for all subcellular fractions. For both cysteine *S*-conjugates, a protein concentration dependent increase in pyruvate formation was observed (Figure 27). The amount of pyruvate formed differed between tissue and whether TCVC or 1123-CYS was used as substrate. Slightly increased pyruvate formation was observed with incubations of 1123-CYS compared to incubations of TCVC.

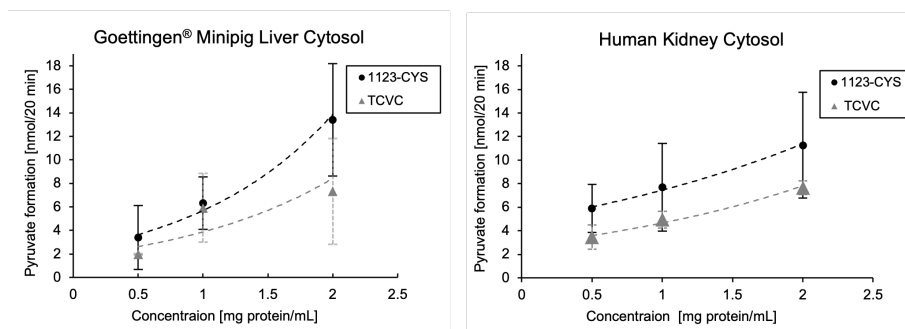


Figure 27 Protein-dependent cleavage of TCVC and 1123-CYS (1.25 mM) resulting in formation of pyruvate. Incubations were performed with cytosolic fractions of minipig liver and human kidney (concentration: (0.5 mg protein/mL); (1 mg protein/mL); (2 mg protein/mL)). Results are presented as mean \pm standard deviation of three independent experiments, each carried out in triplicate.

Inhibition of β -lyases by AOAA

AOAA is a specific inhibitor of pyridoxal 5'-phosphate dependent enzymes, such as β -lyases (Stevens, 1989). To confirm that 1123-CYS is a substrate of β -lyases, incubations with 1123-CYS (1.25 mM) and cytosolic fractions (0.5 mg protein/mL) were carried out in the presence and absence of AOAA (0.625 mM). Cytosolic fractions from Goettingen® Minipig (liver) and human (kidney) were used exemplary for other subcellular fractions. Incubations with TCVC (1.25 mM) in presence of AOAA (0.625 mM) were included as positive control. In the presence of AOAA, a clear reduction in pyruvate formation was observed in incubations of TCVC and renal human cytosol or hepatic Goettingen® Minipig cytosol. Addition of AOAA to incubations of 1123-CYS and renal human cytosol or hepatic Goettingen® Minipig cytosol completely blocked pyruvate formation, thus confirming 1123-CYS as a substrate of β -lyases (Figure 28).

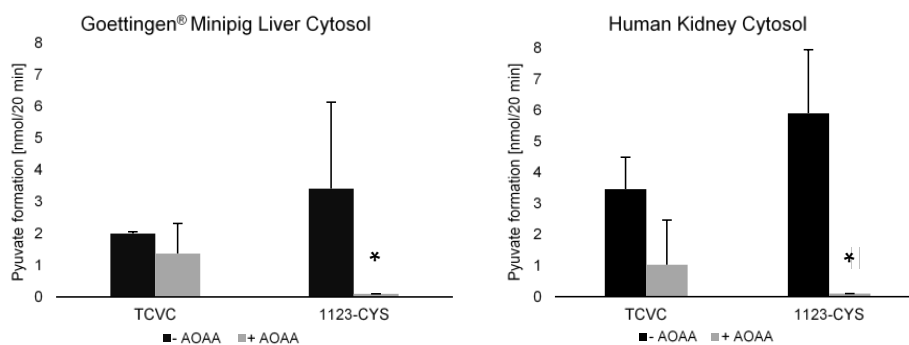


Figure 28 Cleavage of TCVC / 1123-CYS in the absence and presence of AOAA (0.625 mM) in minipig liver and human kidney cytosolic fractions (0.5 mg protein/mL). Bars marked with * indicate that no pyruvate formation was detected. Results are presented as mean \pm standard deviation of three independent experiments, each carried out in triplicate.

5.2.2 Kinetics of β -lyase mediated cleavage of 1123-CYS in renal and hepatic cytosolic fractions

Enzyme kinetics of β -lyase mediated cleavage of 1123-CYS were characterized in renal and hepatic cytosolic fractions of SD rat, human, CD1 mouse, Goettingen[®] Minipig and NZW Rabbit. Incubations were carried out with cytosolic fractions (0.5 mg protein/mL) and 1123-CYS (0.5, 1, 2, 3, 4, 5 mM). Kinetic parameters K_m and V_{max} were determined by Eadie-Hofstee plot and Lineweaver-Burk plot (Lineweaver and Burk, 1934; Hofstee, 1952). Since no significant differences in K_m and V_{max} values obtained by these methods were observed, only data calculated from Eadie-Hofstee plot are shown below (for values calculated from Lineweaver Burk plot see Appendix B, Table B.1).

Figure 29 shows V_{max} and K_m values obtained from liver and kidney cytosolic fractions of the examined species and 1123-CYS. In general, a higher V_{max} value implies enzymatic reaction with higher rates of substrate cleavage, whereas lower V_{max} values imply a lower rate of substrate cleavage. The Michaelis Menten constant K_m describes the affinity of an enzyme to its substrate. Small K_m values imply rapid and high-affinity binding between substrate and enzyme, whereas large K_m values indicate slow and low-affinity binding.

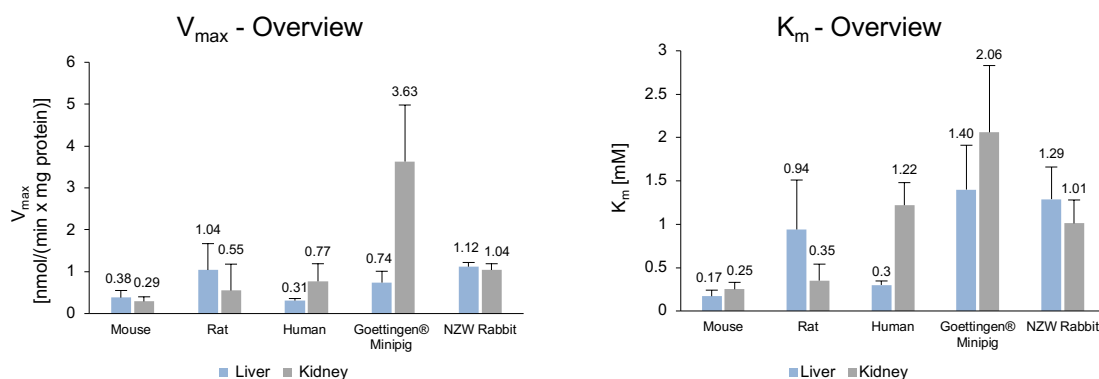


Figure 29 V_{max} (nmol/(min x mg protein) and K_m values (mM)) obtained in liver and kidney cytosol of mice, rats, humans, Goettingen[®] Minipigs and NZW Rabbits. Data analysis was performed with the Eadie-Hofstee plot. Results are presented as mean \pm standard deviation of three independent experiments, each performed in triplicates.

The K_m values obtained in CD1 mouse tissue (liver: 0.17 ± 0.07 mM; kidney: 0.25 ± 0.08 mM) suggest high-affinity binding between β -lyases and 1123-CYS, whereas higher K_m values in Goettingen[®] Minipigs (liver: 1.40 ± 0.51 mM, kidney: 2.06 ± 0.77 mM) indicate a lower-affinity binding between enzyme and substrate. More importantly, however, the markedly higher V_{max} from Goettingen[®] Minipig kidney cytosol (3.63 ± 1.35 nmol/(min x mg protein)) demonstrate a significantly higher β -lyase activity and greater extent of 1123-CYS cleavage as compared to liver and kidney cytosolic fractions of other species, e.g., the low V_{max} values obtained from

CD1 mouse tissue (liver: 0.17 ± 0.07 mM; kidney: 0.25 ± 0.08 mM) which indicate a much lower β -lyase activity and 1123-CYS cleavage.

The plot of the Michaelis-Menten kinetics (Figure 30) provides an overview of β -lyase mediated cleavage of 1123-CYS in the cytosolic fractions of different species. Enzyme kinetic studies revealed an increased β -lyase activity in renal cytosol of Goettingen[®] Minipigs ($V_{\max} = 3.63 \pm 1.35$ nmol/(min x mg protein), $K_m = 2.06 \pm 0.77$ mM) as compared to renal cytosol of human, rat and mouse (human: $V_{\max} = 0.77 \pm 0.26$ nmol/(min x mg protein), $K_m = 1.22 \pm 0.42$ mM; rat: $V_{\max} = 0.55 \pm 0.24$ nmol/(min x mg protein), $K_m = 0.35 \pm 0.19$ mM; mouse: $V_{\max} = 0.29 \pm 0.1$ nmol/(min x mg protein), $K_m = 0.25 \pm 0.08$ mM). β -lyase activity in renal NZW Rabbit cytosol ($V_{\max} = 1.04 \pm 0.15$ nmol/(min x mg protein), $K_m = 1.01 \pm 0.37$ mM) was slightly higher as compared to renal cytosol of human, rat, and mouse but lower than renal Goettingen[®] Minipig cytosol. By comparing the results obtained in liver cytosol, no significant differences in β -lyase activity between species could be observed (Goettingen[®] Minipig: $V_{\max} = 0.74 \pm 0.27$ nmol/(min x mg protein), $K_m = 1.40 \pm 0.51$ mM; human: $V_{\max} = 0.31 \pm 0.05$ nmol/(min x mg protein), $K_m = 0.30 \pm 0.05$ mM; rat: $V_{\max} = 1.04 \pm 0.63$ nmol/(min x mg protein), $K_m = 0.94 \pm 0.57$ mM; mouse: $V_{\max} = 0.38 \pm 0.17$ nmol/(min x mg protein), $K_m = 0.17 \pm 0.07$ mM; NZW Rabbit: $V_{\max} = 1.12 \pm 0.10$ nmol/(min x mg protein), $K_m = 1.29 \pm 0.27$ mM).

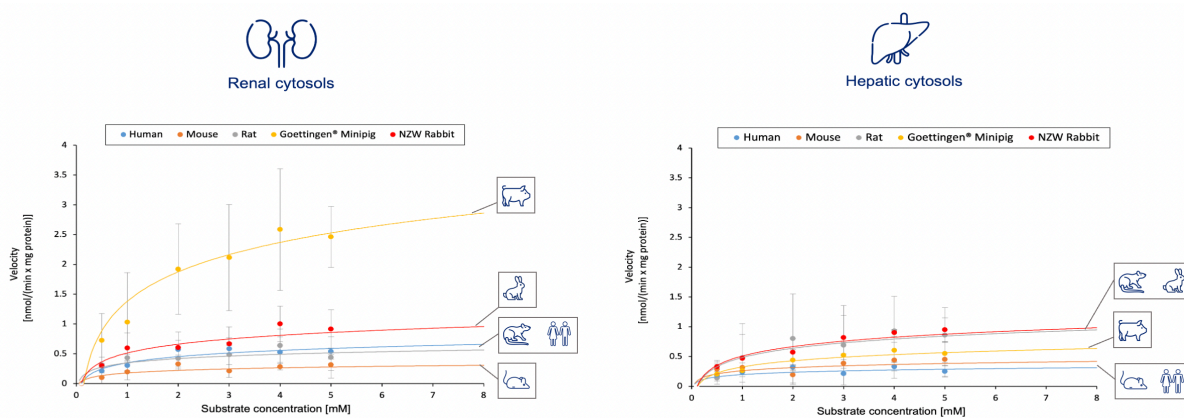


Figure 30 Michaelis-Menten kinetics of β -lyase mediated cleavage of 1123-CYS in renal and hepatic human, mouse, rat, Goettingen[®] Minipig, and NZW Rabbit cytosolic fractions. Results are presented as mean \pm standard deviation of three independent experiments, each performed in triplicates.

5.2.3 Fluorine containing metabolite formation from 1123-CYS in renal and hepatic cytosol monitored by ^{19}F -NMR

Purity reassessment of the 1123-CYS batch used for ^{19}F -NMR investigations

For ^{19}F -NMR studies, a second purification step of 1123-CYS was performed to remove traces of F^- and MFA. 1123-CYS was purified by HPLC (for HPLC parameters see Appendix B, chapter B.1) and purity of the isolated product was assessed with ^{19}F -NMR. Figure 31 displays the ^{19}F -NMR of 1123-CYS (20 mM) in D_2O .

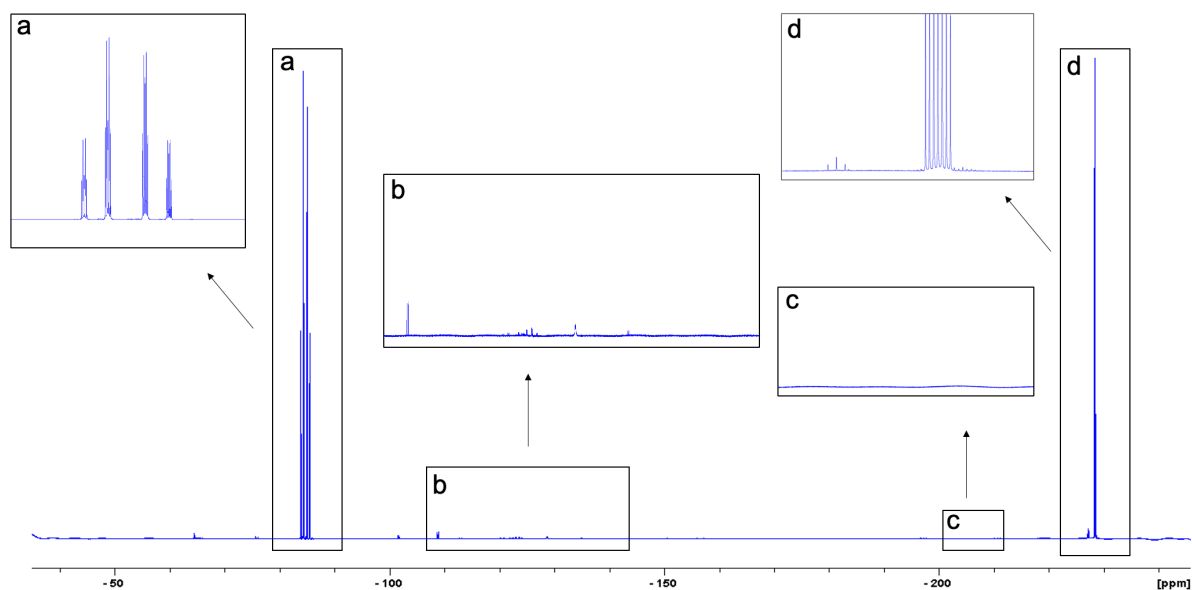


Figure 31 ^{19}F -NMR spectrum of purified 1123-CYS (dissolved in D_2O), with particular attention to important sections of the spectrum (Box a-d).

The two multiplets (m) (box a; box d) are caused by the F_2 -moiety ($\delta = -84.6$ ppm; m) and the F_1 -moiety ($\delta = -228.3$ ppm; m) of 1123-CYS, respectively. The absence of similar signals with smaller signal intensities in the surrounding area of these multiplets implies the absence of 1123-CYS-Ester as a potential contaminant. Furthermore, box d displays a triplet ($\delta = -227.1$ ppm; t, $J_{\text{HF}} = 46.4$ Hz). Chemical shift, hydrogen-fluorine coupling constant (J_{HF}) and multiplicity indicate a molecule containing a FH_2C -unit, but the exact structure could not be identified. As the signal intensity was low, this unknown compound was considered to be a minor impurity, which may not affect analysis of metabolites.

The spectral area displayed in box b ranges from -108.0 ppm to -145.0 ppm. In this area signals with low intensity were detected. The molecular structure of compounds causing these signals are unknown. As their signal intensity was low, compared to the signals corresponding to 1123-CYS (F_2 : $\delta = -84.6$ ppm, m; F_1 : $\delta = -228.3$ ppm, m), their presence was considered to have minimal impact on the results of subsequent incubations. Importantly, no signal corresponding to inorganic fluoride (F^-), which is expected to show a singlet (s) at -120.3 ppm, was detected. It was therefore concluded that the 1123-CYS batch was free of inorganic F^- .

In box c, the chemical shift area from -209 ppm until -223.5 ppm is displayed. If present, the triplet (t) of monofluoroacetic acid (MFA, $\delta = -216.9$ ppm, t) is expected to occur in this range. As no signal was visible at a chemical shift of -216.9 ppm, the 1123-CYS batch was considered to be free of MFA impurities.

Purity assessment of cytosolic fractions

Pure cytosolic fractions of Goettingen[®] Minipigs prepared in-house and humans were screened for fluorine containing metabolites to evaluate absence of fluorine containing impurity. Figure 32 shows the spectra of cytosolic fraction of Goettingen[®] Minipig kidney, human kidney, and human liver. One signal ($\delta = -64.3$ ppm; t, $J_{HF} = 11.2$ Hz) is apparent in the spectra obtained from Goettingen[®] Minipig kidney cytosol. Chemical shift, multiplicity and J_{HF} imply a F_3CH_2 -moiety. Comparison with spectra of standards suggest the presence of 3,3,3-trifluoro-1-propanol. This signal was also present in all analyzed incubations containing Goettingen[®] Minipig cytosol (prepared in-house), but not in commercially obtained human cytosols (XenoTech[®], Lenexa, USA). It is not certain, during which process this contamination was introduced to the in-house prepared cytosolic fraction. A possible contamination could be introduced during the preparation process due to contaminated equipment. Another possibility is the occurrence of 3,3,3-trifluoro-1-propanol in the kidney and liver of the Goettingen[®] Minipig prior to any extraction or incubation. This substance could be introduced to the porcine organism due to feed contamination. Yet, minor contamination with 3,3,3-trifluoro-1-propanol was not considered to negatively affect β -lyase mediated cleavage of 1123-CYS.

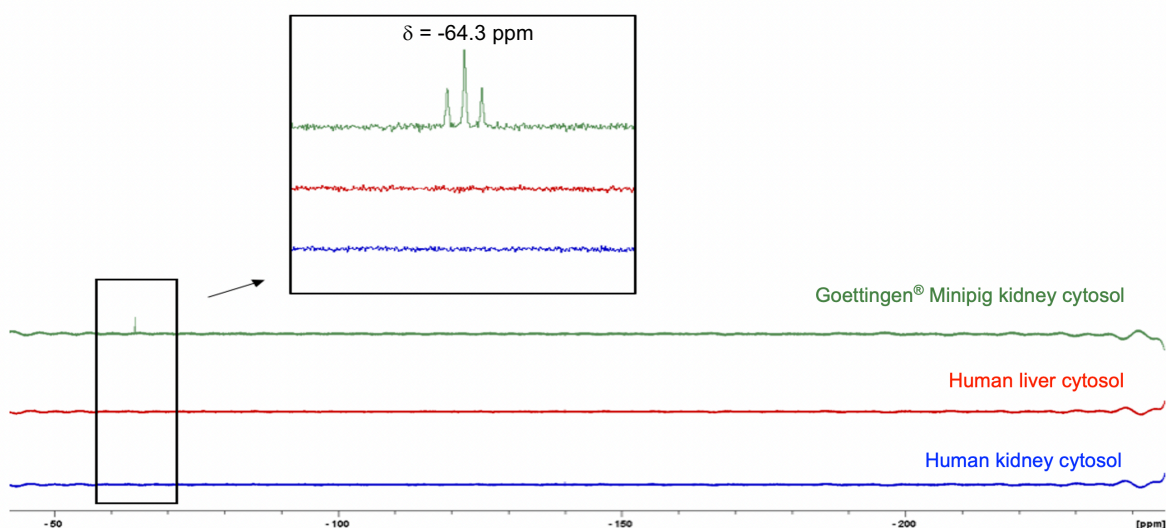


Figure 32 ¹⁹F-NMR spectra of control incubations (top to bottom: Goettingen[®] Minipig kidney cytosol, human liver cytosol, human kidney cytosol). A signal assigned to 3,3,3-trifluoro-1-propanol ($\delta = -64.3$ ppm; t, $J_{HF} = 11.2$ Hz) was observed in renal Goettingen[®] Minipig cytosol. As this signal was not detected in renal and hepatic human cytosol, these fractions were considered to be free of fluorine containing compounds.

Incubations of 1123-CYS and renal Goettingen[®] Minipig cytosol

Since enzyme kinetic data suggested a significantly higher β -lyase activity in renal cytosolic fractions of the Goettingen[®] Minipig as compared to liver or kidney cytosol from other species, ¹⁹F-NMR analysis of metabolites was primarily conducted in incubations of 1123-CYS with Goettingen[®] Minipig kidney cytosol in the presence and absence of the β -lyase inhibitor AOAA.

In incubations of renal cytosol from Goettingen[®] Minipigs with 1123-CYS, the formation of signals assigned to F⁻ (δ = -120.0 ppm; s), MFA (δ = -216.9 ppm; t, J_{HF} = 48.4 Hz) and two MFA-derivatives (FCH₂-groups containing compounds) (MFA-derivative (1) δ = -202.2 ppm; t, J_{HF} = 48.5 Hz; MFA-derivative (2) δ = -220.1 ppm; t, J_{HF} = 48.5 Hz) was detected. Figure 33 displays the ¹⁹F-NMR spectra of aliquots taken at 0 (T_{0 min}) and 60 minutes (T_{60 min}) after start of the reaction. Two areas are marked with black boxes are of special interest (box a, box b). The two multiplets correspond to the F₂-moiety (δ = -84.6 ppm; m) and the F₁-moiety (δ = -228.3 ppm; m) of 1123-CYS, respectively. Box a shows a singlet caused by F⁻ (δ = -120 ppm; s). The triplets marked by box b are assigned to MFA (δ = -216.9 ppm; t, J_{HF} = 48.4 Hz) and two potential MFA-derivatives (MFA-derivative (1) δ = -202.2 ppm; t, J_{HF} = 48.5 Hz; MFA-derivative (2) δ = -220.1 ppm; t, J_{HF} = 48.5 Hz). Exact structures of these MFA-derivatives are unknown. Chemical shift, J_{HF} and multiplicity indicate a FCH₂-unit with unknown substituents. Both compounds can be anticipated to be precursors or successors of MFA and therefore associated with formation of MFA. Also, the chemical shift of MFA-derivative (1) (which appears at a lower chemical shift relative to MFA) suggest a less electronegative substituent at the FCH₂-unit compared to MFA. MFA-derivative (2) (which appears at a higher chemical shift relative to MFA) possibly contains a more electronegative substituent.

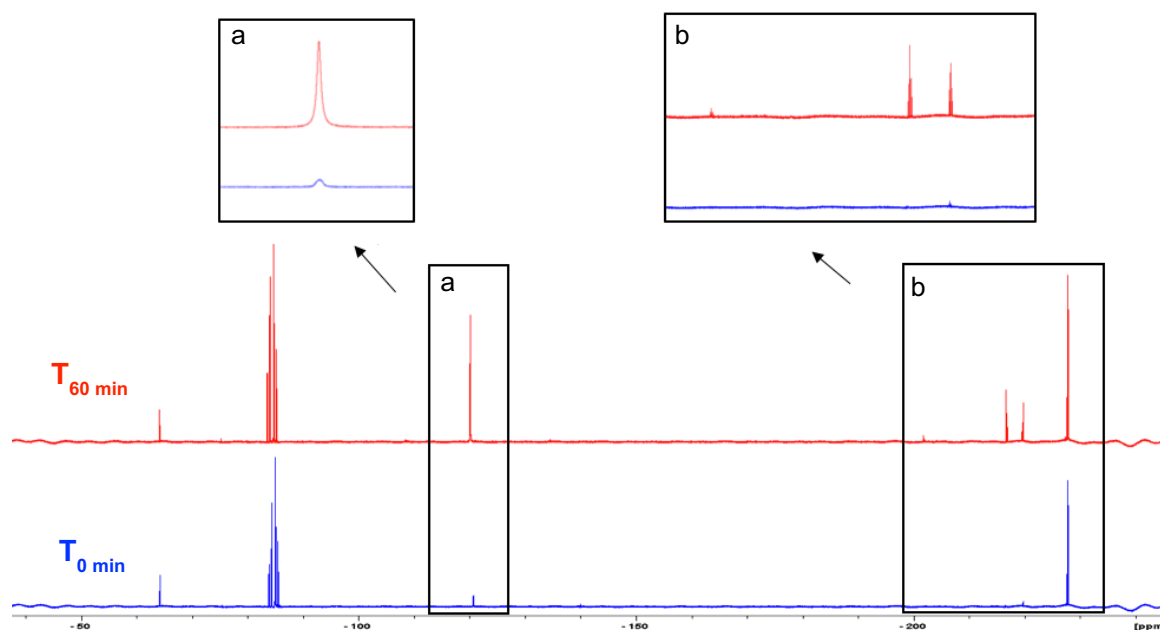


Figure 33 ^{19}F -NMR spectra from aliquots taken at 0 ($T_{0 \text{ min}}$) and 60 minutes ($T_{60 \text{ min}}$) after start of the reaction (renal Goettingen[®] Minipig cytosol incubated with 1123-CYS). Resonances were assigned to 3,3,3-trifluoro-1-propanol ($\delta = -64.3$ ppm; t, $J_{\text{HF}} = 11.2$ Hz); 1123-CYS (F2-moiety ($\delta = -84.6$ ppm; m), F1-moiety ($\delta = -228.3$ ppm; m)); F^- ($\delta = -120.0$ ppm; s); MFA ($\delta = -216.9$ ppm; t, $J_{\text{HF}} = 48.4$ Hz); MFA-derivative (1) ($\delta = -202.2$ ppm; t, $J_{\text{HF}} = 48.5$ Hz), MFA-derivative (2) ($\delta = -220.1$ ppm; t, $J_{\text{HF}} = 48.5$ Hz). By comparing $T_{0 \text{ min}}$ and $T_{60 \text{ min}}$ the formation of F^- , MFA and two MFA-derivatives becomes apparent. Furthermore, integration of signal intensities reveals that the decrease in intensity of the spectra assigned to 1123-CYS is proportional to the increase in intensity of the spectra assigned to MFA, MFA-derivatives, and F^- .

To confirm β -lyases dependent formation of F^- , MFA and MFA-derivatives, incubations were carried out in the presence of AOAA. Figure 34 displays the ^{19}F -NMR spectra of aliquots taken 0 ($T_{0 \text{ min}}$) and 60 minutes ($T_{60 \text{ min}}$) after start of the reaction. Areas of interest are shown in detail (box a and box b). Signals of F^- ($\delta = -120.3$ ppm; s; box a) and MFA ($\delta = -216.7$ ppm; t, $J_{\text{HF}} = 48.5$ Hz; box b) were apparent at low levels in both spectra. However, the signal intensity did not increase with time and no significant change in 1123-CYS signal intensity was detectable.

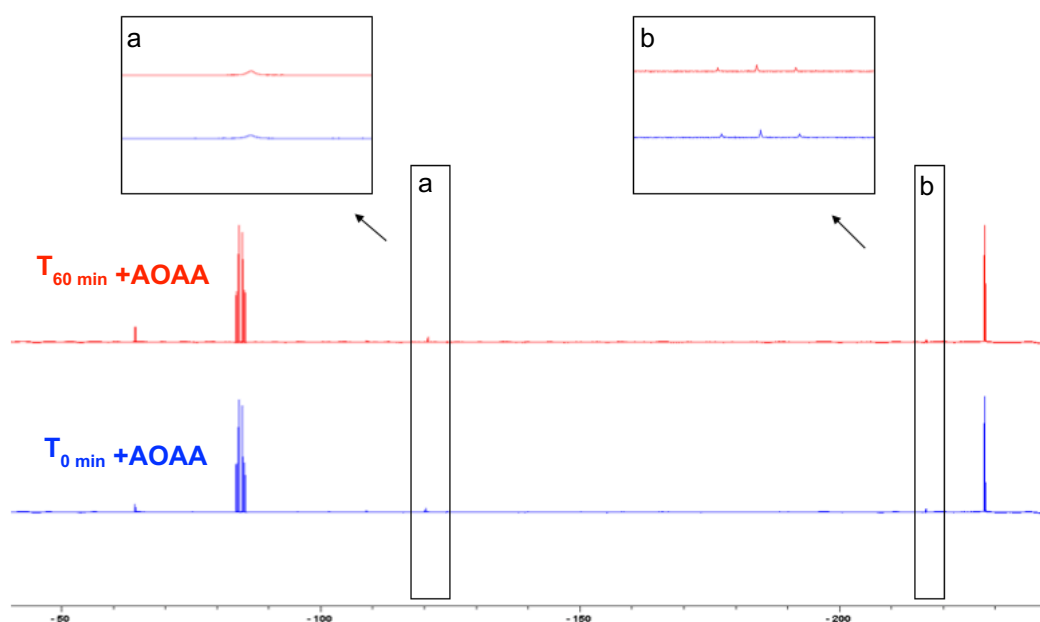


Figure 34 ^{19}F -NMR spectra from aliquots taken at 0 ($T_{0 \text{ min}}$) and 60 minutes ($T_{60 \text{ min}}$) after the start of the reaction in the presence of AOAA (renal Goettingen[®] Minipig cytosol incubated with 1123-CYS). Resonances were assigned to 3,3,3-trifluoro-1-propanol ($\delta = -64.3$ ppm; t, $J_{\text{HF}} = 11.2$ Hz); 1123-CYS (F_2 -moiety ($\delta = -84.6$ ppm; m), F_1 -moiety ($\delta = -228.0$ ppm; m)); F^- ($\delta = -120.0$ ppm; s); MFA ($\delta = -216.7$ ppm; t, $J_{\text{HF}} = 48.5$ Hz). By comparing $T_{0 \text{ min}}$ and $T_{60 \text{ min}}$ no change in signal intensity of MFA and F^- is evident.

Based on these data, it can be concluded that formation of MFA and F^- can be blocked by addition of the specific β -lyase inhibitor AOAA and is therefore dependent on β -lyases.

Incubations of 1123-CYS with renal and hepatic human cytosol

Enzyme kinetic data of human cytosolic fractions (kidney: $V_{\text{max}} = 0.77 \pm 0.26$ [nmol/(min x mg protein)]; liver: 0.31 ± 0.05 [nmol/(min x mg protein)]) suggest a low activity of β -lyase towards 1123-CYS. To support these results, formation of fluorine containing metabolites was monitored in incubations containing 1123-CYS (5 mM) and human cytosol (kidney, liver; (5 mg protein/mL)). Spectra were compared to the ones obtained from incubations of Goettingen[®] Minipig kidney cytosol and 1123-CYS.

Incubations of human kidney cytosol with 1123-CYS showed a low, but time-dependent formation of signals assigned to F^- ($\delta = -119.9$ ppm; s) and MFA ($\delta = -217.1$ ppm; t, $J_{\text{HF}} = 48.4$ Hz). Figure 35 displays the ^{19}F -NMR spectra of aliquots taken 0 ($T_{0 \text{ min}}$ human kidney) and 60 minutes ($T_{60 \text{ min}}$ human kidney) after start of the reaction compared to spectra obtained from an aliquot taken at 60 minutes ($T_{60 \text{ min}}$ Goettingen[®] Minipig kidney) of incubation with Goettingen[®] Minipig kidney cytosol. Box a shows a zoomed-in image of the signal assigned to F^- ($\delta = -119.8$ ppm; s), whereas box b displays the spectral area from -200 to -227 ppm (MFA and MFA-derivative). In human kidney cytosol, intensity of the F^- signal slightly increases with time, suggesting minimal time-dependent formation of F^- . However, the intensity of the signal is only a fraction of the F^- signal obtained with Goettingen[®] Minipig kidney cytosol. Box b shows time-dependent formation of MFA in human kidney cytosol, but no evidence of signals

assigned to the MFA-derivatives detected in renal cytosolic fractions of the Goettingen[®] Minipig. Consistent with the signal corresponding to F⁻, the intensity of the MFA signal in human kidney cytosol is only a fraction of the signal obtained with Goettingen[®] Minipig kidney cytosol. Similar findings were obtained with incubations of human liver cytosol and 1123-CYS (Figure 36).

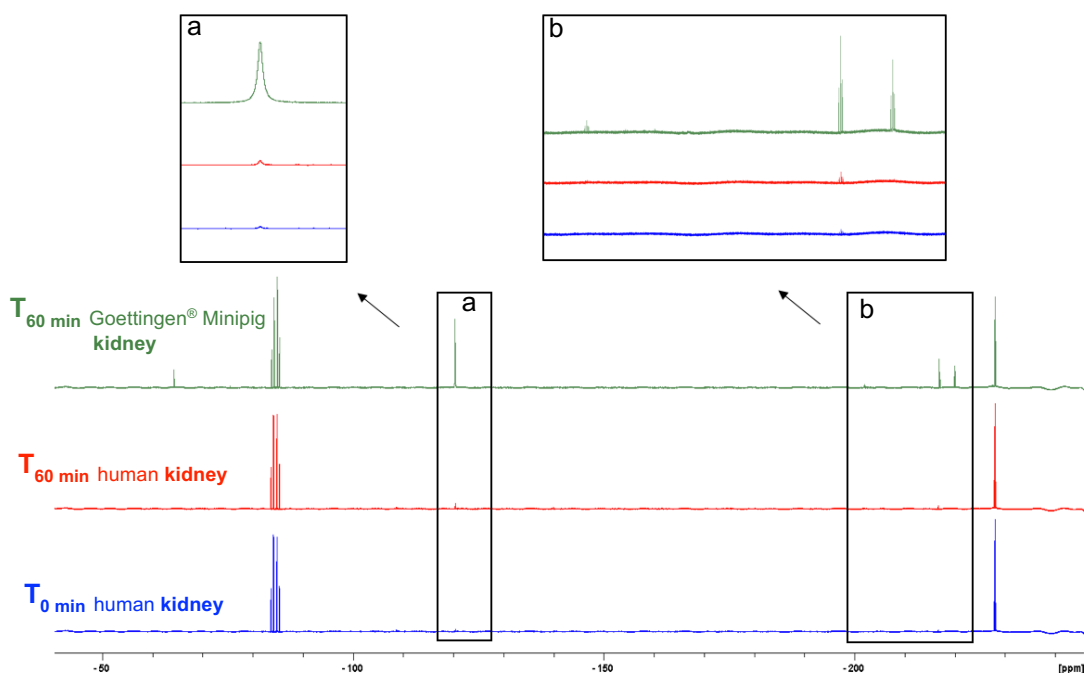


Figure 35 ¹⁹F-NMR spectra from aliquots taken at 0 ($T_{0 \text{ min}}$ human kidney) and 60 minutes ($T_{60 \text{ min}}$ human kidney, $T_{60 \text{ min}}$ Goettingen[®] Minipig kidney) after the start of incubation containing 1123-CYS and human kidney cytosol and Goettingen[®] Minipig kidney cytosol respectively. Resonances were assigned to 3,3,3-trifluoro-1-propanol ($\delta = -64.3$ ppm; t, $J_{\text{HF}} = 11.2$ Hz); 1123-CYS (F_2 -moiety ($\delta = -84.6$ ppm; m), F_1 -moiety ($\delta = -228.1$ ppm; m)); F⁻ ($\delta = -119.9$ ppm; s); MFA ($\delta = -217.1$ ppm; t, $J_{\text{HF}} = 48.4$ Hz); MFA-relative (1) ($\delta = -202.0$ ppm; t, $J_{\text{HF}} = 48.5$ Hz), MFA-relative (2) ($\delta = -220.2$ ppm; t, $J_{\text{HF}} = 48.5$ Hz). By comparing $T_{0 \text{ min}}$ and $T_{60 \text{ min}}$ time-dependent formation of F⁻, MFA is evident in human kidney cytosol. However, the signal intensity of both MFA and F⁻ exhibited only a fraction of the corresponding signals in $T_{60 \text{ min}}$ Goettingen[®] Minipig kidney. Also, the two MFA-relatives are detectable only in incubations of 1123-CYS with Goettingen[®] Minipig cytosol.

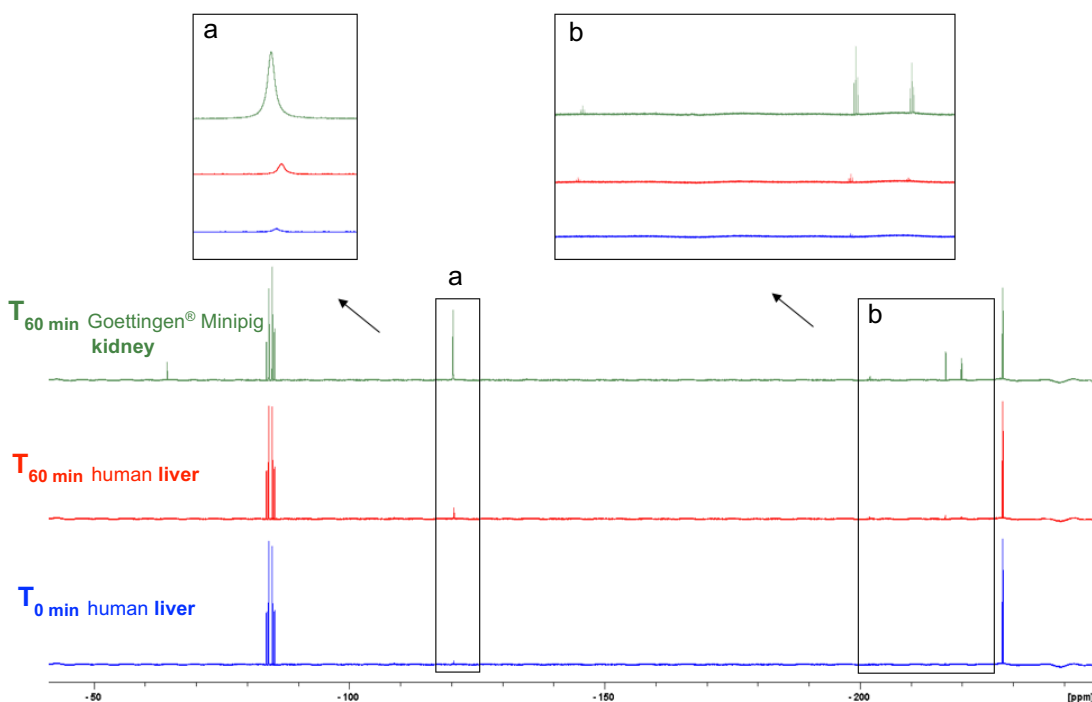


Figure 36 ^{19}F -NMR spectra from aliquots taken at 0 ($T_{0 \text{ min}}$ human liver) and 60 minutes ($T_{60 \text{ min}}$ human liver, $T_{60 \text{ min}}$ Goettingen[®] Minipig kidney) after the start of incubation containing 1123-CYS and human liver cytosol or Goettingen[®] Minipig kidney cytosol, respectively. Resonances were assigned to 3,3,3-trifluoro-1-propanol ($\delta = -64.3$ ppm; t, $J_{\text{HF}} = 11.2$ Hz); 1123-CYS (F_2 -moiety ($\delta = -84.6$ ppm; m), F_1 -moiety ($\delta = -228.1$ ppm; m)); F^- ($\delta = -119.9$ ppm; s); MFA ($\delta = -217.1$ ppm; t, $J_{\text{HF}} = 48.4$ Hz); MFA-relative (1) ($\delta = -202.0$ ppm; t, $J_{\text{HF}} = 48.5$ Hz), MFA-relative (2) ($\delta = -220.2$ ppm; t, $J_{\text{HF}} = 48.5$ Hz). By comparing $T_{0 \text{ min}}$ and $T_{60 \text{ min}}$ time-dependent formation of F^- and MFA is apparent in human liver cytosol. However, the signal intensity of both MFA and F^- exhibited only a fraction of the corresponding signals in $T_{60 \text{ min}}$ Goettingen[®] Minipig kidney.

These findings provide further experimental support for reduced β -lyase activity towards 1123-CYS in human kidney and liver cytosol compared to Goettingen[®] Minipig renal cytosol, thereby confirming the β -lyase enzyme kinetic data.

Incubations of 1123-CYS with renal and hepatic NZW Rabbit cytosol

While NZW Rabbits were found to be susceptible to HFO-1123 toxicity, enzyme kinetic data of NZW Rabbit cytosolic fractions (kidney: $v_{\text{max}} = 1.04 \pm 0.15$ (nmol/(min x mg protein))); liver: $v_{\text{max}} = 1.12 \pm 0.10$ (nmol/(min x mg protein)) suggest a lower activity of β -lyase towards 1123-CYS compared to Goettingen[®] Minipig renal cytosol. To support these results, formation of fluorine containing metabolites was monitored in incubations containing 1123-CYS (5 mM) and NZW Rabbit cytosol (kidney, liver; (5 mg protein/mL)). Spectra were compared to the ones obtained with Goettingen[®] Minipig and human kidney cytosol incubated with 1123-CYS.

In renal and hepatic NZW Rabbit cytosols, the formation of F^- ($\delta = -122.2$ ppm; s), MFA ($\delta = -217.0$ ppm; t, $J_{\text{HF}} = 48.0$ Hz) and three MFA-derivatives (MFA-derivative (I): $\delta = -202.2$ ppm; t, $J_{\text{HF}} = 48.7$ Hz; MFA-derivative (II): $\delta = -208.2$ ppm; t, $J_{\text{HF}} = 47.2$ Hz; MFA-derivative (III): $\delta = -220.1$ ppm; t, $J_{\text{HF}} = 45.7$ Hz) was detected. No significant differences in metabolite formation

between renal and hepatic NZW cytosol were identified after 60 min of incubation (see Appendix B, Figure B.10).

In line with results obtained by spectrometric β -lyase assay, the amounts of F^- , MFA and MFA-derivates formed were lower (especially MFA and MFA-derivative (III)) in renal (Figure 37) and hepatic (Appendix B, Figure B.11) NZW Rabbit cytosol compared to renal Goettingen[®] Minipig cytosol, indicating a lower β -lyase activity in NZW Rabbit cytosols compared to renal Goettingen[®] Minipig cytosol. The formation of MFA-derivative (II) was detected exclusively in renal and hepatic NZW Rabbit cytosol (not in Goettingen[®] Minipig). However, the exact chemical structure of this MFA-derivative is still unknown. Interestingly, MFA-derivates were detected in incubations of Goettingen[®] Minipig and NZW Rabbit renal cytosol but not in human fractions (Figure 38).

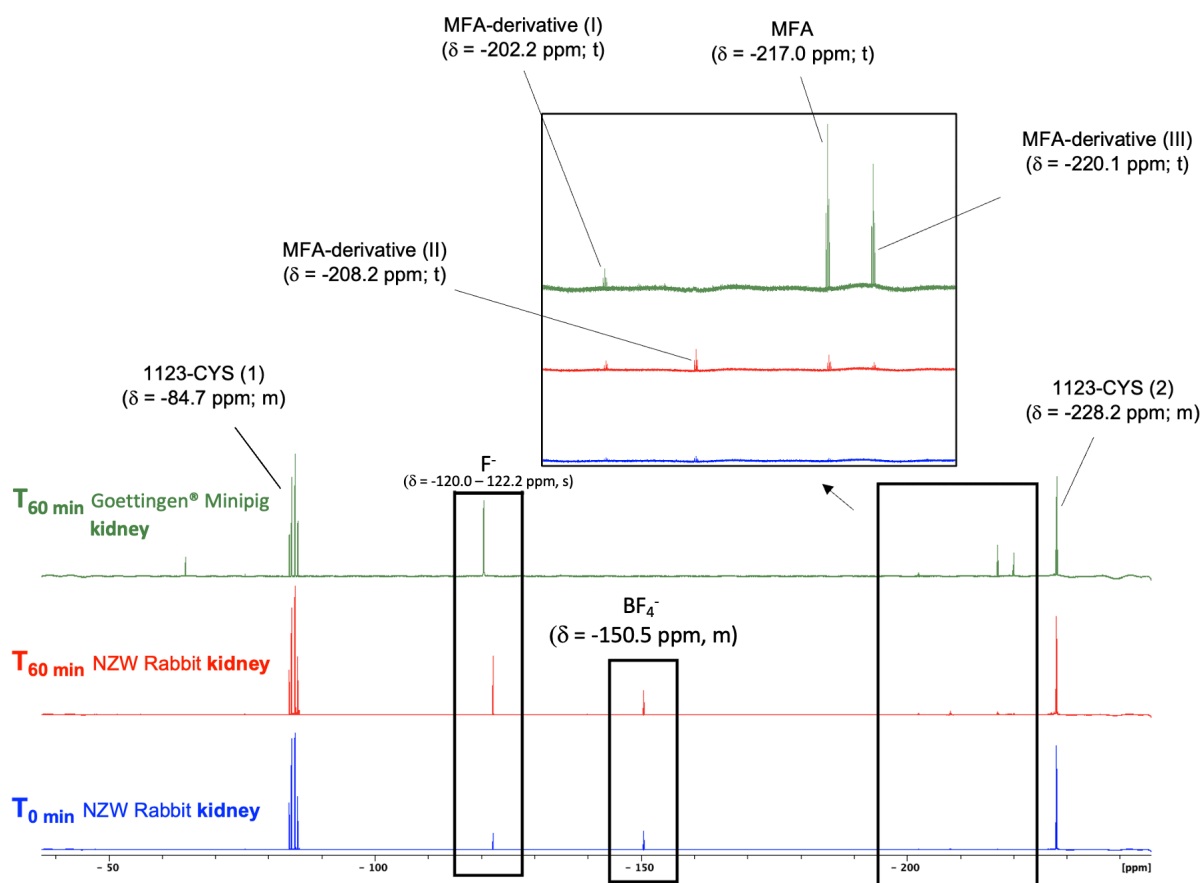


Figure 37 ^{19}F -NMR spectra from aliquots taken at 0 ($T_{0 \text{ min}}$ NZW Rabbit kidney) and 60 minutes ($T_{60 \text{ min}}$ NZW Rabbit kidney, $T_{60 \text{ min}}$ Goettingen[®] Minipig kidney) after the start of incubation containing 1123-CYS and NZW Rabbit kidney cytosol or Goettingen[®] Minipig kidney cytosol, respectively. Resonances were assigned to 3,3,3-trifluoro-1-propanol ($\delta = -64.3$ ppm; t, $J_{HF} = 11.2$ Hz); 1123-CYS (F_2 -moiety ($\delta = -84.7$ ppm; m), F_1 -moiety ($\delta = -228.2$ ppm; m)); F^- ($\delta = -122.2$ ppm; s); MFA ($\delta = -217.0$ ppm; t, $J_{HF} = 48.4$ Hz); MFA-derivative (I) ($\delta = -202.2$ ppm; t, $J_{HF} = 48.5$ Hz),

MFA-derivative (II) ($\delta = -208.2$ ppm; t, $J_{HF} = 48.5$ Hz) and MFA-derivative (III) ($\delta = -220.1$ ppm; t, $J_{HF} = 48.5$ Hz). BF_4^- ($\delta = -150.5$ ppm, m) is most likely formed by the reaction of fluoride formed from 1123-CYS cleavage and borate present in the glass of the NMR-tubes. By comparing $T_{0 \text{ min}}$ and $T_{60 \text{ min}}$ time-dependent formation of F^- , MFA and all MFA-derivatives is evident in NZW Rabbit kidney cytosol. However, the signal intensity of both MFA and MFA-derivatives exhibited only a fraction of the corresponding signals in $T_{60 \text{ min}}$ Goettingen[®] Minipig kidney.

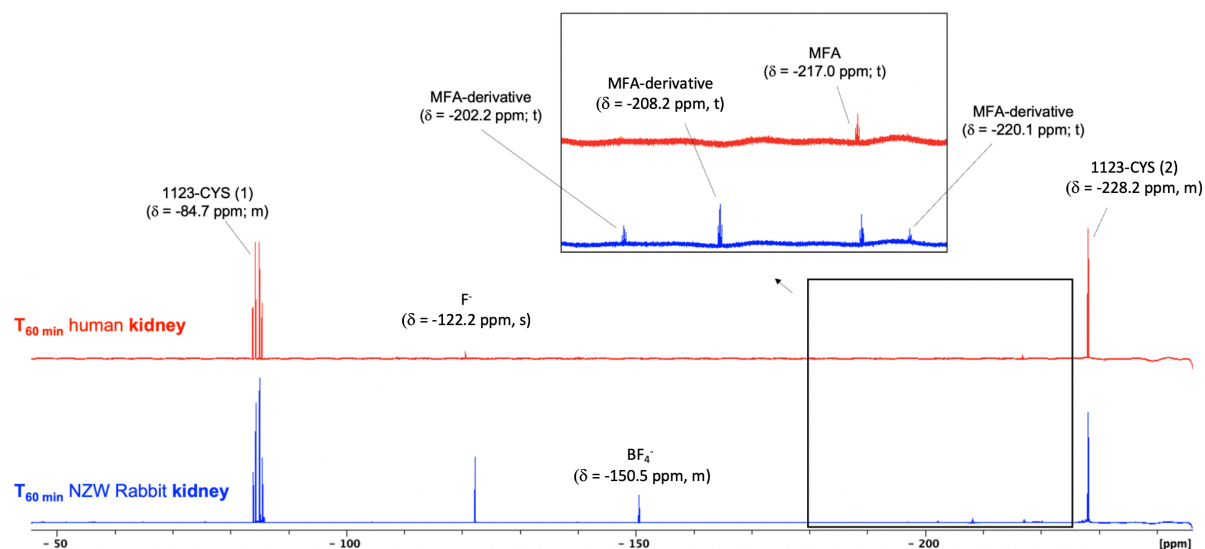


Figure 38 ^{19}F -NMR spectra from aliquots taken 60 minutes ($T_{60 \text{ min}}$ human kidney, $T_{60 \text{ min}}$ NZW Rabbit kidney) after the start of incubation containing 1123-CYS and NZW Rabbit kidney cytosol or human kidney cytosol, respectively. Resonances were assigned to 1123-CYS (F_2 -moiety ($\delta = -84.7$ ppm; m), F_1 -moiety ($\delta = -228.2$ ppm; m)); F^- ($\delta = -122.2$ ppm; s); MFA ($\delta = -217.0$ ppm; t, $J_{HF} = 48.4$ Hz); MFA-derivative (I) ($\delta = -202.2$ ppm; t, $J_{HF} = 48.5$ Hz), MFA-derivative (II) ($\delta = -208.2$ ppm; t, $J_{HF} = 48.5$ Hz), MFA-derivative (III) ($\delta = -220.1$ ppm; t, $J_{HF} = 48.5$ Hz) and BF_4^- ($\delta = -150.5$ ppm; m). BF_4^- is most likely formed by the reaction of fluoride formed from 1123-CYS cleavage and borate present in the glass of the NMR-tubes. Time-dependent formation of F^- , MFA and all MFA-derivatives is evident in NZW Rabbit kidney cytosol. However, human kidney cytosol only shows formation of MFA.

In summary, ^{19}F -NMR analysis revealed formation of F^- , MFA and three MFA-derivatives in renal and hepatic NZW Rabbit cytosol. However, the amounts of F^- , MFA and MFA-derivatives formed in NZW Rabbit cytosol were lower compared to renal Goettingen[®] Minipig cytosol, being in line with the results obtained by the *in vitro* kinetics of 1123-CYS cleavage in cytosolic fraction. Whether formation of the structurally not defined MFA-derivatives, which were detected in Goettingen[®] Minipig and NZW Rabbit cytosols but not in human and rat cytosols, contributes to 1123-CYS toxicity is unknown.

5.3 Effects of 1123-CYS and MFA on cell viability and cellular citrate levels in cell culture

5.3.1 Cytotoxicity of 1123-CYS and MFA¹

To assess if species-differences in toxicity of HFO-1123 can be reproduced in cell culture *in vitro* and to further confirm the role of β -lyases in toxicity of 1123-CYS, cytotoxicity of 1123-CYS was comparatively assessed in HK-2 (human), NRK-52E (rat) and LLC-PK1 (pig) proximal tubular cell lines in the absence and presence of the β -lyase inhibitor AOAA.

Interestingly, the porcine kidney cell line was found to be more susceptible (IC_{50} value: 0.8 mM) to 1123-CYS cytotoxicity as compared to rat (IC_{50} value: 3.4 mM) and human (IC_{50} value: 3.2 mM) proximal tubular cells (Figure 39, Table 10).

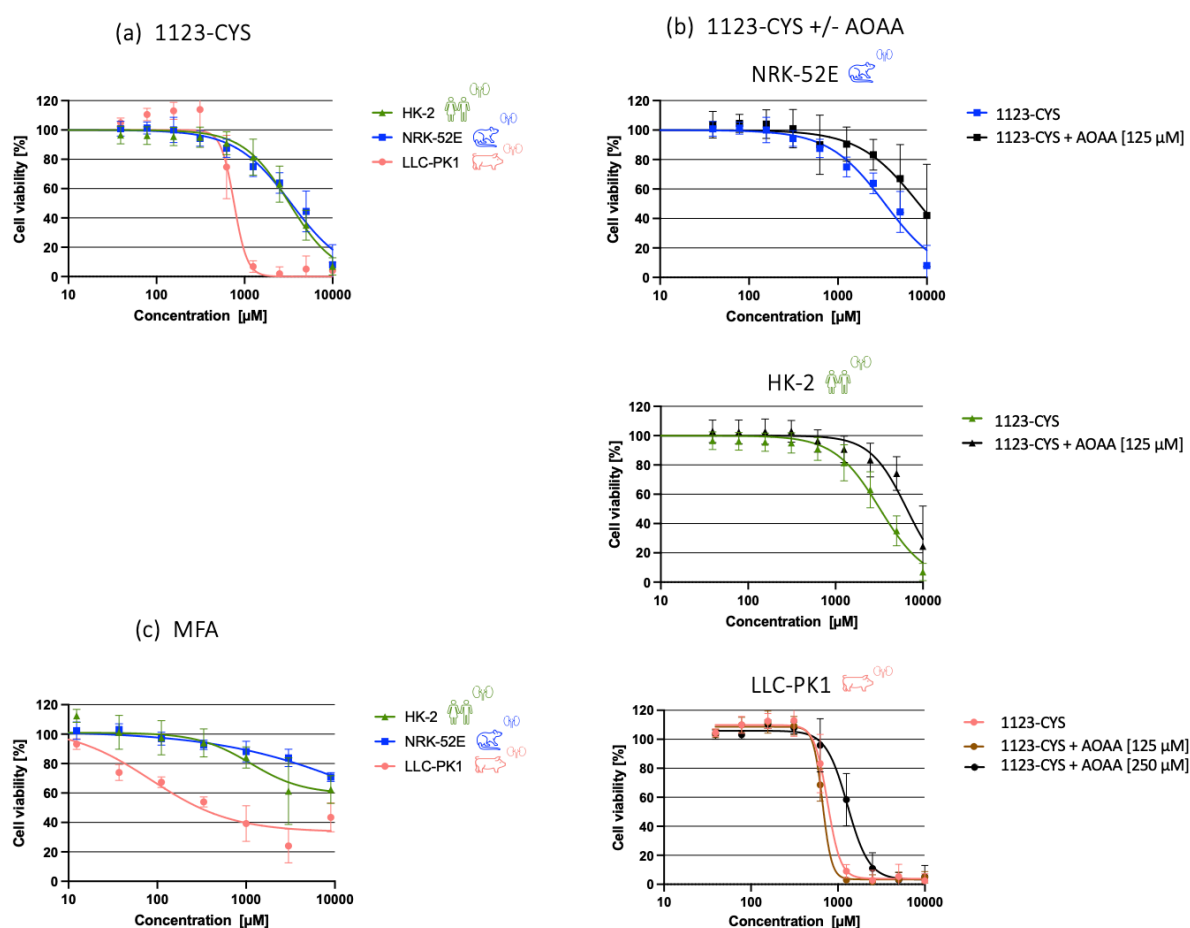


Figure 39 Cell viability of human (HK-2), rat (NRK-52E) and porcine (LLC-PK1) proximal tubular cell lines after 48h treatment with 1123-CYS (a) or MFA (c). Part (b) shows cell viability of HK-2, NRK-52E and LLC-PK1 cells after treatment with 1123-CYS in presence of AOAA (NRK-52E and HK-2: 125 µM AOAA; LLC-PK1: 125 µM / 250 µM AOAA). Results are presented as mean \pm standard deviation of three independent experiments, each performed in triplicates.

¹Cell culture experiments were carried out in collaboration with Johanna Serban, who was responsible for tissue culture maintenance, cell treatment and cytotoxicity testing. Raphael Dekant provided purified 1123-CYS and established the LC-MS/MS method for analysis of cellular citrate. Data acquisition and data analysis were performed by Raphael Dekant.

Table 10 IC₅₀ (mM) values of 1123-CYS cytotoxicity after 48h treatment in the presence and absence of AOAA [125 μM] / [250 μM] and MFA in proximal tubular cell lines (n = 3).

	IC ₅₀ (mM)		
	NRK-52E	HK-2	LLC-PK1
1123-CYS	3.4	3.2	0.8
+ AOAA [125μM]	8.1	6.6	0.7
+ AOAA [250μM]	n.d.	n.d.	1.3
MFA	40.9	16.1	0.6

n.d.: not determined

The β-lyase inhibitor AOAA ameliorated 1123-CYS toxicity in all proximal tubular cell lines, indicating that cytotoxicity of 1123-CYS depends at least to some extent on β-lyase enzyme activity (Table 10). Higher concentrations of AOAA were needed to produce a protective effect in LLC-PK1 cells (250 μM) as compared to NRK-52E and HK-2 cells (125 μM), presumably due to the higher β-lyase activity of porcine kidney as compared to that of other species. Interestingly, MFA was also found to be significantly more toxic in the porcine LLC-PK1 proximal tubular cells as compared to the other *in vitro* cell models.

5.3.2 Effects of 1123-CYS on cellular citrate¹

As cleavage of 1123-CYS to MFA is suspected to be responsible for HFO-1123 toxicity, we set out to test if biochemical changes associated with MFA poisoning also occur in our *in vitro* systems. Within the citric acid cycle, MFA is converted to fluorocitrate, the compound ultimately accountable for toxicity. Fluorocitrate is a potent inhibitor of aconitase, an essential enzyme in the citric acid cycle that catalyzes the turnover of citrate to isocitrate, via the intermediate cis-aconitate (Goncharov et al. (2006)). Accumulation of citrate is observed in experimental animals and mammalian cells exposed to MFA (Buffa and Peters, 1949; Buffa *et al.*, 1973; Gardner *et al.*, 1994) and may thus serve as an indicator of MFA intoxication. Furthermore, Keller *et al.* (1996) detected elevated concentrations of citrate in kidney and heart tissue of rats exposed to haloalkanes that are bioactivated to MFA, resulting in toxicity in experimental animals.

To obtain further evidence for the involvement of MFA in 1123-CYS toxicity, the effects of 1123-CYS on citrate levels were analyzed in human (HK-2), rat (NRK-52E) and porcine (LLC-PK1) proximal tubular cells by LC-MS/MS. MFA was used as a positive control to confirm the suitability of the experimental approach and the analytical method to detect changes in citrate levels. Concentrations of 1123-CYS and MFA used for determination of citrate levels in cell

lysates were chosen based on concentrations of 1123-CYS/MFA leading cytotoxicity observed in cell viability experiments.

Following incubation with MFA, statistically significant changes in citrate levels of cell lysates were observed in LLC-PK1 proximal tubule cells (Figure 40) and thus those in models previously established to be most susceptible to MFA toxicity (Figure 21). In contrast, no statistically significant changes in citrate levels of lysates were observed in NRK-52E, HK-2 and LLC-PK1 cells incubated with 1123-CYS, despite the significant cytotoxicity of 1123-CYS in LLC-PK1 cells in this concentration range. This may suggest that 1123-CYS toxicity may not be solely due to MFA formation and aconitase inhibition.

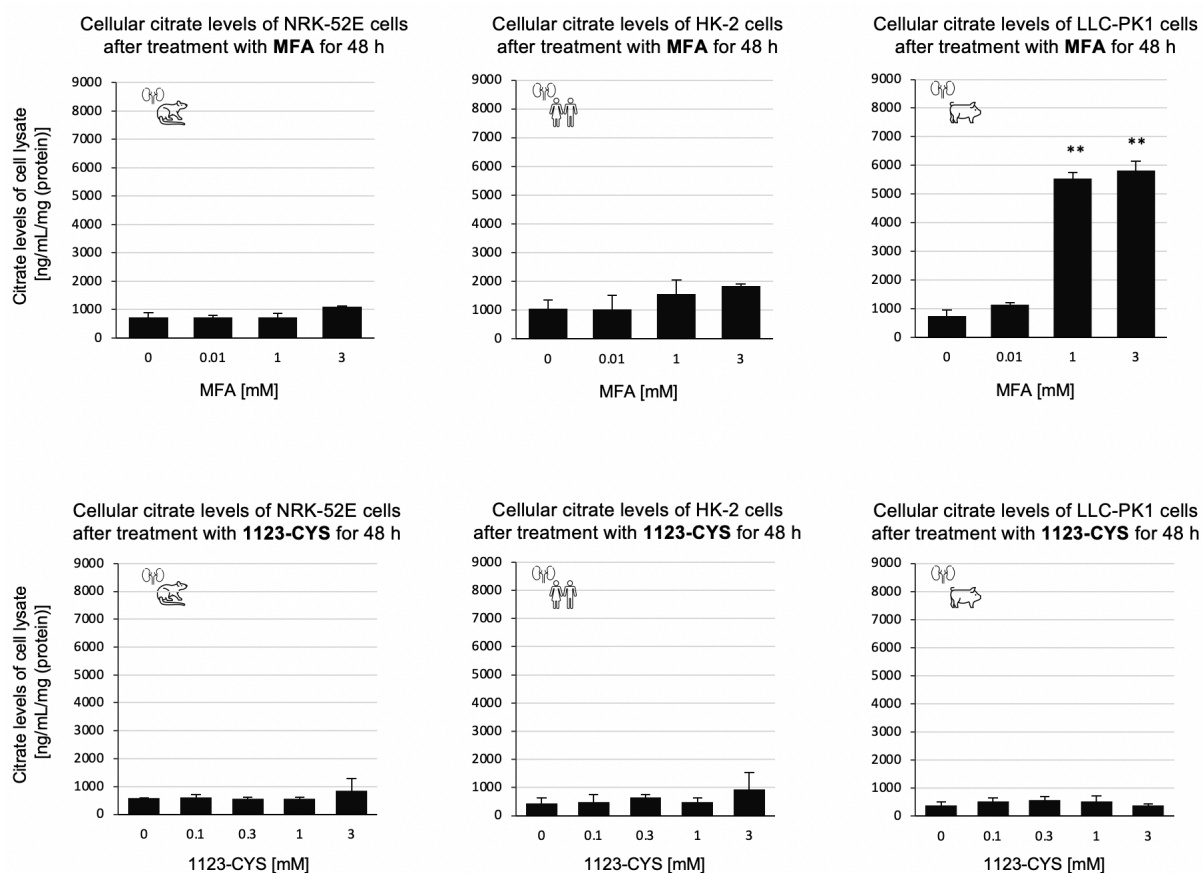


Figure 40 Citrate levels of rat (NRK-52E), human (HK-2) and porcine (LLC-PK1) proximal tubular cell lysates after treatment with MFA (a) and 1123-CYS (b). Statistically significant changes compared to controls were determined by one-way ANOVA with Dunnett's post-hoc test ($p > 0.05$; * $p \leq 0.05$; ** $p \leq 0.01$; *** $p \leq 0.001$).

We did not detect increased citrate levels (compared to controls) in lysates of proximal tubule epithelial cells exposed to 1123-CYS. This may indicate that in the cell models used, 1123-CYS does not lead to the formation of amounts of MFA sufficient to block aconitase. However, results obtained from the cell models in this study may have limited significance for actual *in vivo* conditions, as kidney exhibit several other cell types that may cleave 1123-CYS to MFA and thus lead to an increase in citrate levels.

¹Cell culture experiments were carried out in collaboration with Johanna Serban, who held responsible for tissue culture maintenance, cell treatment and cytotoxicity testing. Raphael Dekant provided purified 1123-CYS and established the LC-MS/MS method for analysis of cellular citrate. Data acquisition and data analysis were performed by Raphael Dekant.

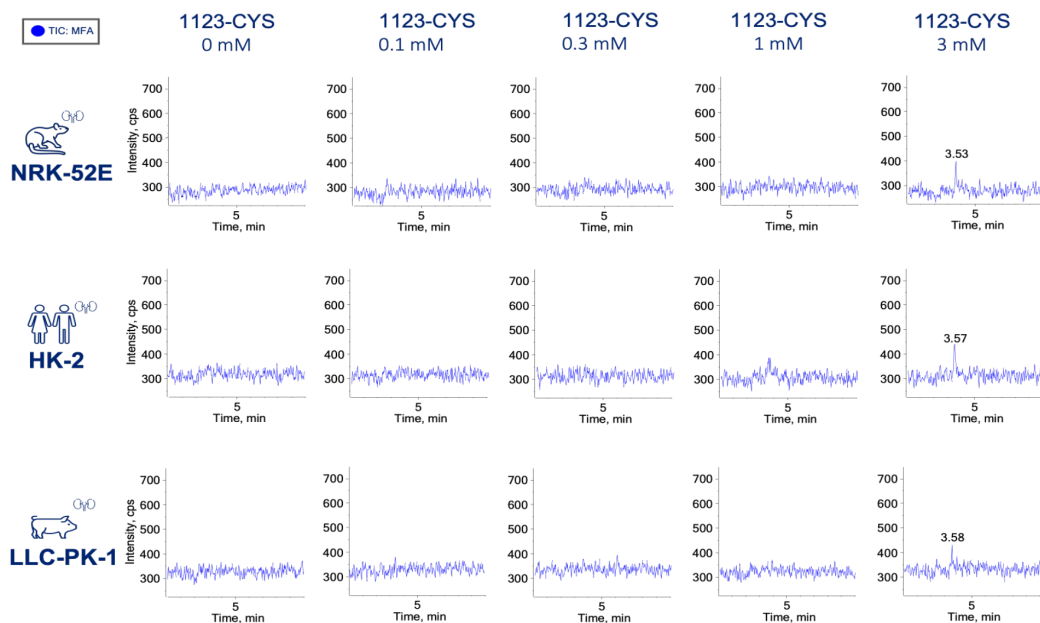
5.3.3 LC-MS/MS analysis of 1123-CYS metabolites in human, rat and porcine proximal tubular cells¹

Since determination of citrate levels in proximal tubular cells treated with 1123-CYS did not completely support MFA as the key toxic metabolite, LC-MS/MS analysis of cells treated with 1123-CYS was conducted to provide direct evidence for MFA formation and to test a possible role of *N*-acetyltransferase mediated biotransformation of 1123-CYS to the corresponding mercapturic acid (1123-CYS-NAc), which may be excreted in urine.

Irrespective of the cell model, MFA was detected at concentrations close to the LOD (approximately 0.5 μ M) in cell lysates treated with the highest concentration (3 mM) of 1123-CYS (Figure 41). In LLC-PK1 cells, which were found to be most susceptible to 1123-CYS toxicity, a concentration dependent increase in 1123-CYS-NAc formation was observed (Figure 41). 1123-CYS-NAc was not detected in NRK-52E or HK-2 cells, suggesting a lower rate of detoxification of 1123-CYS in these cells via the mercapturic acid pathway.

¹Cell culture experiments were carried out in collaboration with Johanna Serban, who was responsible for tissue culture maintenance, cell treatment and cytotoxicity testing. Raphael Dekant provided purified 1123-CYS and established the LC-MS/MS method for analysis of cellular citrate. Data acquisition and data analysis were performed by Raphael Dekant.

(a) TIC of MFA



(b) MRM of 1123-CYS-NAc

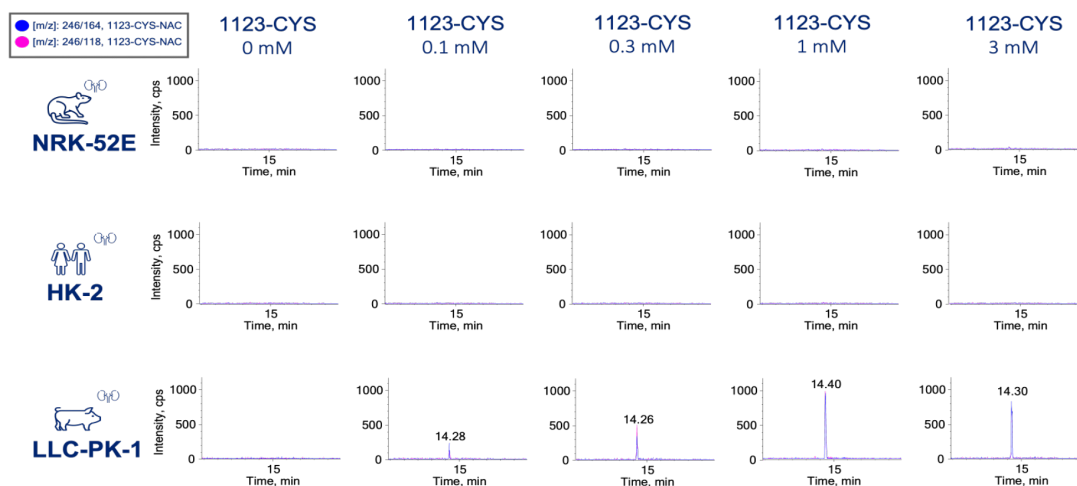


Figure 41 Analysis of MFA (a) and 1123-CYS-NAc (b) formed in NRK-52E, HK-2 and LLC-PK1 cells after treatment with increasing concentrations of 1123-CYS.

5.4 Summary of GST- and β -lyase dependent biotransformation of HFO-1123

Collectively, results from these studies suggest a higher rate of CYP-450 dependent metabolism of HFO-1123 in NZW Rabbit and Goettingen[®] Minipig liver S₉ as compared to human, mice and rat (Table 11). GSH dependent biotransformation of HFO-1123 was most prominent in NZW Rabbit, whereas Goettingen[®] Minipig and human showed the lowest rate of 1123-GSH formation (Table 11). In contrast, β -lyase activity towards 1123-CYS was significantly higher in Goettingen[®] Minipig cytosol as compared to the other species (Table 11). Of all cell lines investigated, porcine proximal tubule cells were found to be most susceptible to 1123-CYS and MFA toxicity (Table 12).

Table 11 Summary of *in vitro* biotransformation of HFO-1123 and 1123-CYS in renal and hepatic subcellular fractions

	Rat	Mouse	NZW Rabbit	G. Minipig	Human
Liver					
<i>S₉ fractions</i>					
CYP-450 mediated biotransformation ¹	+	+	+++	+++	+
1123-GSH ^{1,2}	++	++	+++	+	+
1123-CYS ²	n.d.	n.d.	++	+	+
β -lyase activity ²	n.d.	n.d.	+	n.d.	n.d.
<i>Cytosol</i>					
β -lyase assay ³	+	+	+	+	+
Kidney					
<i>Cytosol</i>					
β -lyase activity ³	+	+	+	+++	+
MFA formation ¹	+	n.e.	++	+++	+
MFA derivatives ¹	n.d.	n.e.	+	++	n.d.

n.d.: not detected; n.e.: not evaluated; +: low, ++: medium, +++: high

¹ evaluated by ¹⁹F-NMR, ² evaluated by LC-MS/MS, ³ evaluated by spectrometric β -lyase assay

Table 12 Summary of cytotoxicity and cellular citrate levels renal proximal tubular cells

	NRK-52E (rat)	HK-2 (human)	LLC-PK1 (pig)
Cytotoxicity¹			
1123-CYS	++	++	+++
MFA	+	+	++
Increased citrate levels²			
1123-CYS	n.d.	n.d.	n.d.
MFA	n.d.	n.d.	++

n.d.: not detected; +: low, ++: medium, +++: high

¹ evaluated by CellTiter-Glo[®] Luminescent Cell Viability Assay, ² evaluated by LC-MS/MS

6 Discussion

Species-differences in biotransformation are considered to account for species-differences in inhalation toxicity observed with HFO-1123 in experimental animals (rat, beagle dogs, Goettingen[®] Minipigs and NZW Rabbits). It was postulated that GSH dependent biotransformation via glutathione S-transferases (GST) and subsequently by β -lyases may play a key role in the bioactivation and toxicity of HFO-1123. Thus, while GST mediated formation of S-(1,1,2-trifluoroethyl)-L-glutathione (1123-GSH) from HFO-1123 in the liver is suggested as the initial step in the metabolism via the mercapturic acid pathway, subsequent cleavage of the corresponding cysteine S-conjugate, S-(1,1,2-trifluoroethyl)-L-cysteine (1123-CYS), via β -lyases presumably to MFA, is assumed to be the critical step in the toxicity of HFO-1123 observed in sensitive species. The aim of the present work was to investigate possible species-differences in the hepatic biotransformation of HFO-1123 and subsequent cysteine S-conjugate β -lyase mediated biotransformation of 1123-CYS in subcellular fractions of susceptible versus less susceptible species and humans as a basis for human risk assessment.

6.1 GST mediated formation of 1123-GSH in hepatic and renal S₉

Characterizing species-differences in GST mediated formation of 1123-GSH *in vitro* is important to understand the initial step of HFO-1123 biotransformation and to draw conclusions on HFO-1123 toxicity *in vivo*. Incubations of hepatic Goettingen[®] Minipig, NZW Rabbit, mouse, rat and human S₉ fractions confirmed HFO-1123 as a substrate for GST mediated biotransformation, leading to the formation of 1123-GSH. Time-dependent formation of 1123-GSH was significantly higher in rat (900.2 ± 118.0 ng/mL), mouse (1053.3 ± 189.8 ng/mL) and NZW Rabbit (986.9 ± 379.7 ng/mL) compared to human (169.9 ± 77.4 ng/mL) and Goettingen[®] Minipig (214.0 ± 78.6 ng/mL) S₉. This is supported by the *in vitro* kinetics of 1123-GSH formation, which indicate an increased GST activity towards HFO-1123 in NZW Rabbit, rat and mouse compared to human and Goettingen[®] Minipig S₉. Compared to GST mediated biotransformation of trichloroethylene (TRI, the chlorine analog of HFO-1123) leading to the time-dependent formation of DCVG, 1123-GSH formation from HFO-1123 is comparably low in hepatic S₉. The lower extent of biotransformation of HFO-1123 compared to TRI may be explained due to increased stability of C-F bonds compared to C-Cl bond.

Across all species, significantly lower amounts of 1123-GSH were detected in the presence of an NADPH regenerating system, indicating CYP-450 mediated biotransformation as an additional route of HFO-1123 metabolism. CYP-450 mediated metabolism, which appears to occur at higher rates in Goettingen[®] Minipig and NZW Rabbit hepatic S₉, is likely to give rise to F⁻, as evidenced by the detection of ¹⁹F-NMR signals corresponding to F⁻ formation in Goettingen[®] Minipig and NZW Rabbit hepatic S₉ in the presence of the NADPH regenerating

system. HFO-1123 undergoes limited CYP-450 dependent biotransformation (judged by the amount of formed F⁻) in rat, mouse and human S₉.

Results obtained are consistent with previous work regarding the *in vitro* biotransformation of HFO-1123 conducted by Yokoyama *et al.* (2018), where formation of 1123-GSH was monitored in hepatic cytosol and microsomes from male SD rats, NZW Rabbits, Goettingen[®] Minipigs, Beagle dogs, cynomolgus monkeys and humans after incubation with HFO-1123. Increased formation of 1123-GSH was observed in SD rat and NZW Rabbit compared to Goettingen[®] Minipig, human, dog, and monkey subcellular fractions. Furthermore, in the presence of NADPH lower amounts of 1123-GSH formed were detected compared to the absence of NADPH. Findings of Yokoyama and colleagues indicate an increased biotransformation of HFO-1123 in subcellular fractions of rats and NZW Rabbits compared to the other species.

Using ¹⁹F-NMR analysis, no fluorine containing metabolites other than F⁻ and 1123-GSH, as the major metabolite formed by GST mediated biotransformation of HFO-1123, were detected in hepatic S₉ fractions incubated with HFO-1123. While ¹⁹F-NMR may not be sufficiently sensitive to detect minor metabolites, these findings overall confirm GST-mediated biotransformation as the major metabolic pathway for HFO-1123. Based on the marked species differences in HFO-1123 inhalation toxicity, it was anticipated that the rate of 1123-GSH formation would be higher in Goettingen[®] Minipig and NZW Rabbits as compared to mice and rats, which appear to be resistant to HFO-1123 toxicity. In contrast, our data suggest that increased GSH mediated biotransformation of HFO-1123 occurs in NZW Rabbit, rat and mouse S₉ fractions compared to Goettingen[®] Minipig S₉.

Since increased GST mediated biotransformation of HFO-1123 in NZW Rabbit, rat and mouse compared to human and Goettingen[®] Minipig hepatic S₉ is not completely in line with the hypothesis of increased biotransformation of HFO-1123 in Goettingen[®] Minipigs and NZW Rabbits being causal for *in vivo* toxicity, differences in the further metabolic fate of 1123-GSH were investigated. LC-MS/MS analysis of 1123-CYS in incubations of HFO-1123 with hepatic S₉ indicated higher rates of cleavage of 1123-GSH to 1123-CYS in NZW Rabbit, human and Goettingen[®] Minipig compared to rat and mouse hepatic S₉, although overall the levels of 1123-CYS found were low compared to 1123-GSH. γ -GTs catalyze the first step in the conversion of GSH S-conjugates to their corresponding cysteine S-conjugates, via a cysteinylglycine S-conjugate intermediate. An inhibitor of γ -GTs is acivicin. It was demonstrated that cytotoxicity of some glutathione S-conjugates derived from nephrotoxic haloalkenes could be reduced in renal proximal tubular cells in the presence of acivicin. For example, acivicin could protect renal tubular cells against S-(1,2-dichlorovinyl)-L-glutathione (DCVG, glutathione S-conjugate derived from trichloroethene) induced toxicity (Elfarra *et al.*, 1986; Lash *et al.*, 1986). However,

the nephrotoxicity of hexachloro-1,3-butadiene could not be reduced by acivicin in rats *in vivo* (Davis, 1988). In the present study, γ -GT mediated cleavage of 1123-GSH in NZW Rabbit hepatic S₉ fractions could be blocked, as evidenced by increased 1123-GSH levels in the presence of acivicin. In contrast, acivicin had no effect on the levels of 1123-GSH in other species. This may indicate that γ -GT dependent processing of 1123-GSH occurs at higher rates in NZW Rabbit hepatic S₉ as compared to liver S₉ of the other species. However, inhibition of γ -GT by acivicin was not paralleled by further cleavage of the cysteinylglycine S-conjugate.

Activity of GSTs and γ -GTs (and additional enzymes involved in processing of haloalkenes via the mercapturic acid pathway) may differ significantly between tissue and mammalian species, making it challenging to evaluate the complete metabolic pathway in one single tissue/*in vitro* system. While GSTs are expressed in hepatic tissue of mammals in highest concentrations, γ -GTs are abundantly expressed at the apical membranes of the renal proximal tubules (Ketterer and Christodoulides, 1994). γ -GT localization is not limited to renal tissue, as a variety of epithelial cells of ducts and glands in e.g. liver, testes, endocervix, prostate sweat glands, brain and spinal cords express γ -GTs, but activity is generally lower compared to renal tissue (Cooper and Hanigan, 2018). Interestingly, levels of γ -GT may differ significantly between mammals and inter-organ biotransformation and trafficking of potential metabolites formed by GSH-conjugation can differ between species. For example, compared to the rat and the rabbit, humans, guinea pigs and pigs exhibit increased levels of hepatic γ -GT activity (Hinchman and Ballatori, 1990). Furthermore, processing of the cysteinylglycine adduct obtained from γ -GT mediated cleavage of the GSH S-conjugate may occur in renal tissue as well. Cysteinylglycine adducts are commonly hydrolyzed by aminopeptidase N (APN) or cysteinylglycine dipeptidase (DPP) to their corresponding cysteine S-conjugates (Poon and Josephy, 2012; Taniguchi, 2012). Both APN and DPP are readily expressed on apical brush-border membranes of epithelial cells in the renal proximal tubules, testes and small intestines and in lower levels in a variety of other organs (Kozak and Tate, 1982) with increased levels being present in renal tissue. Commonly, GSH S-conjugates are cleaved at the brush-boarder membrane of the proximal tubules to their corresponding cysteine S-conjugates by γ -GT and APN/DPP (Hughey *et al.*, 1978; Jones *et al.*, 1988).

An increased β -lyase activity towards 1123-CYS and a thus rapid cleavage of 1123-CYS formed from 1123-GSH in hepatic S₉ might be expected to reduce the amount of 1123-CYS and thus to give a false prediction of the extent of 1123-CYS formation from 1123-GSH. To test if increased β -lyase activity in hepatic S₉ may cause rapid cleavage of 1123-CYS, 1123-CYS formation was evaluated in incubations of HFO-1123 in the presence and absence of AOAA, a specific inhibitor of β -lyases. Results implicate a slightly increased β -lyase activity in NZW Rabbit compared to human, Goettingen[®] Minipig, rat and mouse S₉. However,

differences in β -lyase mediated biotransformation in the liver do not seem to contribute to the cleavage of 1123-GSH, as only low amounts of 1123-CYS were detected in liver S_9 . This is also in line with literature, reporting increased activity of β -lyases towards haloalkenes in renal tissue of different mammalian species (Cooper and Pinto, 2006). Based on the general expression and localization of enzymes that are thought to be involved in the bioactivation of HFO-1123 via the mercapturic acid pathway, inter-organ transport of these potential metabolites is necessary. It is expected that a transfer of 1123-GSH from the liver to other organs (e.g. kidneys) takes place where subsequent biotransformation steps (e.g. γ -GT, DPP, APN and β -lyase) occur.

Overall, the obtained data on liver metabolism of HFO-1123 provide evidence for increased GST mediated biotransformation in NZW Rabbits but not in Goettingen[®] Minipig as compared to less susceptible species. Thus, the results do not fully support the working hypothesis that GSH dependent biotransformation of HFO-1123 via the mercapturic acid pathway in the liver plays a key role in HFO-1123 toxicity.

To understand the contribution of extrahepatic tissues in GST-mediated conjugation of HFO-1123 with GSH, 1123-GSH and 1123-CYS formation was further evaluated in renal S_9 fractions of humans, rats and Goettingen[®] Minipigs. Renal GST mediated biotransformation of haloalkenes is generally low compared to hepatic activity (Hanna and Anders, 2019), but it was found necessary to evaluate 1123-GSH and 1123-CYS formation in renal S_9 in the presence of HFO-1123. While time-dependent formation of 1123-GSH and 1123-CYS was observed in renal S_9 fractions of all species, no species-differences in the levels of 1123-GSH and 123-CYS formed were apparent. However, the levels of 1123-GSH formed were significantly lower in renal S_9 (20 to 50-fold) compared to hepatic S_9 , while no significant differences in formation of 1123-CYS were detected between renal and hepatic fractions. These data suggest that soluble GSTs in renal S_9 fractions unlikely to play a significant role in the initial step of HFO-1123 biotransformation.

6.2 β -lyase mediated biotransformation of 1123-CYS in renal and hepatic cytosols

1123-CYS is expected to be the product of γ -GT, aminopeptidase N and cysteinylglycine dipeptidase mediated cleavage of 1123-GSH and a substrate of β -lyase cleavage leading to the formation of MFA as final toxic metabolite. In general, cysteine S-conjugates derived from haloalkenes may accumulate in the epithelial cells of the kidney where further processing occurs (Cooper and Hanigan, 2018).

β -Lyases are thought to play a pivotal role in bioactivation of 1123-CYS, as they are directly linked to the toxicity of several cysteine S-conjugates derived from haloalkenes as TRI, chlorotrifluoroethylene, 1,1-dibromo-2,2-difluoroethylene and 1,1-dichloro-2,2-difluoroethylene (Boogaard *et al.*, 1989). At least eleven enzymes (e.g. glutamine transaminase K (GTK), mitochondrial and cytosolic aspartate aminotransferase (mitAspAT/cytAspAT), γ -cystathionase and branched-chain aminotransferases (BCAT)) that catalyze the cleavage of cysteine S-conjugate are known to be present in mammalian tissue and are thus collectively referred to as β -lyases (Cooper and Pinto, 2006). All β -lyases are pyridoxal 5'-phosphat dependent and are present in cytosol or mitochondria of mammalian cells. There is evidence for some level of substrate specificity of individual β -lyases. For example DCVC is substrate of GTK and mitAspAT, but not susceptible for γ -cystathionase mediated β -lyase cleavage (Yamauchi *et al.*, 1993; Cooper *et al.*, 2003). Also, the species-specific expression of particular β -lyases is described. Alanine aminotransferase and GABA aminotransferase are reported to be solely express in pigs and mitochondrial and cytosolic BCAT are exclusive to human tissue (Gaskin *et al.*, 1995; Cooper *et al.*, 2003).

β -Lyases can be found in almost all tissues (e.g. kidneys, liver, heart, intestines) of various mammalian species (rat, rabbit, pig, human), but activity of the respective β -lyase may vary significantly between tissue and species. However, the common target of cysteine S-conjugates (e.g. DCVC, TCVC) derived from haloalkenes (e.g. trichloroethylene, tetrachloroethylene) are renal proximal tubular cells. This indicates increased specific activity of β -lyase towards cysteine S-conjugates derived from haloalkenes in the kidney and especially in proximal tubular cells (Cooper and Hanigan, 2018).

Analysis of β -lyase mediated biotransformation of 1123-CYS in hepatic and renal cytosolic fractions of susceptible and non-susceptible species and humans confirmed 1123-CYS as a substrate of β -lyase cleavage. This is supported by the time- and protein concentration dependent formation of pyruvate and fluorine containing metabolites and inhibition of their formation in the presence of the specific β -lyase inhibitor AOAA.

In liver cytosols, β -lyase activity towards 1123-CYS did not differ significantly between species, which suggests that the liver is unlikely the primary organ responsible for possible species-differences in β -lyase mediated biotransformation. However, β -lyase activity with 1123-CYS in renal Goettingen[®] Minipig cytosol was significantly higher compared to hepatic and renal cytosolic fractions from human, rat, mouse and NZW Rabbit. NZW Rabbit renal cytosol showed slightly increased β -lyase activity compared to renal fractions from human, rat and mouse. Enzyme kinetic data obtained by determining pyruvate were further supported by analysis of fluorine containing metabolites using ¹⁹F-NMR. Renal Goettingen[®] Minipig and renal and hepatic NZW Rabbit cytosol incubated with 1123-CYS showed time-dependent formation of MFA, F⁻ and MFA-derivatives. Consistent with the spectrometric assay, the amounts of F⁻, MFA and MFA-derivates formed in NZW Rabbit cytosol were lower compared to renal Goettingen[®] Minipig cytosol. Whether formation of the structurally not defined MFA-derivatives, which were exclusively detected in Goettingen[®] Minipig and NZW Rabbit cytosols but not in human and rat cytosols, contributes to 1123-CYS toxicity is unknown. In the presence of the specific β -lyase inhibitor AOAA, formation of MFA, F⁻ and MFA-derivatives was inhibited, thus confirming that these metabolites are formed via β -lyase mediated cleavage of 1123-CYS. Although MFA and F⁻ formation was also observed in incubations of 1123-CYS with human kidney and liver cytosol, the signal intensities of MFA and F⁻ obtained with human cytosols were significantly lower than those obtained with Goettingen[®] Minipig kidney cytosol. Overall, our ¹⁹F-NMR studies demonstrate that β -lyase mediated cleavage of 1123-CYS, which occurs at significantly higher rates in renal fractions of Goettingen[®] Minipigs as compared to renal and hepatic fractions of other species, gives rise to MFA and F⁻.

These findings are consistent with differences in the urinary excretion of MFA between rats and Goettingen[®] Minipigs after HFO-1123 exposure. The *in vivo* formation and urinary excretion of MFA was evaluated by ¹⁹F-NMR after inhalation exposure of HFO-1123 in rats (exposed to 20,000 ppm HFO-1123 for 4 hours) and Goettingen[®] Minipigs (exposed to 85 and 200 ppm for 4 hours) by Wako and colleagues (2019b; 2019a). In contrast to rats, Goettingen[®] Minipigs excreted traces of MFA as a urinary metabolite after exposure to 200 ppm HFO-1123. This may indicate an increased metabolism of HFO-1123 towards MFA in the Goettingen[®] Minipig *in vivo* being causal for HFO-1123 toxicity.

As HFO-1123 does not lead to nephrotoxicity in inhalation experiments with rats, HU-liver TK-NOG mice, NZW Rabbits and Goettingen[®] Minipigs, it may also possible that β -lyase dependent biotransformation of 1123-CYS leading to MFA occurs in other organs (e.g. cardiac tissue) which may explain symptoms of toxicity after HFO-1123 inhalation exposure. Histopathological changes in cardiac tissue of surviving and moribund NZW Rabbits and Goettingen[®] exposed to HFO-1123, indicate the heart as a target organ of HFO-1123 toxicity.

As porcine cardiac tissue features cytoAspAT (Ueno *et al.*, 1982), β -lyase cleavage of 1123-CYS may be possible. Cleavage of 1123-CYS to MFA in cardiac tissue may lead to interferences of the TCA cycle and may explain histopathological changes of the heart of NZW Rabbits and Goettingen[®] Minipigs. An increased β -lyase mediated metabolism of 1123-CYS to MFA in cardiac tissue of susceptible species, may explain the species differences in toxicity of HFO-1123. It could be necessary to evaluate cleavage of 1123-CYS and formation of MFA in cardiac tissue homogenates (cytosol/microsomes) of susceptible and less susceptible species to evaluate a possible contribution of cardiac metabolism in HFO-1123 (cardio)toxicity.

6.3 β -lyase mediated biotransformation of 1123-CYS and cytotoxicity in cell culture

As described previously β -lyase activity towards cysteine S-conjugates derived from haloalkenes is elevated in proximal tubular cells of the kidney. To further support the observed species differences in β -lyase mediated cleavage of 1123-CYS in renal and hepatic cytosol, cytotoxicity of 1123-CYS was evaluated in rat (NRK-52E), porcine (LLC-PK1) and human (HK-2) renal proximal tubular cell lines.

LLC-PK1 cells were more susceptible to 1123-CYS, compared to human and rat kidney cells, thus reflecting the species-differences observed in HFO-1123 toxicity *in vivo*. Results obtained in cell culture further support a role of β -lyase mediated cleavage in 1123-CYS toxicity, as evidenced by the amelioration of 1123-CYS cytotoxicity in the presence of the β -lyase inhibitor AOAA. Interestingly, higher concentrations of AOAA were required in porcine cell lines to elicit a protective effect against 1123-CYS toxicity compared to rat and human proximal tubular cells. As higher concentrations of AOAA were needed to protect LLC-PK1 cells from 1123-CYS cytotoxicity, this may indicate an elevated β -lyase dependent metabolism of 1123-CYS or/and an increased specific activity of porcine β -lyases towards 1123-CYS leading to cytotoxic metabolites (e.g. MFA).

However, as mentioned previously, at least eleven enzymes are capable of β -cleavage of cysteine S-conjugates and tissue, and species differences in the distribution and specific activity of different β -lyases exist. For example, alanine aminotransferase and GABA aminotransferase are solely expressed in pigs and mitochondrial and cytosolic BCAT are exclusive to human tissue (Cooper and Pinto, 2006). Whether proximal tubular cells used in this study feature similar β -lyase composition as described for *in vivo* conditions is not known.

In addition to species differences in the expression of β -lyase with specific activity towards individual cysteine S-conjugates, uptake and accumulation of the cysteine S-conjugate into the cell system is of major importance. β -Lyases are located in renal cytosol and mitochondria of proximal tubular epithelial cells, thus β -lyase mediated biotransformation of 1123-CYS may

dependent to a great extent on specific transport into renal proximal tubular cells. In general, cysteine S-conjugates and mercapturates can be transferred by diffusion and active transport across cell membranes. Four families of transporters, namely multidrug resistance ABC transporters, amino acid transporters (AAT), organic anion transporters (OAT) and organic anion transporting polypeptide transporters are accountable for active transport of cysteine S-conjugates into renal proximal tubular cells (Hanna and Anders, 2019). Na⁺-dependent probenecid-sensitive OAT-1 (OAT-1) and Na⁺-dependent/independent AAT seem to play a decisive role in the active transport and accumulation of haloalkene derived cysteine S-conjugates, e.g. DCVC, S-(2-chloro-1,1,2-trifluoroethyl)-L-cysteine)-L-cysteine and S-(pentachlorobutadienyl)-L-cysteine in renal proximal tubular *in vitro* systems (Dekant *et al.*, 1994; Wright *et al.*, 1998; Groves *et al.*, 2003). As transport of 1123-CYS into renal tubular cells was not investigated yet, a read-across approach was used to identify possible species differences in transporter expression. In this regard, the transport and accumulation of DCVC was investigated in great detail in renal proximal tubular cells systems, renal proximal tubular cell preparation and isolated renal tubules of various mammalian species. Depending on the mammalian species, different transporters/transporter subtypes were identified of being accountable for transferring DCVC across renal basolateral membranes. OAT-1 and Na⁺-dependent/independent AAT were identified of transporting DCVC proximal tubular cells of rats and NZW rabbit proximal tubular preparations (Schaeffer and Stevens, 1987a; Lash and Anders, 1989). However, in porcine LLC-PK1 cells uptake of DCVC is associated with Na⁺-dependent L-like AAT (Schaeffer and Stevens, 1987b). To our knowledge, the transport of DCVC in isolated human renal proximal tubular cells was not studied yet. However investigations with Chinese hamster ovary cells transfected with human OAT1, suggest involvement of this transporter in the uptake of DCVC in humans (Groves *et al.*, 2003). In summary, studies with DCVC identified OAT1 and Na⁺-dependent/independent AATs to be accountable for transport into renal proximal tubular cells of different mammalian tissue. These may also be accountable for 1123-CYS transport. However, there are no data on the relative expression and activity of these transporters in different species *in vivo* and in the renal cell lines used in the present study. While species-differences in transporter activity for 1123-CYS leading to differences in intercellular concentration of 1123-CYS and subsequent β -lyase mediated metabolism may contribute to species-differences in HFO-1123 toxicity, it should be recognized that expression of transporters and xenobiotic metabolizing enzymes in immortalized cells in culture may not exactly match the physiological conditions *in vivo*. Thus, it is possible that the differential cytotoxicity of 1123-CYS observed in the different renal cell models may reflect an altered physiology state compared to kidney cells *in vivo* rather than true species-specific effects.

Porcine kidney cells were also most susceptible to MFA toxicity. Cytotoxicity of MFA in these cells was associated with a concentration-dependent increase in cellular citrate levels, consistent with inhibition of aconitase. In contrast, no changes in citrate levels were observed in response to 1123-CYS treatment in any of the cell lines investigated, despite significant cytotoxicity of 1123-CYS in all cell lines. This may indicate that 1123-CYS toxicity may – at least in part – involve mechanisms other than MFA formation and aconitase inhibition. Detection of minor amounts of MFA by LC-MS/MS in proximal tubular cell lysates after incubation with 1123-CYS without apparent differences between cell lines, further supports the possibility of an alternative mechanism. Metabolite formation of 1123-CYS in proximal tubular cell lysates monitored by LC-MS/MS revealed the concentration dependent formation of the corresponding mercapturic acid 1123-CYS-NAc only in porcine proximal tubular cell lysates. Commonly, *N*-acetylation of cysteine *S*-conjugates usually presents a mechanism of detoxication. However, bioactivation of *N*-acetyl-*L*-cysteine and cysteine *S*-conjugates of tetrachloroethene and trichloroethene (e.g. *S*-(1,2,2-trichlorovinyl)-*L*-cysteine, *N*-acetyl-*S*-(1,2,-trichlorovinyl)-*L*-cysteine, *N*-acetyl-*S*-(1,2-dichlorovinyl)-*L*-cysteine) by sulfoxidation, resulting in the formation of cytotoxic and mutagenic *N*-acetyl-*L*-cysteine and cysteine *S*-conjugate sulfoxides, is described in literature (Werner *et al.*, 1996; Krause *et al.*, 2003). In general, toxicity of cysteine *S*-conjugates derived from haloalkenes relies on β -lyase dependent cleavage to a reactive metabolite. In contrast their corresponding sulfoxides are not cleaved to a great extent by β -lyases, thus not leading to reactive metabolites (Elfarrar and Krause, 2007). The same applies for sulfoxides derived from *N*-acetyl-*L*-cysteine derivatives formed from haloalkenes. The toxicity of these sulfoxides can be explained, as they are directly acting nucleophiles and Michael acceptors. It is postulated that they are capable of depleting cellular GSH storages in mitochondria associated with production of hydrochloric acid leading to apoptosis in renal tissue (Lash *et al.*, 2003). However, the exact mechanism still needs to be elucidated. Sulfoxides from *N*-acetyl-*L*-cysteine and cysteine *S*-conjugates derived from tetrachloro- and trichloroethene were found to be potent nephrotoxics *in vivo* and did not show toxicity in other organs. Interestingly, *S*-(1,2,2-trichlorovinyl)-*L*-cysteine sulfoxide (TCVCS) exhibits increased nephrotoxicity in rats *in vivo* compared to its corresponding cysteine *S*-conjugate, *S*-(1,2,2-trichlorovinyl)-*L*-cysteine (TCVC) (both compounds are metabolites of tetrachloroethene) (Elfarrar and Krause, 2007). As TCVCS is formed from TCVC *in vitro*, it is anticipated that TCVCS plays a role in nephrotoxicity observed in response to tetrachloroethene. In summary, sulfoxides of *N*-acetyl-*L*-cysteine and cysteine *S*-conjugates derived from tetrachloro- and trichloroethene are associated with the toxicity of these haloalkenes. Whether 1123-CYS-NAc or 1123-CYS are metabolized to their corresponding sulfoxide is yet unknown. If formed to a great extent in the HFO-1123 susceptible species, these sulfoxides could play a role in the species-specific toxicity.



6.4 Summary and Conclusion

A summary of *in vitro* and *in vivo* investigations regarding species differences in biotransformation and toxicity of HFO-1123 performed in the present study is provided in Figure 42. Single exposure of Goettingen[®] Minipigs and NZW Rabbits to HFO-1123 showed mortality and moribundity at concentrations ≥ 500 ppm and ≥ 1250 ppm, respectively (Wako, 2016, 2017). In contrast, toxicity of HFO-1123 in rats was low, with NOAELs for HFO-1123 inhalation exposure in rats $> 20,000$ ppm (Wako, 2014c). Species differences in toxicity are possibly due to a species-specific biotransformation. Within the biotransformation of HFO-1123, GSTs and β -lyases are anticipated to play a key role and species differences in their activity may explain *in vivo* toxicity. Significantly higher β -lyase activity towards 1123-CYS associated with formation of MFA and F⁻ was recorded in renal Goettingen[®] Minipig cytosol as compared to cytosolic fractions of other species. NZW Rabbit hepatic and renal cytosol also showed increased β -lyase activity compared to hepatic and renal fractions from human, rat and mouse. Furthermore, increased β -lyase mediated cytotoxicity of 1123-CYS was observed in porcine proximal tubular cells compared to rat and human cell cultures. Overall, data obtained within this work provide some support for the hypothesis that increased β -lyase mediated cleavage of 1123-CYS and subsequent MFA formation in Goettingen[®] Minipig and NZW Rabbit kidney cytosol contribute to the toxicity of HFO-1123 observed in this species. This is furthermore supported by the detection of MFA in proximal tubular cell systems after incubation with 1123-CYS. The lower β -lyase activity towards 1123-CYS in human cytosolic fractions may suggest that humans may be less susceptible to HFO-1123 toxicity as compared to Goettingen[®] Minipig and NZW Rabbit.

However, liver metabolism of HFO-1123 to 1123-GSH as the initial step in GSH dependent biotransformation via the mercapturic acid pathway was significantly lower in Goettingen[®] Minipig (and human) S₉ as compared to NZW Rabbit and hepatic S₉ fractions of less susceptible species (mouse and rat).

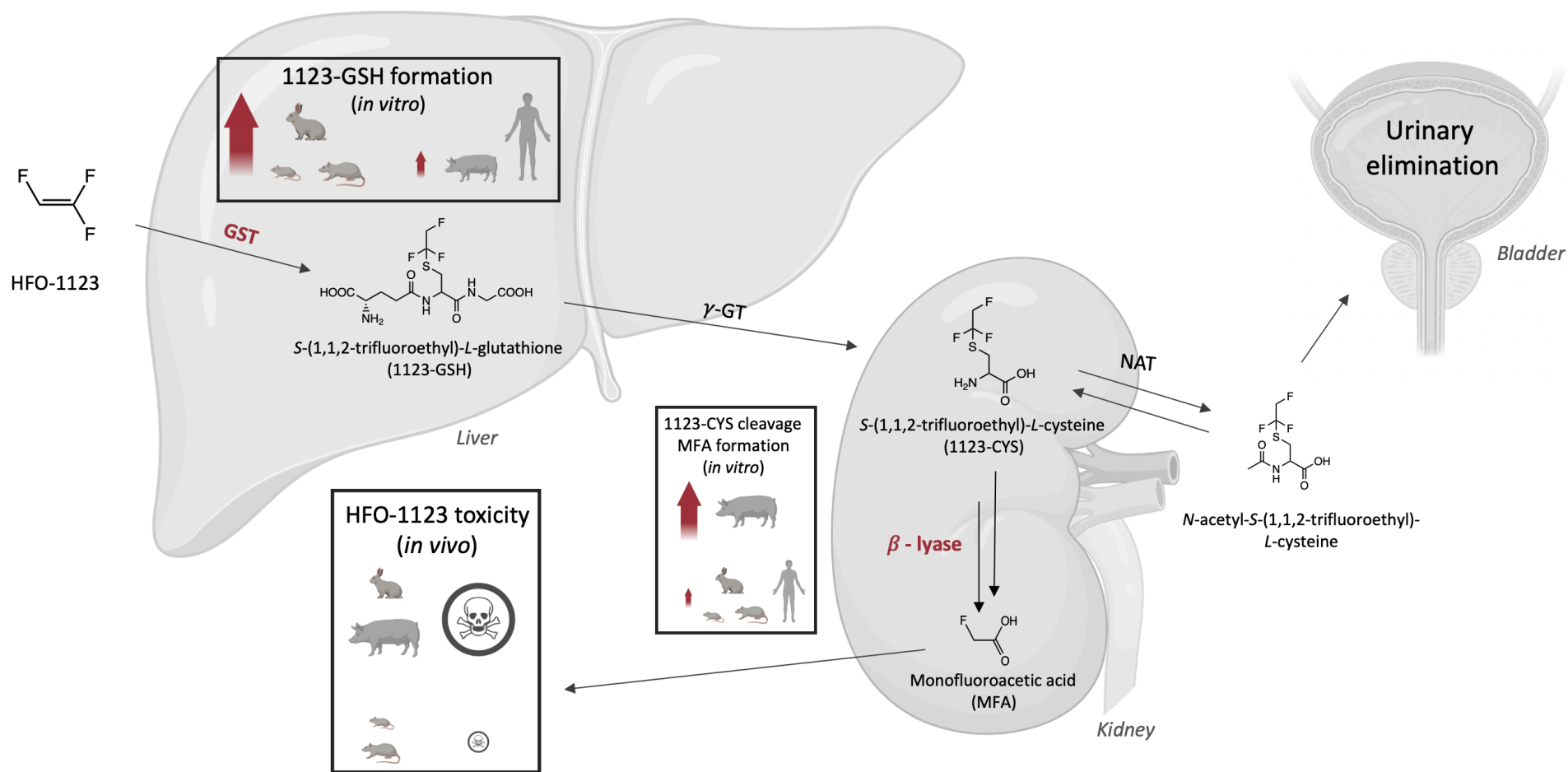


Figure 42 Overview of *in vivo* toxicity of HFO-1123 and *in vitro* species-differences in biotransformation. Results obtained *in vitro* partially support an increased biotransformation of HFO-1123 in the susceptible species (Goettingen[®] Minipig and NZW Rabbit) responsible for toxicity. GSH mediated biotransformation, leading to the formation of 1123-GSH, was increased in NZW Rabbit, rat and mouse hepatic S₉ compared to Goettingen[®] Minipig and human fractions. In contrast, β -lyase mediated cleavage of 1123-CYS leading to MFA formation was increased in renal Goettingen[®] Minipig cytosol compared to other species. Despite increased cytotoxicity of 1123-CYS in porcine proximal tubule cells, increased NAT mediated biotransformation was detected in porcine cells compared to rat and human cell lines. Increased β -lyase cleavage of 1123-CYS and formation 1123-CYS-NAc in porcine cells may indicate enhanced biotransformation of HFO-1123 in this cell line as compared to the other cell models investigated.

Based on the inconsistencies between GST and β -lyase mediated biotransformation, these *in vitro* data do not allow to draw firm conclusions regarding the relative contribution of the mercapturic acid pathway to HFO-1123 biotransformation in kidney and liver in these species *in vivo*. It is conceivable that other organs (e.g., lungs, respiratory epithelium) may participate in GSH dependent biotransformation of HFO-1123. For several halogenated alkenes, biotransformation also occurs in the respiratory system. For example, the initial step in GSH dependent biotransformation of trichloroethylene (TRI), was identified in Clara cells of the bronchial epithelium (next to liver and kidney) and has been postulated to be co-responsible for toxicity (Forkert *et al.*, 2005; Forkert *et al.*, 2006). Based on these findings, it is possible that the respiratory tract may play an important role in the overall metabolism of HFO-1123 *in vivo* and thus may be worth investigating.

In addition to the metabolism of HFO-1123 in organs other than liver and kidney, interorgan transport of GSH S-conjugates, cysteine S-conjugates and metabolites derived thereof may play a vital role in biotransformation and toxicity of HFO-1123. As mentioned before, formation of GSH S-conjugates derived from haloalkenes predominately occurs in hepatic tissue, cysteine S-conjugates in contrast are bioactivated and/or detoxified to a great extent in the kidney. Therefore, metabolism via the mercapturic acid pathways involves complex interorgan transport. In short, GSH conjugates are to a great extent removed from the liver via canicular transporters into the bile (Keppler and König, 2000). In the bile, GSH conjugates may be cleaved by γ -GT and dipeptidases or transported unmodified to the intestines. Within the intestines, intact GSH S-conjugates have several metabolic fates. They can either be excreted by feces, absorbed from the intestine into the systemic circulation, and again delivered to the liver and finally being transported to the kidney or biotransformation by intestinal microbiome (Cooper and Hanigan, 2010). Due to the multitude of organ specific metabolic fates, predicting biotransformation of HFO-1123 in one single *in vitro* system is challenging. Species-differences in organ distribution and interorgan transfer of HFO-1123 and HFO-1123 derived metabolites are most likely and possibly contribute to HFO-1123 toxicity. By evaluating biotransformation of HFO-1123 and derived metabolites in single, isolated *in vitro* systems may give a false prediction on the entire biotransformation of HFO-1123.

To cope with issues originating from isolated *in vitro* systems, modern organ-on-a-chip models might be valuable to study interorgan transport and metabolism of HFO-1123. Organ-on-a-chip models, also known as “tissue chips” or microphysiological systems, are complex, three dimensional microfluid cell culture based *in vitro* systems that can predict the physiologic function of whole organs (e.g., liver, kidney, and lung) more accurately than single two-dimensional cell models (Low *et al.*, 2021). By linking several organ-on-a-chip models of different organs, it is possible to mimic physiologic processes of the whole body, e.g., involvement of multiple organs in biotransformation of xenobiotics or inter organ distribution.

In light of continuous efforts to minimize experiments in animals in order to comply with the 3Rs principle of the animal welfare policy, there is an opportunity for organ-on-a-chip models to become valuable tools for predicting the toxicity of novel chemicals as a basis for human risk assessment. Evaluating HFO-1123 uptake (lung-on-a-chip), metabolism and distribution (liver- and kidney-on-a-chip) in a linked multiorgan microphysiological system may further improve the understanding of HFO-1123 biotransformation and toxicity.

Although MFA formation via β -lyase mediated cleavage presents a plausible mechanism for HFO-1123 toxicity, it cannot be ruled out at present that undetected metabolites formed by biotransformation in liver and kidney may contribute to HFO-1123 toxicity. ^{19}F -NMR identified 1123-GSH and F^- as main metabolites of GSH and CYP-450 dependent metabolism of HFO-1123 in hepatic S_9 . As signals for 1123-GSH were around the LOD for ^{19}F -NMR analysis, potential minor metabolites could not be detected and identified. However, synergistic effects of toxic minor metabolites could play a role in HFO-1123 toxicity. Among minor metabolites 1123-CYS-NAC, the corresponding mercapturic acid of 1123-CYS, may be of interest. Formation of 1123-CYS-NAC was increased in porcine kidney cells (compared to human and rat cell culture) after exposure with 1123-CYS, indicating increased NAT activity in this cell model. Usually, mercapturic acids are readily excreted into urine and detoxified. However, sulfoxidation of halogenated mercapturic acids, leading to cytotoxic and mutagenic *N*-acetylcysteine sulfoxides is described in the literature (Werner *et al.*, 1996). Investigating the formation and toxicity of 1123-CYS-NAC sulfoxides *in vitro* and *in vivo* may help to understand HFO-1123 toxicity. Furthermore, undetected as well as detected metabolites may lead to protein or tissue adducts that could be involved in HFO-1123 toxicity. Protein adduct formation was seen with several HFCFs (e.g., HFCF-123), being responsible for toxicity. Although HFO-1123 was not mutagenic in a bacterial reverse mutation assay, did not show chromosome aberration in cultured mammalian cells (Kamigaito, 2013; Asakura, 2014) and was not clastogenic in an *in vivo* micronucleus study performed in rats (Takasawa, 2015), protein adduct formation may well contribute to HFO-1123 toxicity *in vivo*.

In vivo studies targeting the inhalation toxicity of HFO-1123 in different animal species (rats, Goettingen[®] Minipigs, NZW Rabbits, Beagle dogs, chimeric mice) were conducted from 2014 until 2019. Several different batches of HFO-1123 were used for these inhalation toxicity studies and purity of batches was not consistently monitored. During synthesis of HFO-1123, several halogenated side products may occur at low levels. Despite low concentration of side products, these may well play a potent role in toxicity observed in experimental animals. For example, among potential side products chlorotrifluoroethylene (CTFE) was identified as a general impurity (up to 0.5%) during HFO-1123 synthesis (Hashimoto *et al.*, 2019). The primary target of CTFE toxicity is the kidney, where CTFE has been shown to induce acute necrosis of the renal tubules of different mammalian species (e.g. rats, rabbits, mice, and



guinea pigs). However, degenerative neurological changes were observed in dogs exposed to CTFE (EPA, 2008). Although characteristic symptoms of CTFE toxicity do not completely match symptoms of toxicity observed in susceptible species in response to HFO-1123, it nevertheless appears important to assess if the inconsistencies between different inhalation experiments in which different batches of HFO-1123 were used might be due to impurities with highly toxic compounds. To rule out any concerns regarding potential impurities of the test compound in previous toxicity studies, comparative *in vivo* studies on HFO-1123 biotransformation in susceptible (e.g. Goettingen[®] Minipigs) vs. less susceptible species (e.g. rats) that include stringent characterization of potential impurities seem warranted.

Furthermore, the possibility remains that the high toxicity of HFO-1123 in Goettingen[®] Minipigs and NZW Rabbits may result from a combination of species-differences in biotransformation of HFO-1123 and increased susceptibility of both species to MFA, as suggested by the higher cytotoxicity of MFA in porcine proximal tubule cells and differences in lethal doses of MFA in rabbits (0.5 mg/kg bodyweight (bw)), pigs (0.4-1 mg/kg bw), rats (0.1-5 mg/kg bw) and humans (2-10 mg/kg bw) (Goncharov *et al.*, 2006). Differences in plasma binding of MFA between species may lead to an increased accumulation in susceptible species, leading to increased toxicity in susceptible animals. Differences in accumulation are described for several halogenated carboxylic acids (e.g., trichloroacetic acid, dichloroacetic acid, trifluoroacetic acid, dibromoacetic acid) and may therefore be reasonable anticipated for MFA (Herren-Freund *et al.*, 1987; Davis, 1990; Linder *et al.*, 1994).

Overall, data on *in vitro* biotransformation of HFO-1123 and its cysteine S-conjugate 1123-CYS in subcellular fractions provided no clear conclusion regarding the involvement of the mercapturic acid pathway in the species dependent toxicity of HFO-1123. Thus, the mechanism(s) responsible for the particular susceptibility of Goettingen[®] Minipigs and NZW Rabbits to HFO-1123 inhalation toxicity remain(s) unresolved. Further research may be needed to close these data gaps as a basis for human risk assessment.

The widespread use of low global warming hydrofluoroolefins (HFOs) as refrigerants (and in other applications) will increase steadily within the next decades, as production and application of hydrofluorocarbons (HFCs) and hydrochlorofluorocarbons (HCFCs) with a high global warming potential (GWP) will expire worldwide in 2047 as stipulated by the Kigali amendment to the Montreal protocol in 2016 (Heath, 2017). The phase-out of several HFCs and HCFCs currently being used in a large scale highlights the demand for environmentally friendly, cost-efficient and universally accessible alternatives. Ready access to green cooling is already important today but will become indispensable in the future. The increase in average world temperatures is expected to lead to rising sea levels and extreme drought, leading to uninhabitable areas and tremendous bad harvest. As a consequence of global warming poverty and hunger will prevail among a vast majority of the human population. To tackle the consequences of increasing global temperatures, development of innovative environmentally friendly refrigerants that are cost-efficient and universally accessible will play an important role. Many HFOs that are anticipated for refrigeration meet these demands. However, due to their chemical instability they may pose a health concern for humans. HFOs usually show a low potential for toxicity, but several members (e.g. HFO-1234yf, HFO-1234ze and HFO-1123) exhibit marked species-differences in toxicity that complicate the evaluation of their risk for human health. Despite the great need for new climate friendly refrigerants, the risk for human health that may generate from such compounds needs to be evaluated in detail before their widespread use. It remains challenging to reconcile the need for environmentally friendly innovative refrigerants and the requirements of being harmless for humans and animals. However, this challenge needs to be addressed urgently to maintain a prosperous world and to tackle poverty and hunger while stopping the progress of man-made climate change.

7 Abbreviations

β -lyase	cysteine S-conjugate β -lyase
1123-CYS	S-(1,1,2-trifluoroethyl)-L-cysteine
1123-CYS-NAc	N-acetyl-S-(1,1,2-trifluoroethyl)-L-cysteine
1123-CYS-NAc sulfoxide	N-acetyl-S-(1,1,2-trifluoroethyl)-L-cysteine sulfoxide
1123-GSH	S-(1,1,2-trifluoroethyl)-L-glutathione
AOAA	aminooxyacetic acid
BSA	bovine serum albumin
CFC	chlorofluorocarbon
COSY	Correlation Spectroscopy
d	doublet
DCVC	S-(1,2-dichlorovinyl)-L-cysteine
DCVG	S-(1,2-dichlorovinyl)-L-glutathione
dd	doublet of doublets
DEPT	Distortionless Enhancement by Polarization Transfer
DPP	dipeptidylpeptidase
F ⁻	inorganic fluoride
GSH	glutathione
GST	glutathione S-transferase
HCFC	hydrofluorocarbon
HFC	hydrochlorofluorocarbon
HFO	hydrofluoroolefin
HFO-1123	1,1,2-trifluoroethene
HFP	hexafluoropropylene
HPLC	high performance liquid chromatography
HPLC-DAD	HPLC coupled with a diode array detector
HSQC	Heteronuclear Single Quantum Coherence Spectroscopy
Hz	hertz
Km	kilometers
LC-MS/MS	liquid chromatography coupled with mass spectrometry
m	multiplet
MAP	mercapturic acid pathway

MFA	monofluoroacetic acid
MHz	megahertz
Minipig	Goettingen [®] Minipig
NADPH reg. sys.	NADPH regenerating system
NAT	<i>N</i> -acetyltransferase
NMR	nuclear magnetic resonance
NOELs	no-observed-adverse-effect levels
NZW Rabbit	New Zealand White Rabbit
ppm	parts per million
s	singlet
SD	Sprague Dawley
t	triplet
TCVC	<i>S</i> -(1,2,2-trichlorovinyl)- <i>L</i> -cysteine
TFEC	<i>S</i> -(1,1,2,2-tetrafluoroethyl)- <i>L</i> -cysteine
t_r	retention time
TRI	1,1,2-trichloroethylene
TWA	Time weighted average
V	volt
γ -GT	γ -glutamyltransferase

8 References

- ACS, A.C.S., 2019. Ultraviolet (UV) Radiation (<https://www.cancer.org/cancer/cancer-causes/radiation-exposure/uv-radiation.html>). Last updated 10.07.2019. Accessed at on 07.03.2022.
- ACSNCL, 2017. American Chemical Society National History Chemical Landmarks. Chlorofluorocarbons and Ozone Depletion <http://www.acs.org/content/acs/en/education/whatischemistry/landmarks/cfcs-ozone.html>. Last accessed 17.03.2022.
- Anders, M.W., 1991. Metabolism and toxicity of hydrochlorofluorocarbons: current knowledge and needs for the future. *Environ Health Perspect* **96**, 185-191.
- Anders, M.W., 2008. Chemical Toxicology of Reactive Intermediates Formed by the Glutathione-Dependent Bioactivation of Halogen-Containing Compounds. *Chemical Research in Toxicology* **21**, 145-159.
- Antiñolo, M., Bravo, I., Jiménez, E., Ballesteros, B. and Albaladejo, J., 2017. Atmospheric Chemistry of E- and Z-CF(3)CH=CHF (HFO-1234ze): OH Reaction Kinetics as a Function of Temperature and UV and IR Absorption Cross Sections. *J Phys Chem A* **121**, 8322-8331.
- Arent, D.J., Tol, R.S., Faust, E., Hella, J.P., Kumar, S., Strzepek, K.M., Tóth, F.L., Yan, D., Abdulla, A. and Kheshgi, H., 2015. Key economic sectors and services. *Climate change 2014 impacts, adaptation and vulnerability: part a: global and sectoral aspects*, 659-708.
- Asakura, M., 2014. Chromosome aberration study of trifluoroethene in cultured mammalian cells. *Japan Bioassay Research Center Study No.* 7453.
- Biddle, W., 1998. *A Field Guide to the Invisible*. Volume 1. Henry Holt and Co.
- Boogaard, P.J., N.M. Commandeur, J., Mulder, G.J., Vermeulen, N.P.E. and Nagelkerke, J.F., 1989. Toxicity of the cysteine-S-conjugates and mercapturic acids of four structurally related difluoroethylenes in isolated proximal tubular cells from rat kidney: Uptake of the conjugates and activation to toxic metabolites. *Biochemical Pharmacology* **38**, 3731-3741.
- Bosakowski, T. and Levin, A.A., 1986. Serum citrate as a peripheral indicator of fluoroacetate and fluorocitrate toxicity in rats and dogs. *Toxicol Appl Pharmacol* **85**, 428-436.
- Boucher, R., Hanna, C., Rusch, G.M., Stidham, D., Swan, E. and Vazquez, M., 2003. Hepatotoxicity associated with overexposure to 1,1-dichloro-2,2,2-trifluoroethane (HCFC-123). *AIHA J (Fairfax, Va)* **64**, 68-79.
- Braslavsky, S.E. and Rubin, M.B., 2011. The history of ozone Part VIII. Photochemical formation of ozone. *Photochemical & Photobiological Sciences* **10**, 1515-1520.
- Buffa, P., Guarriero-Boyleva, V. and R., C.-T., 1973. Metabolic effects of fluoroacetate poisoning in animals. *Fluoride*, 224-247.
- Buffa, P. and Peters, R.A., 1949. The *in vivo* formation of citrate induced by fluoroacetate and its significance. *The Journal of physiology* **110**, 488-500.
- Capinha, L., Jennings, P. and Commandeur, J.N.M., 2021. Bioactivation of trichloroethylene to three regioisomeric glutathione conjugates by liver fractions and recombinant human glutathione transferases: Species differences and implications for human risk assessment. *Toxicology Letters* **341**, 94-106.
- Carlowicz, M., 2009. The world we avoided by protecting the ozone layer. <https://earthobservatory.nasa.gov/features/WorldWithoutOzone/page1.php>. NASA. Last accessed on 07.03.2022.

- Coffee, M., 2015. Acute inhalation cardiac sensitization study of HFO-1123 in Beagle dogs. WIL Research Study Number WIL-534028.
- Commandeur, J.N., Oostendorp, R.A., Schoofs, P.R., Xu, B. and Vermeulen, N.P., 1987. Nephrotoxicity and hepatotoxicity of 1,1-dichloro-2,2-difluoroethylene in the rat. Indications for differential mechanisms of bioactivation. *Biochem Pharmacol* **36**, 4229-4237.
- Cook, J.C., Murray, S.M., Frame, S.R. and Hurtt, M.E., 1992. Induction of Leydig cell adenomas by ammonium perfluorooctanoate: a possible endocrine-related mechanism. *Toxicol Appl Pharmacol* **113**, 209-217.
- Cooper, A.J., 1998. Mechanisms of cysteine S-conjugate beta-lyases. *Adv Enzymol Relat Areas Mol Biol* **72**, 199-238.
- Cooper, A.J., Bruschi, S.A., Conway, M. and Hutson, S.M., 2003. Human mitochondrial and cytosolic branched-chain aminotransferases are cysteine S-conjugate beta-lyases, but turnover leads to inactivation. *Biochem Pharmacol* **65**, 181-192.
- Cooper, A.J., Krasnikov, B.F., Niatetskaya, Z.V., Pinto, J.T., Callery, P.S., Villar, M.T., Artigues, A. and Bruschi, S.A., 2011. Cysteine S-conjugate beta-lyases: important roles in the metabolism of naturally occurring sulfur and selenium-containing compounds, xenobiotics and anticancer agents. *Amino Acids* **41**, 7-27.
- Cooper, A.J. and Pinto, J.T., 2006. Cysteine S-conjugate beta-lyases. *Amino Acids* **30**, 1-15.
- Cooper, A.J.L. and Hanigan, M.H., 2010. 4.17 - Enzymes Involved in Processing Glutathione Conjugates. In McQueen, C.A., (Ed.), *Comprehensive Toxicology (Second Edition)*. Elsevier, Oxford, pp. 323-366.
- Cooper, A.J.L. and Hanigan, M.H., 2018. Metabolism of Glutathione S-Conjugates: Multiple Pathways. *Comprehensive Toxicology*, 363-406.
- Cox, P.J., King, L.J. and Parke, D.V., 1972. A study of the possible metabolism of trichlorofluoromethane. *Biochemical Journal* **130**, 13P-14P.
- Cristofori, P., Sauer, A.V. and Trevisan, A., 2015. Three common pathways of nephrotoxicity induced by halogenated alkenes. *Cell Biology and Toxicology* **31**, 1-13.
- Davis, M.E., 1988. Effects of AT-125 on the nephrotoxicity of hexachloro-1,3-butadiene in rats. *Toxicol Appl Pharmacol* **95**, 44-52.
- Davis, M.E., 1990. Subacute toxicity of trichloroacetic acid in male and female rats. *Toxicology* **63**, 63-72.
- Dekant, W., 1996. Toxicology of chlorofluorocarbon replacements. *Environ Health Perspect* **104 Suppl 1**, 75-83.
- Dekant, W., 2003a. Biosynthesis of toxic glutathione conjugates from halogenated alkenes. *Toxicology Letters* **144**, 49-54.
- Dekant, W., 2003b. Biosynthesis of toxic glutathione conjugates from halogenated alkenes. *Toxicol Lett* **144**, 49-54.
- Dekant, W., Berthold, K., Vamvakas, S., Henschler, D. and Anders, M.W., 1988. Thioacylating intermediates as metabolites of S-(1,2-dichlorovinyl)-L-cysteine and S-(1,2,2-trichlorovinyl)-L-cysteine formed by cysteine conjugate beta-lyase. *Chem Res Toxicol* **1**, 175-178.
- Dekant, W., Koob, M. and Henschler, D., 1990. Metabolism of trichloroethene--in vivo and in vitro evidence for activation by glutathione conjugation. *Chem Biol Interact* **73**, 89-101.
- Dekant, W., Vamvakas, S. and Anders, M.W., 1994. Formation and Fate of Nephrotoxic and Cytotoxic Glutathione S-Conjugates: Cysteine Conjugate β -Lyase Pathway. In Anders, M.W., Dekant, W., (Eds.), *Advances in Pharmacology*. Academic Press, pp. 115-162.



- Dekant, W., Vamvakas, S., Berthold, K., Schmidt, S., Wild, D. and Henschler, D., 1986. Bacterial beta-lyase mediated cleavage and mutagenicity of cysteine conjugates derived from the nephrocarcinogenic alkenes trichloroethylene, tetrachloroethylene and hexachlorobutadiene. *Chem Biol Interact* **60**, 31-45.
- Dincer, I., 2018. Comprehensive Energy Systems. In Dincer, I., (Ed.), *Comprehensive Energy Systems*. Elsevier, Oxford, pp. 435-474.
- Dong, Y., Coleman, M. and Miller, S.A., 2021. Greenhouse Gas Emissions from Air Conditioning and Refrigeration Service Expansion in Developing Countries. *Annual Review of Environment and Resources* **46**, 59-83.
- E.U., 2002. European Commission Decision 2002/657/EC of 12 August 2002 implementing Council Directive 96/23/EC concerning the performance of analytical methods and the interpretation of results. *Official Journal of the European Communities* **50**, 8-36.
- Eadie, G.S., 1942. THE INHIBITION OF CHOLINESTERASE BY PHYSOSTIGMINE AND PROSTIGMINE. *Journal of Biological Chemistry* **146**, 85-93.
- ECETOC, 2009. European Centre for Ecotoxicology and Toxicology of Chemicals (ECETOC). Evaluation of Cardiac Sensitization Test Methods, Technical Report No. 105, ECETOC. Brussels, Belgium: ECETOC.
- ECHA, 2022a. Hexafluoropropene. Brief profile. European Chemicals Agency. Helsinki Available from: <https://echa.europa.eu/de/substance-information/-/substanceinfo/100.003.753>. Last accessed 03.05.2022.
- ECHA, 2022b. Tetrafluoroethylene. Brief profile. European Chemicals Agency. Helsinki. Available from: <http://echa.europa.eu/registration-dossier/-/registered-dossier/15453/1>. Last accessed 03 Mai 2022.
- Egger, A.E., 2003. Composition of earth's atmosphere. Vol. EAS (5). <https://www.visionlearning.com/en/library/Earth-Science/6/Composition-of-Earths-Atmosphere/107>. Last accessed 17.03.2022.
- Egyed, M. and Brisk, Y., 1965. Experimental fluoroacetamid poisoning in mice, rats and sheep. *Refuah veterinarith*, 274-278.
- Elfarra, A.A. and Hwang, I.Y., 1990. In vivo metabolites of S-(2-benzothiazolyl)-L-cysteine as markers of in vivo cysteine conjugate beta-lyase and thiol glucuronosyl transferase activities. *Drug Metabolism and Disposition* **18**, 917.
- Elfarra, A.A. and Hwang, I.Y., 1993. Targeting of 6-mercaptopurine to the kidneys. Metabolism and kidney-selectivity of S-(6-purinyl)-L-cysteine analogs in rats. *Drug Metab Dispos* **21**, 841-845.
- Elfarra, A.A., Jakobson, I. and Anders, M.W., 1986. Mechanism of S-(1,2-dichlorovinyl)glutathione-induced nephrotoxicity. *Biochem Pharmacol* **35**, 283-288.
- Elfarra, A.A. and Krause, R.J., 2007. S-(1,2,2-Trichlorovinyl)-L-cysteine Sulfoxide, a Reactive Metabolite of S-(1,2,2-Trichlorovinyl)-L-cysteine Formed in Rat Liver and Kidney Microsomes, Is a Potent Nephrotoxicant. *Journal of Pharmacology and Experimental Therapeutics* **321**, 1095-1101.
- Elfarra, A.A., Krause, R.J., Last, A.R., Lash, L.H. and Parker, J.C., 1998. Species- and Sex-Related Differences in Metabolism of Trichloroethylene To Yield Chloral and Trichloroethanol in Mouse, Rat, and Human Liver Microsomes. *Drug Metabolism and Disposition* **26**, 779.
- Elfarra, A.A., Lash, L.H. and Anders, M.W., 1987. Alpha-ketoacids stimulate rat renal cysteine conjugate beta-lyase activity and potentiate the cytotoxicity of S-(1,2-dichlorovinyl)-L-cysteine. *Molecular Pharmacology* **31**, 208.

- EPA, 2008. United States Environmental Protection Agency. Acute Exposure Guideline Levels (AEGs) for Chlorotrifluoroethylene (CAS Reg. No. 79-38-9).
- EPA, 2011. United States Environmental Protection Agency. Toxicological review of Trichloroethylene (CAS No. 79-01-6) In Support of Summary Information on the Integrated Risk Information System (IRIS).
- Farman, J.C., Gardiner, B.G. and Shanklin, J.D., 1985. Large losses of total ozone in Antarctica reveal seasonal ClO_x/NO_x interaction. *Nature* **315**, 207-210.
- Fisher, D.A., Hales, C.H., Filkin, D.L., Ko, M.K.W., Sze, N.D., Connell, P.S., Wuebbles, D.J., Isaksen, I.S.A. and Stordal, F., 1990. Model calculations of the relative effects of CFCs and their replacements on stratospheric ozone. *Nature* **344**, 508-512.
- Flegal, R. and Smith, D., 1992. Lead Levels in Preindustrial Humans. *New England Journal of Medicine* **326**, 1293-1294.
- Forkert, P.G., Baldwin, R.M., Millen, B., Lash, L.H., Putt, D.A., Shultz, M.A. and Collins, K.S., 2005. Pulmonary bioactivation of trichloroethylene to chloral hydrate: relative contributions of CYP2E1, CYP2F, and CYP2B1. *Drug Metab Dispos* **33**, 1429-1437.
- Forkert, P.G., Millen, B., Lash, L.H., Putt, D.A. and Ghanayem, B.I., 2006. Pulmonary bronchiolar cytotoxicity and formation of dichloroacetyl lysine protein adducts in mice treated with trichloroethylene. *J Pharmacol Exp Ther* **316**, 520-529.
- Gardell, S.J. and Tate, S.S., 1980. Affinity labeling of gamma-glutamyl transpeptidase by glutamine antagonists. Effects of the gamma-glutamyl transferase and proteinase activities. *FEBS Lett* **122**, 171-174.
- Gardner, P.R., Nguyen, D.D. and White, C.W., 1994. Aconitase is a sensitive and critical target of oxygen poisoning in cultured mammalian cells and in rat lungs. *Proc Natl Acad Sci U S A* **91**, 12248-12252.
- Gaskin, P.J., Adcock, H.J., Buckberry, L.D., Teesdale-Spittle, P.H. and Shaw, P.N., 1995. The C-S lysis of L-cysteine conjugates by aspartate and alanine aminotransferase enzymes. *Hum Exp Toxicol* **14**, 422-427.
- Godin, C., Drerup, J. and Vinegar, A., 1993. Conditions influencing the rat liver microsomal metabolism of 2, 2,-dichloro-1, 1, 1-trifluoroethane (HCFC-123). *Drug metabolism and disposition* **21**, 551-553.
- Goh, C.S., Hodgson, D.R., Fearnside, S.M., Heller, J. and Malikides, N., 2005. Sodium monofluoroacetate (Compound 1080) poisoning in dogs. *Aust Vet J* **83**, 474-479.
- Goncharov, N.V., Jenkins, R.O. and Radilov, A.S., 2006. Toxicology of fluoroacetate: a review, with possible directions for therapy research. *J Appl Toxicol* **26**, 148-161.
- Green, T., Dow, J., Ellis, M.K., Foster, J.R. and Odum, J., 1997. The role of glutathione conjugation in the development of kidney tumours in rats exposed to trichloroethylene. *Chemico-Biological Interactions* **105**, 99-117.
- Green, T. and Odum, J., 1985. Structure/activity studies of the nephrotoxic and mutagenic action of cysteine conjugates of chloro- and fluoroalkenes. *Chem Biol Interact* **54**, 15-31.
- Groves, C.E., Muñoz, L., Bahn, A., Burckhardt, G. and Wright, S.H., 2003. Interaction of cysteine conjugates with human and rabbit organic anion transporter 1. *J Pharmacol Exp Ther* **304**, 560-566.
- Gustavsson, J., Cederberg, C., Sonesson, U., Van Otterdijk, R. and Meybeck, A., 2011. Global food losses and food waste. FAO Rome, pp.
- Hanna, P.E. and Anders, M.W., 2019. The mercapturic acid pathway. *Crit Rev Toxicol* **49**, 819-929.



- Harris, J.W., Pohl, L.R., Martin, J.L. and Anders, M.W., 1991. Tissue acylation by the chlorofluorocarbon substitute 2,2-dichloro-1,1,1-trifluoroethane. *Proceedings of the National Academy of Sciences* **88**, 1407-1410.
- Hashimoto, M., Otsuka, T., Fukushima, M., Okamoto, H., Hayamizu, H., Ueno, K. and Akasaka, R., 2019. Development of New Low-GWP Refrigerants–Refrigerant Mixtures Including HFO-1123. *Science and Technology for the Built Environment* **25**, 776-783.
- Heath, E.A., 2017. Amendment to the Montreal Protocol on Substances that Deplete the Ozone Layer (Kigali Amendment). *International Legal Materials* **56**, 193-205.
- Herren-Freund, S.L., Pereira, M.A., Khoury, M.D. and Olson, G., 1987. The carcinogenicity of trichloroethylene and its metabolites, trichloroacetic acid and dichloroacetic acid, in mouse liver. *Toxicol Appl Pharmacol* **90**, 183-189.
- Hinchman, C.A. and Ballatori, N., 1990. Glutathione-degrading capacities of liver and kidney in different species. *Biochem Pharmacol* **40**, 1131-1135.
- Hodnebrog, Ø., Etminan, M., Fuglestedt, J.S., Marston, G., Myhre, G., Nielsen, C.J., Shine, K.P. and Wallington, T.J., 2013. Global warming potentials and radiative efficiencies of halocarbons and related compounds: A comprehensive review. *Reviews of Geophysics* **51**, 300-378.
- Hoet, P., Buchet, J.-P., Sempoux, C., Nomiyama, T., Rahier, J. and Lison, D., 2001. Investigations on the liver toxicity of a blend of HCFC-123 (2,2-dichloro-1,1,1-trifluoroethane) and HCFC-124 (2-chloro-1,1,1,2-tetrafluoroethane) in guinea-pigs. *Archives of Toxicology* **75**, 274-283.
- Hoet, P., Graf, M.L., Bourdi, M., Pohl, L.R., Duray, P.H., Chen, W., Peter, R.M., Nelson, S.D., Verlinden, N. and Lison, D., 1997. Epidemic of liver disease caused by hydrochlorofluorocarbons used as ozone-sparing substitutes of chlorofluorocarbons. *Lancet* **350**, 556-559.
- Hofstee, B.H., 1952. On the evaluation of the constants V_m and K_M in enzyme reactions. *Science* **116**, 329-331.
- Hughey, R.P., Rankin, B.B., Elce, J.S. and Curthoys, N.P., 1978. Specificity of a particulate rat renal peptidase and its localization along with other enzymes of mercapturic acid synthesis. *Arch Biochem Biophys* **186**, 211-217.
- IARC, 2016. International Agency of Research on Cancer. IARC Monographs on the Evaluation of Carcinogenic Risks to Humans Volume 110: Perfluorooctanoic Acid, Tetrafluoroethylene, Dichloromethane, 1,2-Dichloropropane, and 1,3-Propane Sultone. <https://monographs.iarc.who.int/wp-content/uploads/2018/06/mono110-02.pdf>. Last accessed 03 May 2022.
- Iyer, R.A. and Anders, M.W., 1996. Cysteine conjugate beta-lyase-dependent biotransformation of the cysteine S-conjugates of the sevoflurane degradation product compound A in human, nonhuman primate, and rat kidney cytosol and mitochondria. *Anesthesiology* **85**, 1454-1461.
- Jones, T.W., Qin, C., Schaeffer, V.H. and Stevens, J.L., 1988. Immunohistochemical localization of glutamine transaminase K, a rat kidney cysteine conjugate beta-lyase, and the relationship to the segment specificity of cysteine conjugate nephrotoxicity. *Mol Pharmacol* **34**, 621-627.
- Kamigaito, T., 2013. Mutagenicity test of trifluoroethene using microorganisms (reverse mutation assay of trifluoroethene in bacteria). Japan Bioassay Research Center Study Number 6354. Japan Bioassay Research Center, Japan Industrial Safety and Health Association.
- Keller, D.A., Roe, D.C. and Lieder, P.H., 1996. Fluoroacetate-mediated toxicity of fluorinated ethanes. *Fundam Appl Toxicol* **30**, 213-219.

- Keppler, D. and König, J.G., 2000. Hepatic Secretion of Conjugated Drugs and Endogenous Substances. *Semin Liver Dis* **20**, 265-272.
- Ketterer, B. and Christodoulides, L.G., 1994. Enzymology of cytosolic glutathione S-transferases. *Adv Pharmacol* **27**, 37-69.
- Kishida, K., Akaki, Y., Sasabe, T., Yamamoto, C. and Manabe, R., 1990. Glutathione Conjugation of Methazolamide and Subsequent Reactions in the Ciliary Body In Vitro. *Journal of Pharmaceutical Sciences* **79**, 638-642.
- Kitman, J.L., 2000. *The Secret History of Lead*, The Nation, pp.
- Klaassen, C.D., 2013. *Casarett and Doull's toxicology: the basic science of poisons*. McGraw-Hill New York. Volume 1236. .
- Koob, M. and Dekant, W., 1991. Bioactivation of xenobiotics by formation of toxic glutathione conjugates. *Chemico-Biological Interactions* **77**, 107-136.
- Kozak, E.M. and Tate, S.S., 1982. Glutathione-degrading enzymes of microvillus membranes. *Journal of Biological Chemistry* **257**, 6322-6327.
- Krause, R.J., Lash, L.H. and Elfarra, A.A., 2003. Human kidney flavin-containing monooxygenases and their potential roles in cysteine s-conjugate metabolism and nephrotoxicity. *J Pharmacol Exp Ther* **304**, 185-191.
- Lash, L.H., 2007. Methods for measuring cysteine S-conjugate beta-lyase activity. *Curr Protoc Toxicol* **Chapter 6**, Unit6.13.
- Lash, L.H. and Anders, M.W., 1989. Uptake of nephrotoxic S-conjugates by isolated rat renal proximal tubular cells. *J Pharmacol Exp Ther* **248**, 531-537.
- Lash, L.H., Chiu, W.A., Guyton, K.Z. and Rusyn, I., 2014. Trichloroethylene biotransformation and its role in mutagenicity, carcinogenicity and target organ toxicity. *Mutation Research/Reviews in Mutation Research* **762**, 22-36.
- Lash, L.H., Elfarea, A.A. and Anders, M.W., 1986. S-(1,2-dichlorovinyl)-L-homocysteine-induced cytotoxicity in isolated rat kidney cells. *Archives of Biochemistry and Biophysics* **251**, 432-439.
- Lash, L.H., Fisher, J.W., Lipscomb, J.C. and Parker, J.C., 2000. Metabolism of trichloroethylene. *Environ Health Perspect* **108 Suppl 2**, 177-200.
- Lash, L.H., Nelson, R.M., Van Dyke, R.A. and Anders, M.W., 1990. Purification and characterization of human kidney cytosolic cysteine conjugate beta-lyase activity. *Drug Metab Dispos* **18**, 50-54.
- Lash, L.H. and Parker, J.C., 2001. Hepatic and Renal Toxicities Associated with Perchloroethylene. *Pharmacological Reviews* **53**, 177.
- Lash, L.H., Putt, D.A., Hueni, S.E., Krause, R.J. and Elfarra, A.A., 2003. Roles of necrosis, Apoptosis, and mitochondrial dysfunction in S-(1,2-dichlorovinyl)-L-cysteine sulfoxide-induced cytotoxicity in primary cultures of human renal proximal tubular cells. *J Pharmacol Exp Ther* **305**, 1163-1172.
- Li, Y.-n., Tao, J.-j., Han, Y.-c., Han, X. and Qin, J., 2014. Numerical and Experimental Study on the Diffusion Property of Difluoromethane (HFC-32) in Leakage. *Procedia Engineering* **71**, 34-43.
- Lind, R.C., Gandolfi, A.J. and Hall, P.D.L.M., 1995. Biotransformation and Hepatotoxicity of HCFC-123 in the Guinea Pig: Potentiation of Hepatic Injury by Prior Glutathione Depletion. *Toxicology and Applied Pharmacology* **134**, 175-181.
- Linder, R.E., Klinefelter, G.R., Strader, L.F., Suarez, J.D., Roberts, N.L. and Dyer, C.J., 1994. Spermatotoxicity of dibromoacetic acid in rats after 14 daily exposures. *Reprod Toxicol* **8**, 251-259.

- Lineweaver, H. and Burk, D., 1934. The Determination of Enzyme Dissociation Constants. *Journal of the American Chemical Society* **56**, 658-666.
- Loizou, G.D., Urban, G., Dekant, W. and Anders, M., 1994. Gas-uptake pharmacokinetics of 2, 2-dichloro-1, 1, 1-trifluoroethane (HCFC-123). *Drug metabolism and disposition* **22**, 511-517.
- Longstreth, J., 1988. Cutaneous malignant melanoma and ultraviolet radiation: a review. *Cancer Metastasis Rev* **7**, 321-333.
- Low, L.A., Mummery, C., Berridge, B.R., Austin, C.P. and Tagle, D.A., 2021. Organs-on-chips: into the next decade. *Nature Reviews Drug Discovery* **20**, 345-361.
- Lowry, O.H., Rosebrough, N.J., Farr, A.L. and Randall, R.J., 1951. Protein measurement with the Folin phenol reagent. *J Biol Chem* **193**, 265-275.
- MacFarlane, M., Schofield, M., Parker, N., Roelandt, L., David, M., Lock, E.A., King, L.J., Goldfarb, P.S. and Gibson, G.G., 1993. Dose-dependent induction or depression of cysteine conjugate beta-lyase in rat kidney by N-acetyl-S-(1,2,3,4,4-pentachloro-1,3-butadienyl)-L-cysteine. *Toxicology* **77**, 133-144.
- Maidment, G., 2014. Sustaining the Future - Inspiring a Generation, <https://ior.org.uk/technical/rachp-technical?search=Sustaining%20the%20Future%20&state=a>. Institute of Refrigeration at Nelson Hayden Lecture Theatre.
- McGrayne, S., 2001. *Prometheans in the Lab: Chemistry and the Making of the Modern World. Volume 2.* ISBN: 0071350071. McGraw-Hill Professional.
- McGregor, G.R., Bessmoulin, P., Ebi, K. and Menne, B., 2015. Heatwaves and health: guidance on warning-system development. WMOP.
- McKinney, L.L., Weakley, F.B., Eldridge, A.C., Campbell, R.E., Cowan, J.C., Picken, J.C. and Biester, H.E., 1957. S-(DICHLOROVINYL)-L-CYSTEINE: AN AGENT CAUSING FATAL APLASTIC ANEMIA IN CALVES¹. *Journal of the American Chemical Society* **79**, 3932-3933.
- McNeill, J.R., 2000. *Something new under the sun: An environmental history of the the twentieth-century world.* WW Norton&Co. Reprint Edition.
- Mergner, G.W., Blake, D.A. and Helrich, M., 1975. Biotransformation and elimination of ¹⁴C-trichlorofluoromethane (FC-11) and ¹⁴C-dichlorodifluoromethane (FC-12) in man. *Anesthesiology* **42**, 345-351.
- Molina, M.J. and Rowland, F.S., 1974. Stratospheric sink for chlorofluoromethanes: chlorine atom-catalysed destruction of ozone. *Nature* **249**, 810-812.
- Mondal, D., Hori, Y., Kariya, K., Miyara, A. and Jahangir Alam, M., 2020. Measurement of Viscosity of a Binary Mixture of R1123 + R32 Refrigerant by Tandem Capillary Tube Method. *International Journal of Thermophysics* **41**, 83.
- Monks, T.J. and Lau, S.S., 1994. Glutathione conjugation as a mechanism for the transport of reactive metabolites. *Adv Pharmacol* **27**, 183-210.
- Montine, T.J., Amarnath, V., Picklo, M.J., Sidell, K.R., Zhang, J. and Graham, D.G., 2000. Dopamine mercapturate can augment dopaminergic neurodegeneration. *Drug Metab Rev* **32**, 363-376.
- Murphy, R.C. and Gijón, M.A., 2007. Biosynthesis and metabolism of leukotrienes. *Biochem J* **405**, 379-395.
- Myhre, G., Shindell, D., Bréon, F.M., Collins, W., Fuglestedt, J., Huang, J., Koch, D., Lamarque, J.F., Lee, D., Mendoza, B., Nakajima, T., Robock, A., Stephens, G., Takemura, T. and Zhang, H. (Eds.), 2013. *Anthropogenic and natural radiative forcing.* Cambridge University Press, Cambridge, UK.

- NASA, N.A.a.S.A., 2022. Media Usage Guidelines. <https://www.nasa.gov/multimedia/guidelines/index.html> Author: Daines, Gary. Updated: 04.01.2022, Last accessed on 18.03.2022.
- Nelson, S.D. and Pearson, P.G., 1990. Covalent and Noncovalent Interactions in Acute Lethal Cell Injury Caused by Chemicals. *Annual Review of Pharmacology and Toxicology* **30**, 169-195.
- Newman, P.A., 2018. NASA Ozone Watch, What is a Dobson unit? NASA, <https://ozonewatch.gsfc.nasa.gov/facts/dobson.html>, pp.
- Newman, P.A., Oman, L.D., Douglass, A.R., Fleming, E.L., Frith, S.M., Hurwitz, M.M., Kawa, S.R., Jackman, C.H., Krotkov, N.A., Nash, E.R., Nielsen, J.E., Pawson, S., Stolarski, R.S. and Velders, G.J.M., 2009. What would have happened to the ozone layer if chlorofluorocarbons (CFCs) had not been regulated? *Atmos. Chem. Phys.* **9**, 2113-2128.
- NIDDK, 2012. Halothane, LiverTox: Clinical and Research Information on Drug-Induced Liver Injury. National Institute of Diabetes and Digestive and Kidney Diseases, Bethesda (MD), pp.
- Nishimura, T., Hu, Y., Wu, M., Pham, E., Suemizu, H., Elazar, M., Liu, M., Idilman, R., Yurdaydin, C., Angus, P., Stedman, C., Murphy, B., Glenn, J., Nakamura, M., Nomura, T., Chen, Y., Zheng, M., Fitch, W.L. and Peltz, G., 2013. Using chimeric mice with humanized livers to predict human drug metabolism and a drug-drug interaction. *J Pharmacol Exp Ther* **344**, 388-396.
- NRC, 2000. National Research Council. Spacecraft Maximum Allowable Concentrations for Selected Airborne Contaminants: Volume 4. doi:10.17226/9786. 386.
- Okajima, K., Inoue, M., Morino, Y. and Itoh, K., 1984. Topological aspects of microsomal N-acetyltransferase, an enzyme responsible for the acetylation of cysteine S-conjugates of xenobiotics. *Eur J Biochem* **142**, 281-286.
- Ozaki, K., Fujiwara, T., Nakamura, Y. and Takahashi, E., 1998. Isolation and mapping of a novel human kidney- and liver-specific gene homologous to the bacterial acetyltransferases. *J Hum Genet* **43**, 255-258.
- Pattison, F.L.M., 1959. Toxic Aliphatic Fluorine Compounds.
- Pearce, F., 2017. The one-man environmental disaster. *New Scientist* **234**, 42-43.
- Peters, T., 2016. Clean Cold and the Global Goals. Available online at: <https://www.birmingham.ac.uk/research/energy/research/clean-cold-global-goals/clean-cold-and-the-global-goals.aspx> Editor: Strahan, David. University of Birmingham. (Last.
- Poon, J.C. and Josephy, P.D., 2012. Hydrolysis of S-aryl-cysteinylglycine conjugates catalyzed by porcine kidney cortex membrane dipeptidase. *Xenobiotica* **42**, 1178-1186.
- Proudfoot, A.T., Bradberry, S.M. and Vale, J.A., 2006. Sodium Fluoroacetate Poisoning. *Toxicological Reviews* **25**, 213-219.
- Ramanathan, V., 1975. Greenhouse Effect Due to Chlorofluorocarbons: Climatic Implications. *Science* **190**, 50-52.
- Reinhardt, C.F., Azar, A., Maxfield, M.E., Smith, P.E. and Mullin, L.S., 1971. Cardiac Arrhythmias and Aerosol "Sniffing". *Archives of Environmental Health: An International Journal* **22**, 265-279.
- Rowland, F.S., 2006. Stratospheric ozone depletion. *Philosophical Transactions of the Royal Society B: Biological Sciences* **361**, 769-790.
- Rusch, G.M., 2018. The development of environmentally acceptable fluorocarbons. *Crit Rev Toxicol* **48**, 615-665.

- Rusch, G.M., Tveit, A., Muijser, H., Tegelenbosch-Schouten, M.M. and Hoffman, G.M., 2013. The acute, genetic, developmental and inhalation toxicology of trans-1,3,3,3-tetrafluoropropene (HFO-1234ze). *Drug Chem Toxicol* **36**, 170-180.
- Schaeffer, V.H. and Stevens, J.L., 1987a. Mechanism of transport for toxic cysteine conjugates in rat kidney cortex membrane vesicles. *Mol Pharmacol* **32**, 293-298.
- Schaeffer, V.H. and Stevens, J.L., 1987b. The transport of S-cysteine conjugates in LLC-PK1 cells and its role in toxicity. *Mol Pharmacol* **31**, 506-512.
- Schmidt, T., Bertermann, R., Rusch, G.M., Hoffman, G.M. and Dekant, W., 2012. Biotransformation of 2,3,3,3-tetrafluoropropene (HFO-1234yf) in male, pregnant and non-pregnant female rabbits after single high dose inhalation exposure. *Toxicology and Applied Pharmacology* **263**, 32-38.
- Schmidt, T., Bertermann, R., Rusch, G.M., Tveit, A. and Dekant, W., 2013. Biotransformation of trans-1-chloro-3,3,3-trifluoropropene (trans-HCFO-1233zd). *Toxicology and Applied Pharmacology* **268**, 343-351.
- Schuster, P., Bertermann, R., Rusch, G.M. and Dekant, W., 2009. Biotransformation of trans-1,1,1,3-tetrafluoropropene (HFO-1234ze). *Toxicology and Applied Pharmacology* **239**, 215-223.
- Snel, H., Saavedra, Y. and Koomen, I., 2018. Hotspot Analysis on Food Loss and Waste in African Agriculture; Literature review. Wageningen Centre for Development Innovation, Wageningen University & Research. WCDI-18-047.
- Stevens, J.L., 1989. Quantitation of multiple pathways for the metabolism of nephrotoxic cysteine conjugates using selective inhibitors of L-alpha-hydroxy acid oxidase (L-amino acid oxidase) and cysteine conjugate beta-lyase. *Drug Metabolism and Disposition* **17**, 297.
- Takasawa, H., 2015. Bone marrow micronucleus assay of HFO-1123 in rats. LSI Medience Corporation, Study Number B150614. LSI Medience Corporation.
- Takebayashi, T., Kabe, I., Endo, Y., Tanaka, S., Miyauchi, H., Nozi, K., Imamiya, S., Takahashi, K. and Omae, K., 1998. Acute liver dysfunction among workers exposed to 2,2-dichloro-1,1,1-trifluoroethane A case report. *Journal of Occupational Health* **40**, 169-170.
- Tanaka, S., Kabe, I., Takebayashi, T., MIYAUCHI, H., NOZI, K., TAKAHASHI, K., SEKI, Y. and OMAE, K., 1998. Environmental and biological monitoring of 2, 2-dichloro-1, 1, 1-trifluoroethane (HCFC-123). *Journal of occupational health* **40**, 348-349.
- Taniguchi, N., 2012. *Glutathione centennial: molecular perspectives and clinical implications*. Elsevier.
- Taniguchi, N. and Ikeda, Y., 1998. c-Glutamyl transpeptidase: catalytic mechanism and gene expression. *Adv Enzymol Relat Areas Mol Biol* **72**, 239-278.
- Taylor, H.R., West, S.K., Rosenthal, F.S., Muñoz, B., Newland, H.S., Abbey, H. and Emmett, E.A., 1988. Effect of ultraviolet radiation on cataract formation. *N Engl J Med* **319**, 1429-1433.
- Townsend, D.M., Deng, M., Zhang, L., Lopus, M.G. and Hanigan, M.H., 2003. Metabolism of Cisplatin to a nephrotoxin in proximal tubule cells. *J Am Soc Nephrol* **14**, 1-10.
- Tveit, A., Rusch, G.M., Muijser, H. and Tegelenbosch-Schouten, M.M., 2013. The acute, developmental, genetic and inhalation toxicology of 2,3,3,3-tetrafluoropropene (HFO-1234yf). *Drug Chem Toxicol* **36**, 412-420.
- Ueno, H., Likos, J.J. and Metzler, D.E., 1982. Chemistry of the inactivation of cytosolic aspartate aminotransferase by serine O-sulfate. *Biochemistry* **21**, 4387-4393.

- UN, 2016. United Nations, Transforming our world: The 2030 agenda for sustainable development, <https://stg-wedocs.unep.org/bitstream/handle/20.500.11822/11125/unepswiosm1inf7sdg.pdf?sequence=1> Last accessed on 13.06.2022.
- UN, 2020. United Nations Guidelines. Sustainable Development Goals, Guidelines for the use of the SDG logo including colour wheel and 17 icons. https://www.un.org/sustainabledevelopment/wp-content/uploads/2019/01/SDG_Guidelines_AUG_2019_Final.pdf
- UNEP, 2009. Handbook for the Montreal Protocol on Substances that Deplete the Ozone Layer. In Program, U.N.E., (Ed.). United Nations Environment Program, Nairobi, pp.
- Urban, G. and Dekant, W., 1994. Metabolism of 1, 1-dichloro-2, 2, 2-trifluoroethane in rats. *Xenobiotica* **24**, 881-892.
- Urban, G., Speerschneider, P. and Dekant, W., 1994. Metabolism of the chlorofluorocarbon substitute 1, 1-dichloro-2, 2, 2-trifluoroethane by rat and human liver microsomes: the role of cytochrome P450 2E1. *Chemical research in toxicology* **7**, 170-176.
- Wako, K., 2013. An acute inhalation toxicity study of HFO-1123 in rats. Mitsubishi Chemical Medience Corporation Study Number B130422.
- Wako, K., 2014a. A 2-week repeated dose toxicity study by nose-only inhalation exposure of HFO-1123 in rats. Mitsubishi Chemical Medience Corporation. Study Number B131119.
- Wako, K., 2014b. A 13-week repeated dose nose-only inhalation toxicity study of HFO-1123 in rats.: LSI Medience Corporation, Study Number B140184.
- Wako, K., 2014c. An acute inhalation toxicity study of HFO-1123 in rats. LSI Medience Corporation. Study Number B14613.
- Wako, K., 2015a. A prenatal developmental toxicity study by inhalation exposure of HFO-1123 in rats LSI Medience Corporation, Study Number B150437.
- Wako, K., 2015b. A reproduction/developmental toxicity screening test of HFO-1123 in rats LSI Medience Corporation, Study Number B140850
- Wako, K., 2016. A dose-finding study for a prenatal developmental toxicity study by inhalation exposure of HFO-1123 in rabbits. LSI Medience Corporation. Study Number B160007.
- Wako, K., 2017. A subacute inhalation toxicity study of HFO-1123 in minipigs (14-day study). LSI Medience Corporation. Study Number B160900.
- Wako, K., 2018a. An acute inhalation toxicity study of HFO-1123 in chimeric mice with humanized livers.:LSI Medience Corporation, Study Number B180272.
- Wako, K., 2018b. A subacute toxicity study of HFO-1123 in female minipigs (14-day study). LSI Medience Corporation. Study Number B180581.
- Wako, K., 2019a. A blood citrate concentration measurement study by inhalation exposure of HFO-1123 in minipigs. LSI Medience Corporation. Study Number B180581.
- Wako, K., 2019b. A blood citrate concentration measurement study by inhalation exposure of HFO-1123 in rats. LSI Medience Corporation, pp.
- WEEL, 2009. Workplace Environmental Exposure Level. Workplace Environmental Exposure Level Committee 2,3,3,3 tetrafluoropropene. Falls Church: American Industrial Hygiene Association.
- WEEL, 2012. Workplace Environmental Exposure Level. Workplace Environmental Exposure Level Committee, 1,3,3,3-Tetrafluoropropylene. OARS WEEL, Workplace Environmental Exposure Level, Cincinnati, OH.

- Werner, M., Birner, G. and Dekant, W., 1996. Sulfoxidation of Mercapturic Acids Derived from Tri- and Tetrachloroethene by Cytochromes P450 3A: A Bioactivation Reaction in Addition to Deacetylation and Cysteine Conjugate β -Lyase Mediated Cleavage. *Chemical Research in Toxicology* **9**, 41-49.
- Wright, S.H., Wunz, T.M., North, J. and Stevens, J.L., 1998. Na-dependent transport of S-(1,2-dichlorovinyl)-L-cysteine by renal brush-border membrane vesicles. *J Pharmacol Exp Ther* **285**, 162-169.
- Wurzel, K.A., 2005. Freons. In Wexler, P., (Ed.), *Encyclopedia of Toxicology (Second Edition)*. Elsevier, New York, pp. 384-385.
- Yamauchi, A., Stijntjes, G.J., Commandeur, J.N.M. and Vermeulen, N.P.E., 1993. Purification of Glutamine Transaminase K/Cysteine Conjugate β -Lyase from Rat Renal Cytosol Based on Hydrophobic Interaction HPLC and Gel Permeation FPLC. *Protein Expression and Purification* **4**, 552-562.
- Yokoyama, H., 2018. *In vitro* metabolism of HFO-1123. LSI Medience Corporation. Study number: B170678.
- Zanovello, A., Ferrara, R., Tolando, R., Bortolato, S., White, I.N. and Manno, M., 2001. Bioactivation and toxicity *in vitro* of HCFC-123 and HCFC-141b: role of cytochrome P450. *Toxicol Lett* **124**, 139-152.

Appendix A Additional Methods

A.1 HPLC-DAD parameters used for 1123-CYS purification

1123-CYS was synthesized by AGC Inc. . Purification of crude 1123-CYS was performed using an HP 1090 HPLC system (Agilent Technologies, Santa Clara, USA) equipped with a photodiode array detector (DAD) on a Partisil ODS 3 C18 column (250 x 8 mm, 5 µm; Bischoff Chromatography, Leonberg, Germany). Water (containing 0.1% formic acid) and methanol (containing 0.1% formic acid) were used as eluents. For gradient elution, the concentration of eluents was changed as follows: 0-15 min 100% water, 15-25 min linear gradient to 5% water, 25-30 min 5% water, 30-35 min linear gradient to 100% water). Detection wavelength was set to 225 nm.

A.2 ¹⁹F-NMR based analysis of fluorine containing metabolites**Table A. 1** Summary of different sample workup procedures applied to stop the enzymatic reaction at the end of the incubation period used for ¹⁹F-NMR analysis of fluorine metabolites formed from β -lyase mediated cleavage of 1123-CYS

Incubations were performed as described in chapter 3.5.1	
Workup Nr. 1 (addition of TCA)	Removed aliquots were placed on ice and 0.2 mL of ice cold trichloroacetic acid (TCA) was added. After centrifugation at 20,000 x g and 4°C for 15 minutes, D ₂ O was added to supernatants, yielding a total volume of 0.8 mL. Until analysis, samples were stored at -80°C.
Workup Nr. 2 (no specific workup)	To stop the enzymatic reaction, the removed aliquots were placed on ice and D ₂ O was added, yielding a total volume of 0.8 mL. Until analysis, samples were stored at -80°C.
Workup Nr. 3 (centrifugation)	Removed aliquots were placed on ice and immediately centrifuged at 20,000 x g and 4°C for 15 minutes. To the obtained supernatants D ₂ O was added, yielding a total volume of 0.8 mL. Until analysis, samples were stored at -80°C.
Workup Nr. 4 (acetonitrile)	Removed aliquots were placed on ice and 0.2 mL of ice-cold acetonitrile was added immediately. After centrifugation at 20,000 x g and 4°C for 15 minutes, D ₂ O was added to the supernatants, yielding a total volume of 0.8 mL. Until analysis, samples were stored at -80°C.
Workup Nr. 5 (ultracentrifugation)	Removed aliquots were placed on ice and immediately centrifuged at 164,000 x g and 4°C for 30 minutes. D ₂ O was added to the supernatants, yielding a total volume of 0.8 mL. Until analysis, samples were stored at -80°C.



A.3 HPLC-DAD parameters used for 1123-GSH purification

Purification of crude 1123-GSH was performed using an HP 1090 HPLC system (Agilent Technologies, Santa Clara, USA) equipped with a photodiode array detector (DAD) on a Hypersil C18 column (250 x 8 mm, 5 µm; Bischoff Chromatography, Leonberg, Germany). Water (containing 0.1% formic acid) and acetonitrile (ACN) (containing 0.1% formic acid) were used as eluents with a flow rate of 4 mL/min. For gradient elution, the concentration of eluents was changed as follows: linear gradient from 0 to 20% ACN in 20 min, 20-22 min linear gradient to 95% ACN, 22-25min 95% ACN, 25-27 min linear gradient to 0% ACN). Detection wavelength was set to 235 nm. 1123-GSH eluted at a retention time of 8.91 minutes

Appendix B Additional Figures & Tables

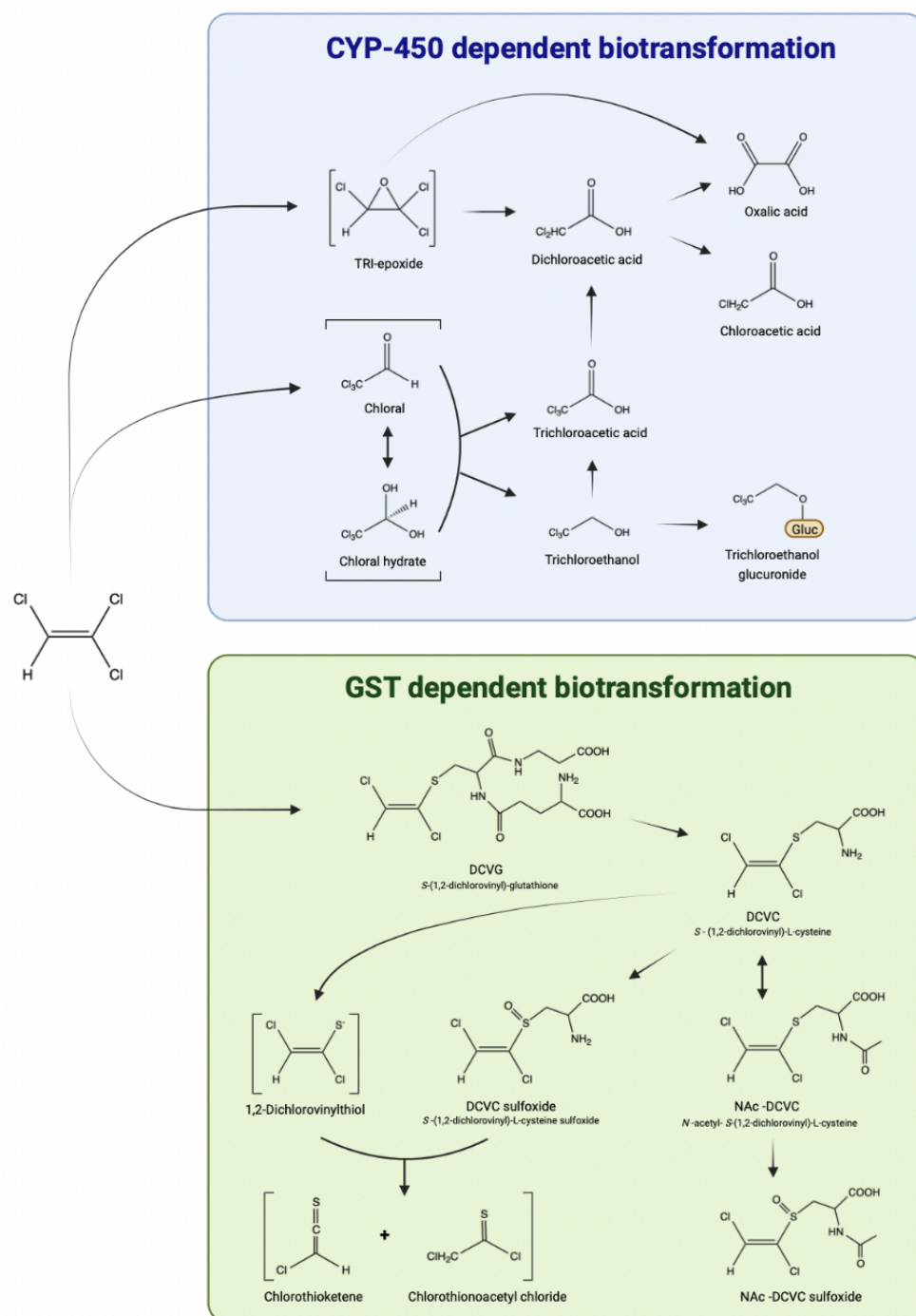


Figure B. 1 Main pathways of trichloroethene (TRI) metabolism. CYP-450 and GST dependent biotransformation play the major role in TRI biotransformation, leading to a multitude of metabolites responsible for TRI induced toxicity. GST mediated formation of S-(1,2-dichlorovinyl)-glutathione (DCVG) is the initial step of the mercapturic acid pathway. Subsequent degradation of DCVG results in the formation of S-(1,2-dichlorovinyl)-L-cysteine (DCVC). DCVC may be cleaved by β -lyases or subject for N-acetylation via N-acetyltransferases. Figure modified from Lash *et al.* (2014). Created with BioRender.com

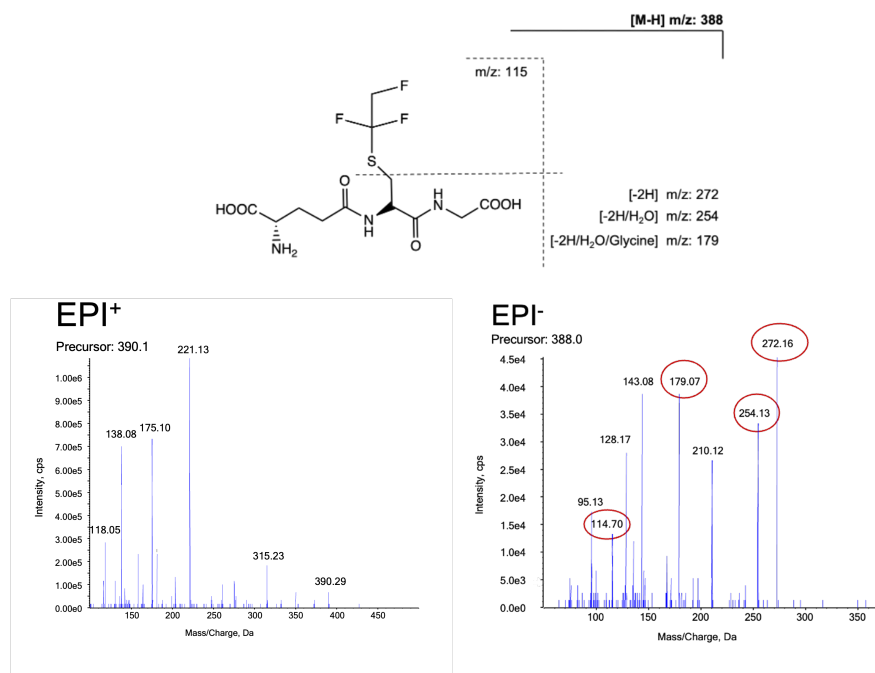


Figure B. 2 Enhanced product ion (EPI) spectra obtained in positive and negative ionization from synthesized 1123-GSH. Positive ionisation showed increased sensitivity compared to negative ionisation and was used for all further LC-MS/MS analysis.

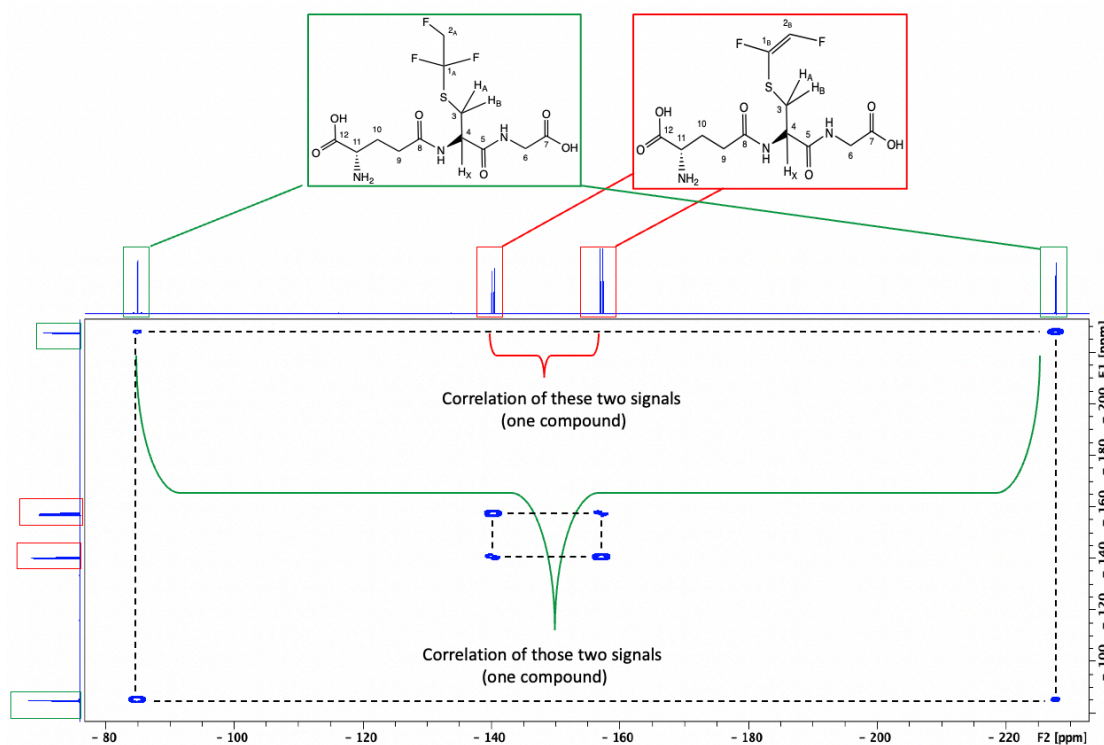


Figure B. 3 ^{19}F , ^{19}F $\{^1\text{H}\}$ -correlation NMR of 1123-GSH batch after HPLC-DAD purification revealing *trans*-(1,2-difluoro-ethylen)-L-glutathione as a side product of synthesis. In this figure the ^{19}F -NMR spectrum (vertical axis) is projected against the ^{19}F $\{^1\text{H}\}$ -NMR (^1H decoupled ^{19}F -NMR) spectrum resulting in a two-dimensional COSY spectrum. Investigations were performed in D_2O at 25 °C at a spectrometer frequency of 376.6 Hz.

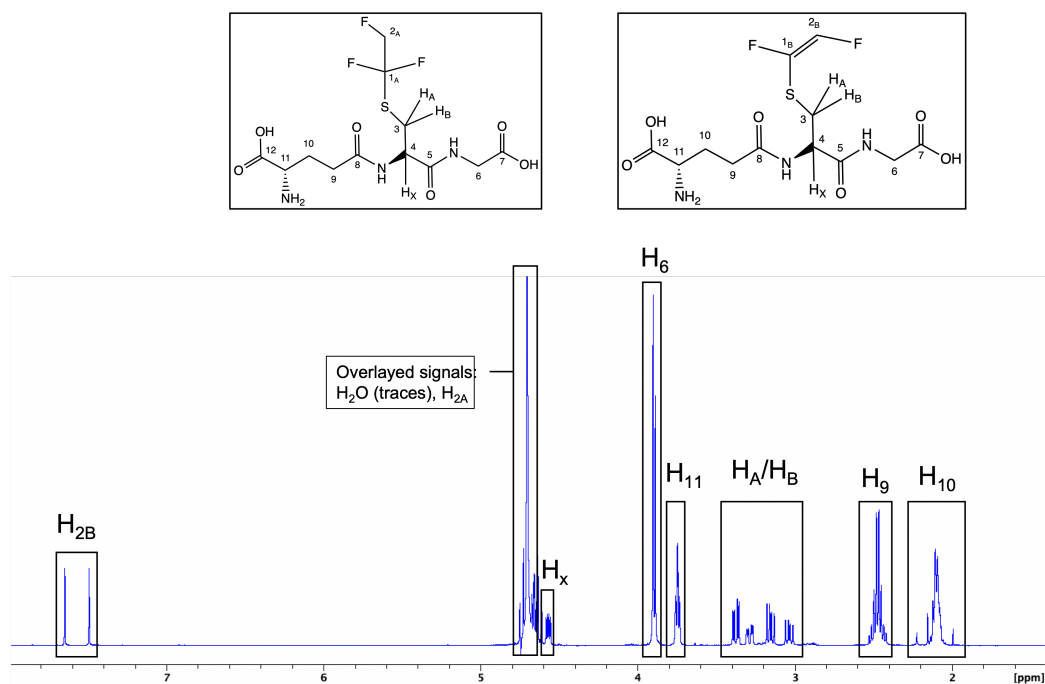


Figure B. 4 $^1\text{H-NMR}$ spectrum of 1123-GSH batch after HPLC-DAD purification revealing *trans*-(1,2-difluoroethenyl)-L-glutathione as a side product of synthesis. Investigations were performed in D_2O at 25°C at a spectrometer frequency of 500.1 Hz.

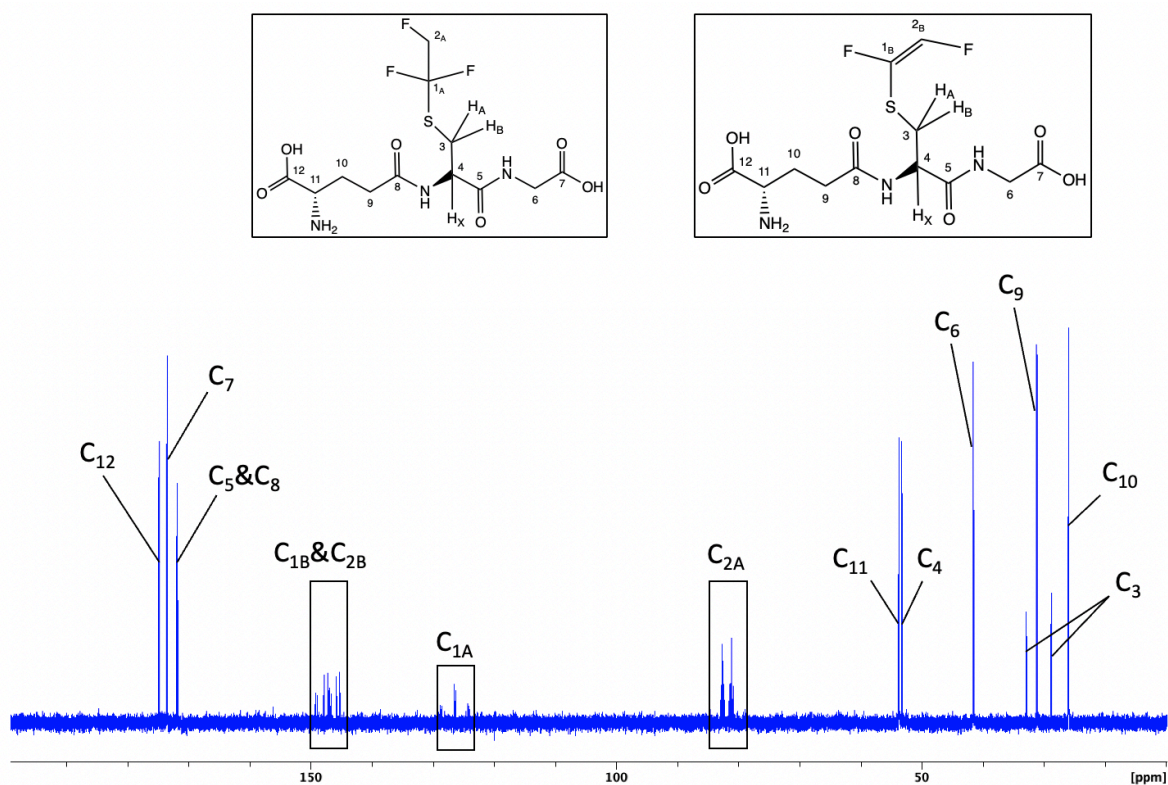


Figure B. 5 $^{13}\text{C-NMR}$ spectrum of 1123-GSH batch after HPLC-DAD purification revealing *trans*-(1,2-difluoroethenyl)-L-glutathione as a side product of synthesis. Investigations were performed in D_2O at 25°C at a spectrometer frequency of 125.8 Hz.

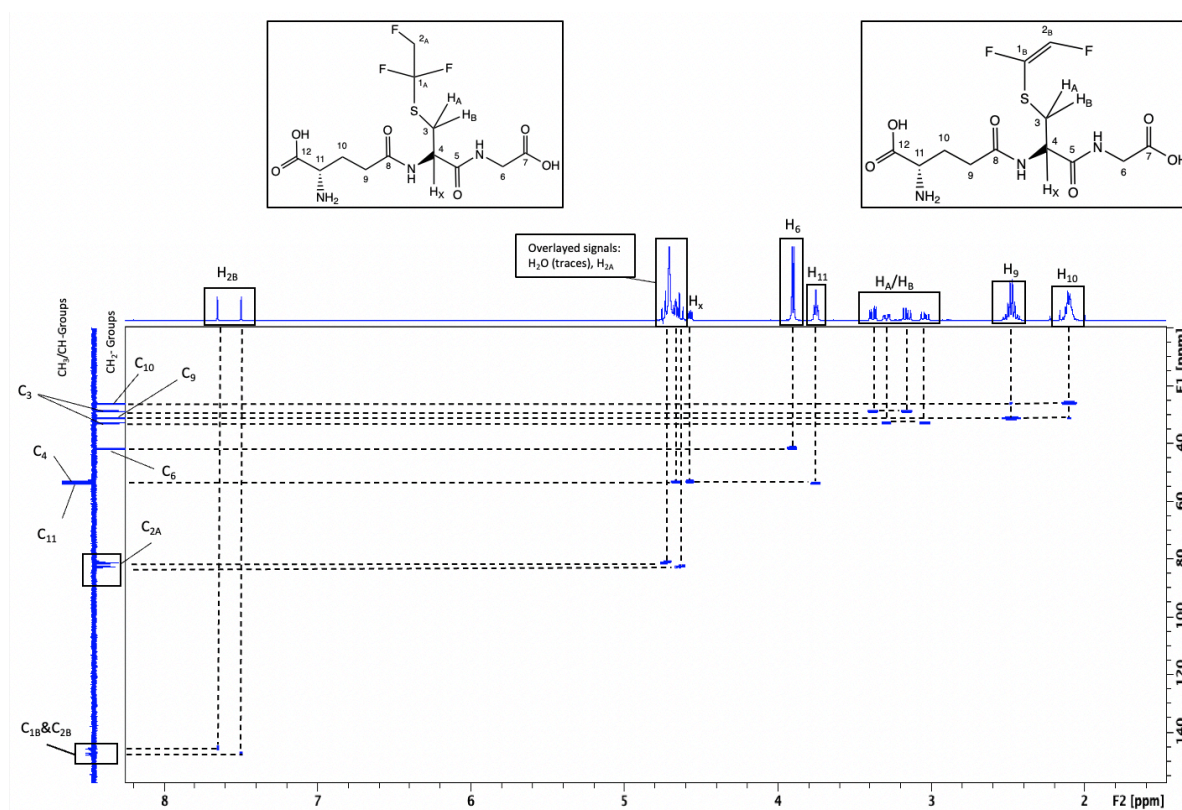


Figure B. 6 $^{13}\text{C}, ^1\text{H}$ -HSQC NMR spectra of 1123-GSH batch after HPLC-DAD purification revealing *trans*-(1,2-difluoroethylenyl)-L-glutathione as a side product of synthesis. In this figure the ^{13}C -DEPT135 spectrum (vertical axis) is projected against the ^1H -NMR spectrum resulting in a two-dimensional HSQC spectrum. Investigations were performed in D_2O at 25°C . ^1H -NMR and ^{13}C -DEPT135 NMR spectra were recorded at a spectrometer frequency of 500.1 Hz and 125.8 Hz, respectively.

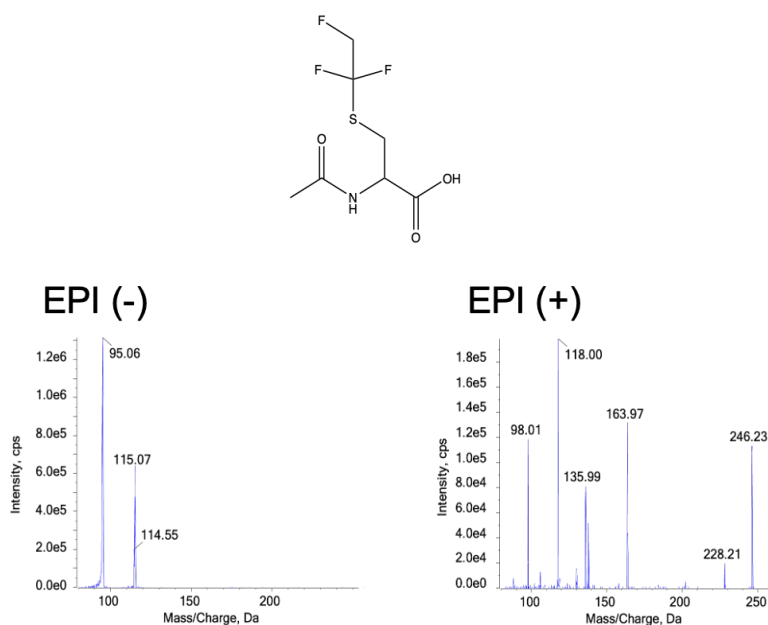


Figure B. 7 Enhanced product ion (EPI) spectra obtained in positive and negative ionization from the product of 1123-CYS-NAC synthesis. Fragmentation pattern indicating successful synthesis of 1123-CYS-NAC

Species-differences in the *in vitro* biotransformation of trifluoroethene (HFO-1123)

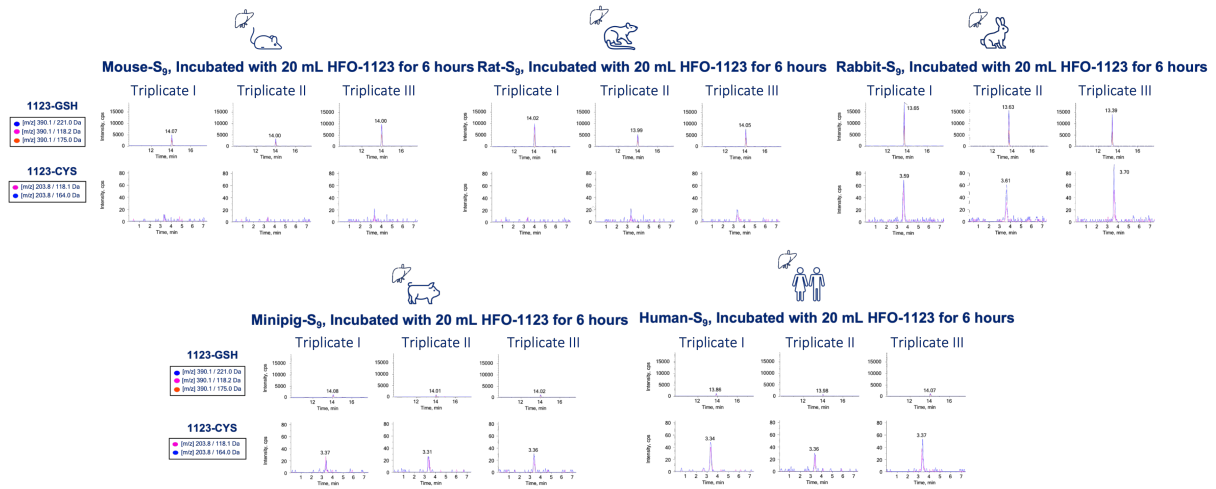


Figure B. 8 Species-differences in 1123-CYS formation in hepatic rat, mouse, human, NZW Rabbit and Goettingen[®] Minipig S₉ fractions. Results of three independently performed experiments (Triplicate I, Triplicate II, Triplicate III) are shown.

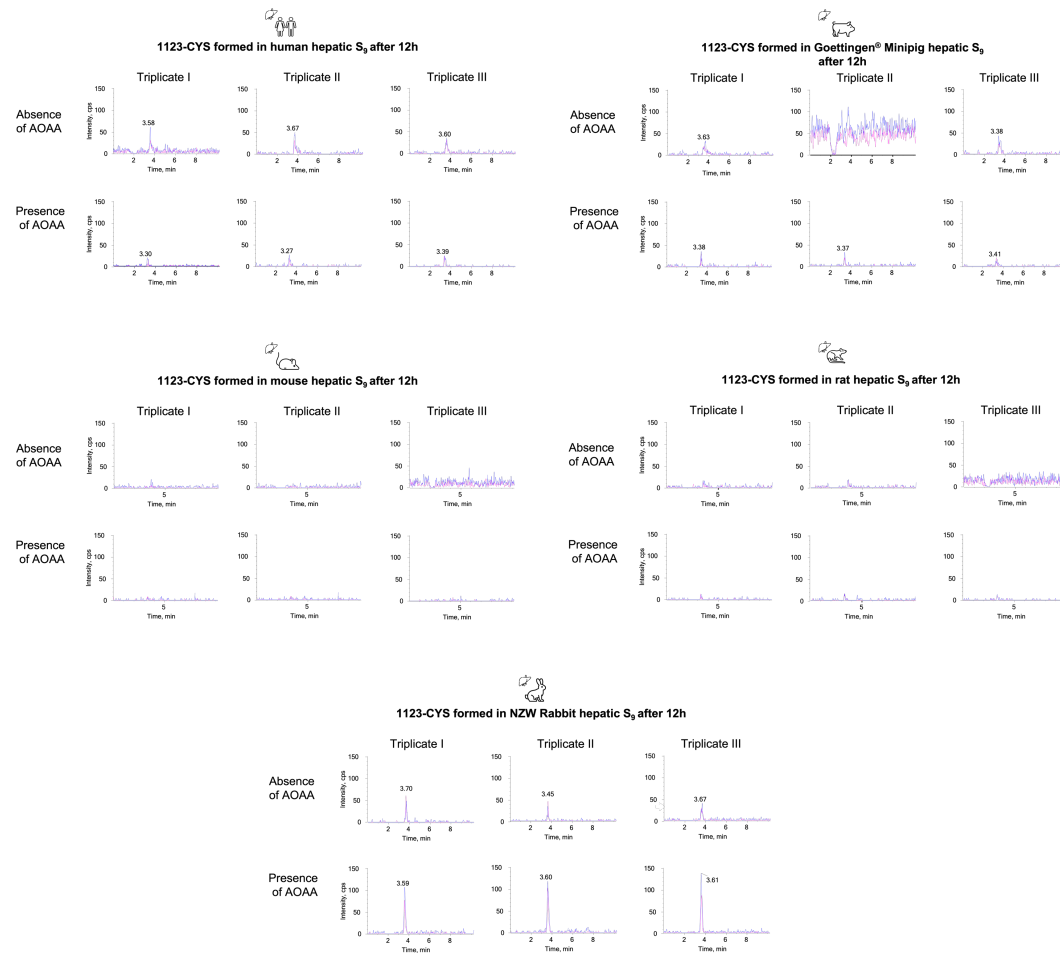


Figure B. 9 Differences in 1123-CYS formation in hepatic S₉ fractions in the presence or absence of the β -lyase inhibitor AOAA. Results of three independently performed experiments (Triplicate I, Triplicate II, Triplicate II) are shown.

Table B. 1 V_{max} and K_m values of 1123-CYS cleavage in renal and hepatic cytosolic fractions determined by Eadie – Hofstee Plot and the Lineweaver – Burk Plot (Lineweaver and Burk, 1934; Eadie, 1942).

		Eadie - Hofstee		Lineweaver - Burk	
		V_{max}	K_m	V_{max}	K_m
		[nmol (pyruvate formed)/(mg protein x min)]	[mM]	[nmol (pyruvate formed)/(mg protein x min)]	[mM]
Human	Kidney	0.77 ± 0.26	1.22 ± 0.42	0.83 ± 0.29	1.50 ± 0.53
	Liver	0.31 ± 0.05	0.30 ± 0.05	0.29 ± 0.05	0.27 ± 0.04
CD1 Mouse	Kidney	0.29 ± 0.1	0.25 ± 0.08	0.33 ± 0.1	0.62 ± 0.2
	Liver	0.38 ± 0.17	0.17 ± 0.07	0.35 ± 0.16	0.16 ± 0.07
SD Rat	Kidney	0.55 ± 0.24	0.35 ± 0.19	0.55 ± 0.23	0.36 ± 0.2
	Liver	1.04 ± 0.63	0.94 ± 0.57	1.14 ± 0.69	1.13 ± 0.68
Goettingen® Minipig	Kidney	3.63 ± 1.35	2.06 ± 0.77	3.55 ± 1.33	2.03 ± 0.76
	Liver	0.74 ± 0.27	1.40 ± 0.51	0.71 ± 0.25	1.32 ± 0.48
NZW Rabbit	Kidney	1.04 ± 0.15	1.01 ± 0.37	1.14 ± 0.14	0.83 ± 0.42
	Liver	1.12 ± 0.10	1.29 ± 0.27	1.06 ± 0.23	1.15 ± 0.17

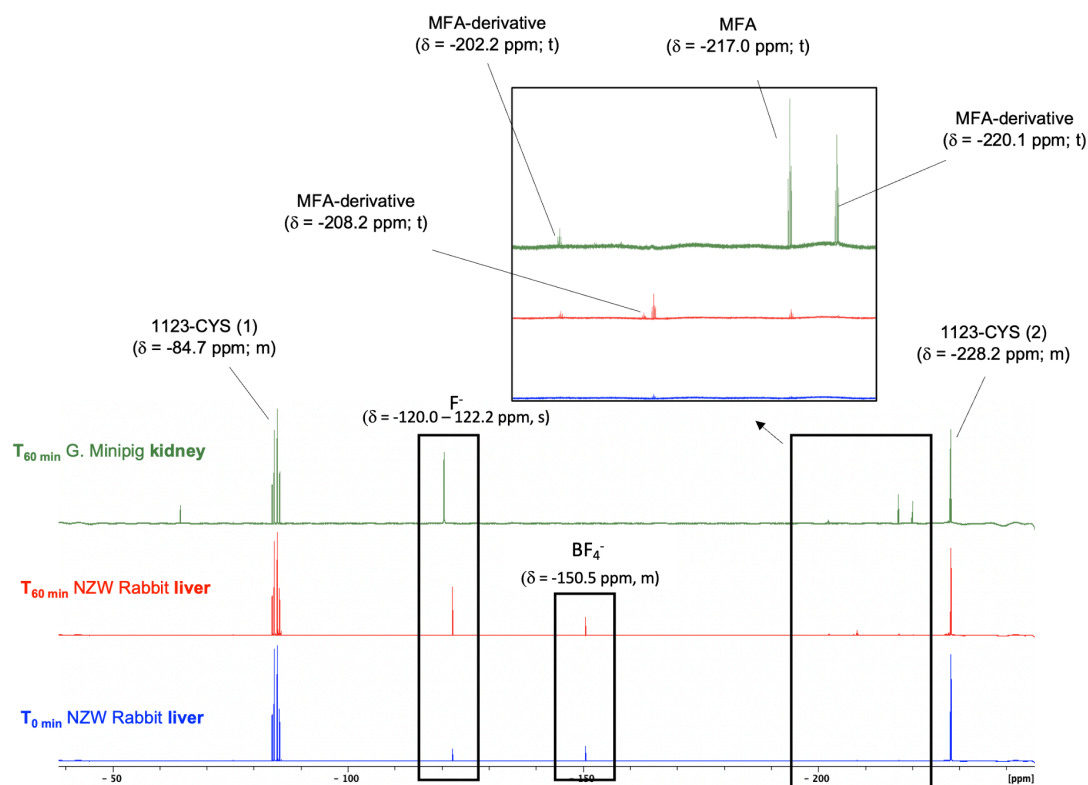


Figure B. 10 ^{19}F -NMR spectra from aliquots taken at 0 ($T_{0 \text{ min}}$ NZW Rabbit liver) and 60 minutes ($T_{60 \text{ min}}$ NZW Rabbit liver, $T_{60 \text{ min}}$ Goettingen[®] Minipig kidney) after the start of incubation containing 1123-CYS and NZW Rabbit liver cytosol or Goettingen[®] Minipig kidney cytosol, respectively. Resonances were assigned to 3,3,3-trifluoro-1-propanol ($\delta = -64.3$ ppm; t, $J_{\text{HF}} = 11.2$ Hz); 1123-CYS (F_2 -moiety ($\delta = -84.7$ ppm; m), F_1 -moiety ($\delta = -228.2$ ppm; m)); F^- ($\delta = -122.2$ ppm; s); MFA ($\delta = -217.0$ ppm; t, $J_{\text{HF}} = 48.4$ Hz); MFA-derivative (I) ($\delta = -202.2$ ppm; t, $J_{\text{HF}} = 48.5$ Hz), MFA-derivative (II) ($\delta = -208.2$ ppm; t, $J_{\text{HF}} = 48.5$ Hz) and MFA-derivative (III) ($\delta = -220.1$ ppm; t, $J_{\text{HF}} = 48.5$ Hz). By comparing $T_{0 \text{ min}}$ and $T_{60 \text{ min}}$ time-dependent formation of F^- , MFA and all MFA-derivatives is evident in NZW Rabbit kidney cytosol. However, the signal intensity of both MFA and MFA-derivatives exhibited only a fraction of the corresponding signals in $T_{60 \text{ min}}$ Goettingen[®] Minipig kidney.

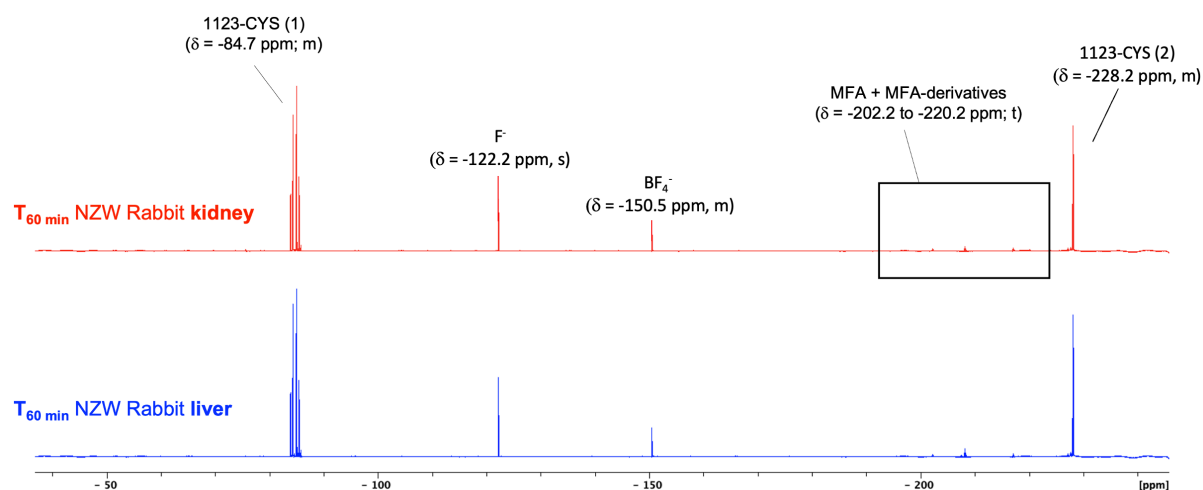


Figure B. 11 ^{19}F -NMR spectra from aliquots extracted 60 minutes after the start of incubations containing 1123-CYS and NZW Rabbit liver (blue) and NZW Rabbit kidney (red) cytosol. Resonances were assigned to 1123-CYS (F_2 -moiety ($\delta = -84.7$ ppm; m), F_1 -moiety ($\delta = -228.2$ ppm; m)); F^- ($\delta = -122.2$ ppm; s); BF_4^- ($\delta = -150.5$ ppm, m), MFA ($\delta = -217.0$ ppm; t, $J_{\text{HF}} = 48.4$ Hz); MFA-derivative (I) ($\delta = -202.2$ ppm; t, $J_{\text{HF}} = 48.5$ Hz), MFA-derivative (II) ($\delta = -208.2$ ppm; t, $J_{\text{HF}} = 48.5$ Hz) and MFA-derivative (III) ($\delta = -220.1$ ppm; t, $J_{\text{HF}} = 48.5$ Hz). No significant differences in metabolite formation were determined between liver and kidney cytosol.

List of figures

Figure 1 United Nations <i>Sustainable Development Goals</i> with regard to universal, cost-efficient clean refrigeration according to the <i>Clean Cold and the Global Goals</i> report of the Birmingham Energy Institute (2016).....	8
Figure 2 Chemical structures of exemplary CFCs.....	10
Figure 3 Negative influence of CFCs on stratospheric ozone and related health risks.....	12
Figure 4 Computational model of global stratospheric ozone depletion from 1974 until 2064 (A and B) and changes in global in UV-index (C) if CFCs were not phased out.....	14
Figure 5 Chemical structures of exemplary HCFCs and HFCs.....	15
Figure 6 <i>In vitro</i> and <i>in vivo</i> biotransformation of HCFC-123.	17
Figure 7 CYP-450 and GST dependent biotransformation of HFO-1234ze in rodents.	21
Figure 8 The mercapturic acid pathway in bioactivation and detoxification of xeno- and endobiotics.	25
Figure 9 Pulmonary uptake (A), hepatic transport (B) and proposed biotransformation (C) of HFO-1123 with account for its toxicity in sensitive species.....	33
Figure 10 Cellular effects of monofluoroacetic acid (MFA) that may contribute to its toxicity according to Proudfoot <i>et al.</i> (2006).	34
Figure 11 Overview of the experimental approach for determining GST mediated formation of 1123-GSH after incubation of HFO-1123 with subcellular S ₉ fractions of Goettingen [®] Minipigs, NZW Rabbits, SD rats, CD1 mice and humans.	40
Figure 12 Overview of the experimental approach to determine β-lyase mediated cleavage of 1123-GSH after incubation of HFO-1123 with renal and hepatic cytosolic fractions of Goettingen [®] Minipigs, NZW Rabbits, SD rats, CD1 mice and humans.....	43
Figure 13 Coupling of the cysteine S-conjugate β-lyase reaction and the <i>D</i> -lactate dehydrogenase reaction to detect pyruvate formation.	44
Figure 14 Cell systems (A) and cell culture investigations (B) used to evaluate cytotoxicity and cellular citrate which may arise from β-lyase mediated cleavage of 1123-CYS to MFA and subsequent inhibition of aconitase	50
Figure 15 ¹⁹ F-NMR analysis of the purified 1123-GSH synthesis product. Besides 1123-GSH (δ = -85.0 ppm, m; δ = -227.8 ppm, m), a second GSH conjugate was found to be present.	53
Figure 16 LC-MS/MS chromatograms showing time-dependent formation of DCVG in mouse, rat, human and Goettingen [®] Minipig hepatic S ₉ after incubation with TRI (1 mM). ...	54

- Figure 17** Comparison of 1123-GSH formation in purchased vs. in-house prepared Goettingen® Minipig S₉ (left graph) and mouse hepatic S₉ (right graph), showing no significant differences in the activity of 1123-GSH formation between both Goettingen® Minipig S₉, thus confirming the suitability of S₉ prepared in-house for further investigations..... 55
- Figure 18** Time-dependent formation of 1123-GSH (ng/mL) in hepatic S₉ fractions of mice, rats, NZW Rabbits, Goettingen® Minipigs and humans in the presence (marked in grey) or absence (marked in blue) of the NADPH regenerating system. 56
- Figure 19** Velocity of 1123-GSH formed (ng 1123-GSH/mL/h) in hepatic S₉ fractions of mice, rats, NZW Rabbits, Goettingen® Minipigs and humans after incubation with HFO-1123 (4, 6, 8, 10, 12, 20 mL) in the gas phase..... 58
- Figure 20** LC/MS-MS analysis of 1123-GSH and 1123-CYS formed in 6h-incubations of 20 mL HFO-1123 with hepatic S₉ fractions (rat, mouse, NZW Rabbit, human, and Goettingen® Minipig)..... 59
- Figure 21** Time-depended formation of 1123-GSH (ng/mL) in hepatic S₉ fractions of mice, rats, NZW Rabbits, Goettingen® Minipigs and humans in the presence or absence acivicin.60
- Figure 22** LC-MS/MS analysis of 1123-CYS ([m/z]: 203.18/118.1 Da, 203.18/164.0 Da) in 12h-incubations of hepatic S₉ of rats, mice, Goettingen® Minipigs, humans and NZW Rabbits with HFO-1123 61
- Figure 23** ¹⁹F-NMR spectra of rat, mouse, human, Goettingen® Minipig and NZW Rabbit hepatic S₉ subcellular fractions incubated with HFO-1123 (0.89 mmol / 20 ml) in the presence and absence of either GSH or the NADPH regenerating system..... 63
- Figure 24** Time-dependent formation of 1123-GSH ([m/z]: 390.1/221.0 Da, 390.1/118.2 Da, 390.1/175.0 Da) and 1123-CYS ([m/z]: 203.8/118.1 Da, 203.8/164.0 Da) in Goettingen® Minipig, human and rat renal S₉ fractions. 65
- Figure 25** LC-MS/MS chromatograms of 1123-CYS batch before and after purification via HPLC. Before HPLC purification distinct signals of 1123-CYS ester (t_r = 14.56 min) and cystine (t_r = 1.96 min) were detected next to 1123-CYS (t_r = 3.65 min), revealing a contamination with both substances.. 67
- Figure 26** ¹⁹F-NMR Spectra of purified 1123-CYS (20 mM)..... 68
- Figure 27** Protein-dependent cleavage of TCVC and 1123-CYS (1.25 mM) resulting in formation of pyruvate. 69
- Figure 28** Cleavage of TCVC / 1123-CYS in the absence and presence of AOAA (0.625 mM) in minipig liver and human kidney cytosolic fractions (0.5 mg protein/mL). 69

Figure 29 V_{\max} (nmol/(min x mg protein) and K_m values (mM)) obtained in liver and kidney cytosol of mice, rats, humans, Goettingen [®] Minipigs and NZW Rabbits.....	70
Figure 30 Michaelis-Menten kinetics of β -lyase mediated cleavage of 1123-CYS in renal and hepatic human, mouse, rat, Goettingen [®] Minipig, and NZW Rabbit cytosolic fractions.	71
Figure 31 ¹⁹ F-NMR spectrum of purified 1123-CYS (dissolved in D ₂ O), with particular attention to important sections of the spectrum (Box a-d).....	72
Figure 32 ¹⁹ F-NMR spectra of control incubations (top to bottom: Goettingen [®] Minipig kidney cytosol, human liver cytosol, human kidney cytosol)	73
Figure 33 ¹⁹ F-NMR spectra from aliquots taken at 0 ($T_{0 \text{ min}}$) and 60 minutes ($T_{60 \text{ min}}$) after start of the reaction (renal Goettingen [®] Minipig cytosol incubated with 1123-CYS).....	75
Figure 34 ¹⁹ F-NMR spectra from aliquots taken at 0 ($T_{0 \text{ min}}$) and 60 minutes ($T_{60 \text{ min}}$) after the start of the reaction in the presence of AOAA (renal Goettingen [®] Minipig cytosol incubated with 1123-CYS).....	76
Figure 35 ¹⁹ F-NMR spectra from aliquots taken at 0 ($T_{0 \text{ min}}$ human kidney) and 60 minutes ($T_{60 \text{ min}}$ human kidney, $T_{60 \text{ min}}$ Goettingen [®] Minipig kidney) after the start of incubation containing 1123-CYS and human kidney cytosol and Goettingen [®] Minipig kidney cytosol respectively.	77
Figure 36 ¹⁹ F-NMR spectra from aliquots taken at 0 ($T_{0 \text{ min}}$ human liver) and 60 minutes ($T_{60 \text{ min}}$ human liver, $T_{60 \text{ min}}$ Goettingen [®] Minipig kidney) after the start of incubation containing 1123-CYS and human liver cytosol or Goettingen [®] Minipig kidney cytosol, respectively.	78
Figure 37 ¹⁹ F-NMR spectra from aliquots taken at 0 ($T_{0 \text{ min}}$ NZW Rabbit kidney) and 60 minutes ($T_{60 \text{ min}}$ NZW Rabbit kidney, $T_{60 \text{ min}}$ Goettingen [®] Minipig kidney) after the start of incubation containing 1123-CYS and NZW Rabbit kidney cytosol or Goettingen [®] Minipig kidney cytosol, respectively.....	79
Figure 38 ¹⁹ F-NMR spectra from aliquots taken 60 minutes ($T_{60 \text{ min}}$ human kidney, $T_{60 \text{ min}}$ NZW Rabbit kidney) after the start of incubation containing 1123-CYS and NZW Rabbit kidney cytosol or human kidney cytosol, respectively.....	80
Figure 39 Cell viability of human (HK-2), rat (NRK-52E) and porcine (LLC-PK1) proximal tubular cell lines after 48h treatment with 1123-CYS (a) or MFA (c).....	81
Figure 40 Citrate levels of rat (NRK-52E), human (HK-2) and porcine (LLC-PK1) proximal tubular cell lysates after treatment with MFA (a) and 1123-CYS (b).....	83
Figure 41 Analysis of MFA (a) and 1123-CYS-NAc (b) formed in NRK-52E, HK-2 and LLC-PK1 cells after treatment with increasing concentrations of 1123-CYS.	85

Figure 42 Overview of <i>in vivo</i> toxicity of HFO-1123 and <i>in vitro</i> species-differences in biotransformation.	98
Figure B. 2 Main pathways of trichloroethene (TRI) metabolism. CYP-450 and GST dependent biotransformation play the major role in TRI biotransformation, leading to a multitude of metabolites responsible for TRI induced toxicity.....	122
Figure B. 2 Enhanced product ion (EPI) spectra obtained in positive and negative ionization from synthesized 1123-GSH.....	123
Figure B. 3 ¹⁹ F, ¹⁹ F { ¹ H}-correlation NMR of 1123-GSH batch after HPLC-DAD purification revealing <i>trans</i> -(1,2-difluoro-ethylen)-L-glutathione as a side product of synthesis.....	123
Figure B. 4 ¹ H-NMR spectrum of 1123-GSH batch after HPLC-DAD purification revealing <i>trans</i> -(1,2-difluoro-ethylen)-L-glutathione as a side product of synthesis.....	124
Figure B. 5 ¹³ C-NMR spectrum of 1123-GSH batch after HPLC-DAD purification revealing <i>trans</i> -(1,2-difluoro-ethylen)-L-glutathione as a side product of synthesis.....	124
Figure B. 6 ¹³ C, ¹ H-HSQC NMR spectra of 1123-GSH batch after HPLC-DAD purification revealing <i>trans</i> -(1,2-difluoroethylen)-L-glutathione as a side product of synthesis.....	125
Figure B. 7 Enhanced product ion (EPI) spectra obtained in positive and negative ionization from the product of 1123-CYS-NAC synthesis.....	125
Figure B. 8 Species-differences in 1123-CYS formation in hepatic rat, mouse, human, NZW Rabbit and Goettingen [®] Minipig S ₉ fractions.....	126
Figure B. 9 Differences in 1123-CYS formation in hepatic S ₉ fractions in the presence or absence of the β-lyase inhibitor AOAA.....	126
Figure B. 10 ¹⁹ F-NMR spectra from aliquots taken at 0 and 60 minutes after the start of incubation containing 1123-CYS and NZW Rabbit liver cytosol or Goettingen [®] Minipig kidney cytosol, respectively.....	128
Figure B. 11 ¹⁹ F-NMR spectra from aliquots extracted 60 minutes after the start of incubations containing 1123-CYS and NZW Rabbit liver (blue) and NZW Rabbit kidney (red) cytosol.....	129

List of tables

Table 1 Classes of refrigerants and their climatic properties.....	18
Table 2 Study design and results of acute toxicity and <i>in vivo</i> biotransformation studies conducted with HFO-1123 in experimental animals.....	28
Table 3 Study design and results of repeated dose toxicity studies conducted with HFO-1123 in experimental animals	29
Table 4 Study design and results of developmental and reproductive toxicity studies conducted with HFO-1123 in experimental animals.....	30
Table 5 Pipetting scheme for sample and blank incubations used to determine β -lyase mediated cleavage of cysteine S-conjugates in cytosolic fractions.....	45
Table 6 Mass spectrometer settings Q1 (m/z), Q3 (m/z) and Collision Energy (V) used for LC-MS/MS analyses	48
Table 7 List of cell culture media and supplements.....	49
Table 8 Origin of proximal tubular kidney cells and composition of cell-specific culture media	49
Table 9 Concentration of 1123-GSH (ng/mL) formed after incubation of mouse, rat NZW Rabbit, Goettingen [®] Minipig and human hepatic S ₉ fractions with 0.4 mmol HFO-1123.	57
Table 10 IC ₅₀ (mM) values of 1123-CYS cytotoxicity after 48h treatment in the presence and absence of AOAA [125 μ M] / [250 μ M] and MFA in proximal tubular cell lines (n = 3)	82
Table 11 Summary of <i>in vitro</i> biotransformation of HFO-1123 and 1123-CYS in renal and hepatic subcellular fractions.....	86
Table 12 Summary of cytotoxicity and cellular citrate levels renal proximal tubular cells.....	87
Table A. 2 Summary of different sample workup procedures applied to stop the enzymatic reaction at the end of the incubation period used for ¹⁹ F-NMR analysis of fluorine metabolites formed from β -lyase mediated cleavage of 1123-CYS.....	120
Table A. 3 Summary of different sample workup procedures applied to stop the enzymatic reaction at the end of the incubation period used for ¹⁹ F-NMR analysis of fluorine metabolites formed from β -lyase mediated cleavage of 1123-CYS.....	127

Acknowledgements

First of all, I would like to thank my principle supervisor Prof. Dr. Angela Mally for the constant support and guidance throughout this project. I am deeply grateful to you, Angela, for professional and personal communication and help over the last three years. Furthermore, I cannot express enough thanks to the other committee members, Prof. Dr. Lehmann and Dr. Bertermann, for their continued support and encouragements. Especially, I want to thank you, Rüdiger, that you provided me with knowledge regarding all forms of NMR and for the great service of your NMR unit. In this regard, I also want to thank Marie-Luise Schäfer and Laura Wolz for their support during NMR analysis.

Words cannot express my gratitude to you Wolfgang, for your invaluable advice, continuous support, and patience during this project.

I would like to express my deepest appreciation to AGC Inc. for funding this project. Especially to Motoki Shinohara for the excellent communication and support during this project.

My completion of this project could not have been accomplished without the support of the members of my working group, Nataly, Heike, Hannelore, Christina, Christine, Bene. I would like to offer my special thanks to Johanna and Sanya for their contribution to this project.

I could not have undertaken this journey without the support and help of my caring mother Hedda, thank you for always being there for me. From the bottom of my heart, I want to thank Joa, Flo and Jaro for your love and support during the last years and many more to come! Finally, to my caring, loving and supportive wife, Jule: my deepest gratitude and love. Your encouragements when times got rough are much appreciated and duly noted.